Synthesis, Characterization and Applications of Modified TiO_2 Systems

Thesis submitted to

Cochin University of Science and Technology

in partial fulfillment of the requirements for the degree of

Doctor of Philosophy

in

Chemistry

Under the Faculty of Science

by

Mothi Krishna Mohan

Under the Supervision of

Dr. S. Sugunan

Department of Applied Chemistry
Cochin University of Science and Technology
Kochi - 682 022

June 2014

Synthesis, Characterization and Applications of Modified TiO_2 Systems

Ph. D. Thesis under the Faculty of Science

Author:

Mothi Krishna Mohan
Research Fellow, Department of Applied Chemistry
Cochin University of Science and Technology
Kochi -682 022
Email: mothikrishnamohan@gmail.com

Research Guide:

Dr. S. Sugunan
Emeritus Professor
Department of Applied Chemistry
Cochin University of Science and Technology
Kochi - 682 022
Email: ssg@cusat.ac.in

Department of Applied Chemistry
Cochin University of Science and Technology
Kochi - 682 022
India

June 2014

DEPARTMENT OF APPLIED CHEMISTRY
COCHIN UNIVERSITY OF SCIENCE AND TECHNOLOGY
KOCHI - 682 022, INDIA

Dr. S. Sugunan
Emeritus Professor

16-05-2014

Certificate

This is to certify that the thesis entitled **"Synthesis, Characterization and Applications of Modified TiO_2 Systems"** submitted for the award of the Degree of Doctor of Philosophy in Chemistry of the Cochin University of Science and Technology, is a record of original research work carried out by **Mr. Mothi Krishna Mohan** under my supervision and guidance in the Department of Applied Chemistry, and further that it has not formed the part of any other thesis previously.

Kochi-22

Dr. S. Sugunan
(Supervising Guide)

Declaration

I hereby declare that the thesis entitled **"Synthesis, Characterization and Applications of Modified TiO_2 Systems"** submitted for the award of Ph.D. Degree, is based on the original work done by me under the guidance of **Dr. S. Sugunan**, Professor (Emeritus), Department of Applied Chemistry, Cochin University of Science and Technology and further that it has not previously formed the basis for the award of any other degree.

Kochi-22 **Mothi Krishna Mohan**

16-05-2014

DEPARTMENT OF APPLIED CHEMISTRY

COCHIN UNIVERSITY OF SCIENCE AND TECHNOLOGY
KOCHI - 682 022, INDIA

Dr. S. Sugunan
Emeritus Professor

16-05-2014

Certificate

This is to certify that all the relevant corrections and modifications suggested by the audience during the pre-synopsis seminar presented by **Mr. Mothi Krishna Mohan,** and recommended by the doctoral committee of the candidate have been incorporated in the thesis entitled **"Synthesis, Characterization and Applications of Modified TiO_2 Systems"**.

Kochi-22

Dr. S. Sugunan
(Supervising Guide)

Dedicated to

my Dearest parents and sisters

Acknowledgements

Dr. S. Sugunan – My supervising guide, for his guidance, for the affection and freedom offered during my research period.

Dr. N. Manoj – Head of the Department, for the help, suggestions and instrumental facility.

Dr. K. Sreekumar – Former Head of the Department. For the freedom, guidance and suggestions offered during photovoltaic device fabrication and testing.

Dr. K. Girish Kumar – Former Head of the Department.

Dr. S. Prathapan – Doctoral committee member. For the help received during photo-oxidation reactions.

All other faculty members, administrative staff and librarian - For the help and support.

UGC-DAE consortium – For various analyses

Salim Al Harthi, Oman – For XPS measurements.

IIT Mumbai – For TEM analysis.

Dr. R. Ramesh, School of Chemistry, Bharathidasan University, Trichy- For EPR measurements.

STIC CUSAT- For various analyses.

DRDO, UGC-BSR – For financial assistance.

Friends of Department of Applied Chemistry, Department of Physics and Photonics – For the love and support.

My dear labmates – For the help and affection.

My family members.

Mothi Krishna Mohan

Preface

Nowadays, many n-type semiconductors are studied and applied in several application fields, such as energy production, smart-materials technology, environment depollution, chemical synthesis, whereas p-type semiconductors are rarely used because of their limited presence in nature and their usually too small band-gap. Our material of interest is the physically and chemically superior TiO_2. The thesis reports the applications of the modified forms of TiO_2 in different fields.

Semiconductor photocatalysis attracted much attention during the last two three decades due to their low environmental impact. Among various semiconductors, titania paves more attention due to its non-toxicity, low cost, stability and better catalytic activity. But due to its large band gap, the spectral response is in the UV region which constitutes only 4-5% of the sun light. Band gap narrowing is an effective way to change the spectral response of TiO_2 to the visible region. Here we have used a co-doping technique for the modification of TiO_2 to transfer its spectral response. The prepared catalysts were successfully employed for the removal of some hazardous herbicides such as Atrazine and Metolachlor using visible region of the electromagnetic spectrum. These catalysts were also found to be very active in the photo-oxidation reactions. By using these catalysts, we have converted some antracene based polycyclic aromatic hydrocarbons to industrially and medically vital anthraquinone. The compounds were separated and purified by column chromatographic technique.

TiO_2 is thermally inactive in nature. But it can be act as a better support. Cu/Pd bimetallic supported on TiO_2 systems were prepared by Sol-Gel followed impregnation method and applied to synthetically important Suzuki coupling reaction. Various parameters such as effect of catalyst, effect of solvent and effect of base were evaluated.

Photovoltaic cells are the devices which convert solar energy to electrical energy by using photovoltaic effect of semiconductors. TiO_2 is the most commonly used semiconducting material in dye sensitized solar cells due to its low cost and high power conversion efficiency. A device which absorbs sun light with a layer of organic molecule and directly converts it to electric energy is known as organic solar cells. We have fabricated an inverted heterojunction device using TiO_2 as the n-type material and conjugated polymer MEH-PPV as the p-type material. Two fullerene derivatives such as ICBA and PCBM were introduced in order to improve the power conversion efficiency. Spin coating technique was adopted for the fabrication of the entire device.

Nonlinear optics deals with the variation of frequency, phase and other physical properties of the material due to the impact of an applied electric field. Nowadays almost all photonic technologies are based on nonlinear optics where photons are used for signal transmission and processing. Fabricated bare and noble metal modified thin films of TiO_2 by spray pyrolysis technique and well characterized. Third order nonlinear optical properties of these thin films were measured by Z-Scan technique. Here most of the materials showed saturable absorption (SA) behavior and some materials exhibited reverse saturable absorption (RSA). Both SA and RSA have got immense applications in electronic devices.

Contents

Chapter 1

Introduction and Literature Survey

Contents

The modern microelectronics applications are mainly based on semiconductor technologies. Moreover, building materials, health care products, materials for special applications and much more, often employ semiconductors. TiO_2 is a widely accepted superior semiconductor material for diverse applications due to its better physical and chemical properties. It is a sophisticated material to play a vital role in helping solve serious environmental and pollution challenges in a benign manner. It is also very useful to curtail energy crisis through effective utilization of solar energy based on photovolataic and water-splitting devices. This thesis deals with the modification of TiO_2 for various applications including photocatalysis, thermal reaction, photovoltaics and non-linear optics. General introduction of each topic is shown below.

1.1. Heterogeneous Photocatalysis

Nowadays environmental pollution has increased extensively due to industrial as well as manmade activities. Complete removal of the

pollutants for a clean, green and salubrious environment is the centre point of attraction in today's scientific world. Pollutants from various sources cause serious ecological problems as the biodegradation of these pollutants is slow and conventional methods adopted for their removal are ineffective and environmentally not compatible [1]. Increased use of chemicals and the presence of recalcitrant pollutants in environment forced the researchers to develop highly efficient methods for their removal. Photocatalysis by semiconductors are widely investigated advanced oxidation process (AOP), which can be considered as an effective and superior method than conventional methods employed for detoxification. Heterogeneous semiconductor photocatalysis has recently got immense significance due to its heavy application in environmental pollution control [2]. Generally, photocatalysis is the acceleration of a photoreaction in the presence of a catalyst. In heterogeneous photocatalysis, reactants and catalysts are in different phases and most of the photoinduced molecular transformations and reactions take place at the surface of the catalyst [3]. Photoexcitation of semiconductors suspended in different solvents or in gaseous mixtures facilitate redox reactions concurrently and this event accomplishes a selective oxidation or complete oxidative degradation of a weakly adsorbed molecule [4]. Photocatalysis can be divided into two kinds of processes depending on the mode of activation. They are 1) catalyzed photoreaction 2) sensitized photoreaction. In catalyzed photoreaction initial excitation occurs on the adsorbate molecule and catalyst itself can be firstly excited in sensitized mode of activation. Initial excitation followed by subsequent electron or energy transfer leads to chemical reactions in the heterogeneous photocatalytic process [3]. Suspended semiconductor photocatalysts are stable to photolysis conditions and are able

to carry out a large number of oxidative conversions per active site without the loss of semiconductor's redox capacity so that these redox reactions are considered under heterogeneous photocatalysis [4,5]. Without photocatalyst, light alone cannot initiate any kind of photoreactions. Now semiconductor based photocatalysis have got much attention due to its benign nature. Compared to p-type semiconductors n-type materials are widely applicable in various fields such as energy production, smart-materials technology, environment depollution, chemical synthesis etc. Organic transformations by semiconductor mediated photocatalysis is another area of interest [4,6]. The reactions accomplished through heterogeneous photocatalysis include oxidations, oxidative cleavages, reductions, substitutions etc.

1.1.1. TiO_2- Superior Semiconductor Photocatalyst

Semiconductor mediated photocatalysis now emerged as a hot topic due to its diverse applications. Semiconductors are applicable in modern microelectronics, building materials, health care products, materials for special applications and much more due to their chemical and physical properties. It can catalyze a variety of chemical reactions including oxidation, reduction, C-H bond activation and C-C bond forming reactions. Pristine semiconductors are intrinsic and doped semiconductors are known as extrinsic. Extrinsic semiconductors with larger electron concentration are known as n-type and those with larger hole concentration are known as p-type. The catalytic properties of semiconductors are related to the electronic structure and processes occurring inside and on the surface of them. Semiconductors are the materials whose conductivity lies between metals and insulators and are known to be good photocatalysts. Generally a photocatalytic reaction starts with the generation of excitons upon band gap

irradiation. In metals, due to the continuum of electronic states either oxidation or reduction can be feasible. But a semiconductor is characterized by the absence of continuum of states. An energetically closely spaced array of orbitals composed by the valence electrons of the material is called valance band and higher energetic spaced array formed by the unoccupied orbitals is called conduction band. The void region between the top of the filled valance band and the bottom of the vacant conduction band is called band gap (Fig.1.1). Due to the large band gap, insulators require high energy for electronic excitation. If the semiconductor remains intact and charge transfer takes place to the adsorbed species continuously and exothermically, the process is termed as heterogeneous photocatalysis [3].

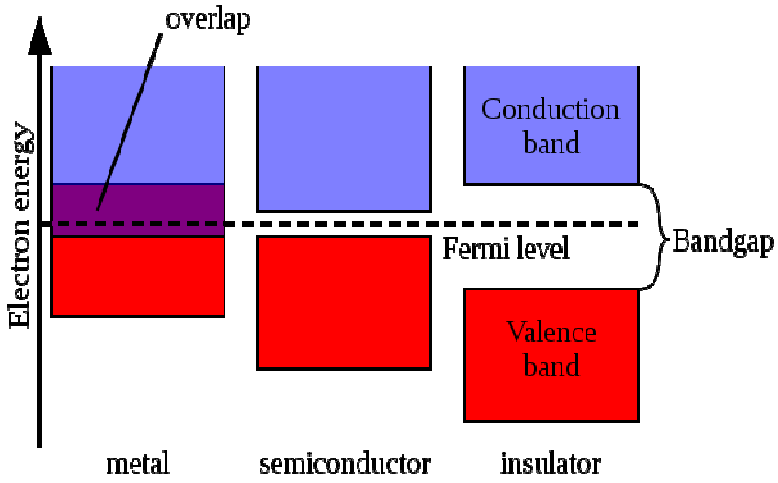

Fig.1.1. Band structure of metal, semiconductor and insulator

A suitable semiconductor photocatalyst has to satisfy some requirements. It should be chemically inert, environmentally benign, non-photocorrosive, cost effective, having high surface area, broad absorption spectra with high absorption coefficient and must be capable of extended use

without substantial loss of photoactivity. A lot of semiconductors having different band gap and electronic structure are available and some of them are shown in Fig.1.2. Among various semiconductors, TiO_2 has got much attention due to its superior physical and chemical properties. But relatively high cost of photocatalytically active anatase was found to be uneconomical for large scale water treatment operations. Photocatalytic removal of pollutants from the environment can be performed using other semiconductors having narrower band gap which are strongly sensitive towards visible region of electromagnetic spectrum. The narrower band gap of metal calcogenides such as CdS, ZnO and CdSe make these materials to undergo photo-corrosion process although they are very active in visible region. Due to similar band gap, photocatalytic activity of TiO_2 and ZnO are somewhat comparable. But structural instability due to photo-corrosion under UV light decreases the photocatalytic efficiency of ZnO in aqueous solution. TiO_2 is the only material which perfectly satisfies the features of an ideal semiconductor photocatalyst and has been used extensively.

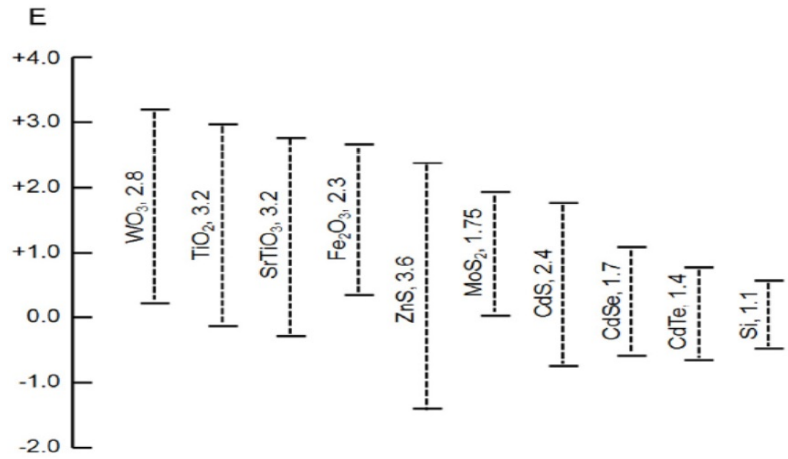

Fig. 1.2. Band gap of various Semiconductors

The photocatalytic activity of a semiconductor is mainly controlled by a) the light absorption properties, e.g., light absorption spectrum and coefficient b) reduction and oxidation rates on the surface by the electron and hole c) rate of electron-hole recombination [7]. Two major events of heterogeneous photocatalysis are 1) Generation of electron-hole pair 2) Adsorption of the target molecule on the surface. Larger surface area with constant density of adsorbates increases the rate of photocatalytic reaction. But if the surface is a defective site, it results in a faster recombination thereby decreases the photocatalytic activity. Higher temperature treatments improve the crystalline nature of the material that reduces the bulk defects which in turn positively influence the photocatalytic activity. Photocatalysis is a complex process which depends not only on one factor but on several factors such as crystallinity, surface area, density of adsorbates, pH, surface morphology etc. So the direct correlation of physical properties with the photocatalytic activity is a quite arduous process. The efficiency of a photocatalytic reaction can be expressed in terms of quantum yield. In heterogeneous systems actual light absorbed is very difficult to determine due to the scattering of light by semiconductor surface. In these systems efficiency is quoted as an apparent quantum yield. For an ideal system, quantum yield is given by a simple equation which is shown below

$$\Phi \alpha \frac{k_{CT}}{k_{CT} + k_R} \text{ ---------- (1.1)}$$

Where k_{CT} is the rate of charge transfer and k_R is the rate of recombination. Modifications of semiconductor surfaces are very helpful to improve the quantum yield of a photocatalytic process.

After the discovery of Fujishima and Honda, enormous work has been done on TiO_2 in order to explore its potential in various fields. Why TiO_2 can be considered as the king of photocatalysts? The answer is as follows; TiO_2, a cost effective, non-photo corrosive, highly efficient, bio-compatible and environmentally benign material having high redox capacity is the most widely investigated photocatalyst [8] due to its heavy application in the decomposition of pollutants in both gaseous and liquid phases [9-13].

1.1.2. General Mechanism of Semiconductor Photocatalysis

Irradiation of a solid semiconductor with light of the appropriate wavelength is the basis of photocatalysis [13]. Photo illumination of metal oxide semiconductor with energy exceeding their band gap generates mobile charge carriers (electrons and holes) within the particle [14]. The photon absorption induces a charge separation and also is responsible to produce a highly energetic electron and a lower-energy vacancy in the conduction and valance band respectively (Fig.1.3). The intermediate species thus formed is called electron-hole pair. Immediately after the formation, majority of charge carriers of the semiconductor undergo non-radiative electron-hole pair recombination. Rest of the charge carriers become trapped within band gap states characterized as hole traps, shallow electron traps and deep electron traps [14]. In the excited state, back electron transfer to hole to initiate electron-hole recombination is thermodynamically feasible. But due to the absence of some states in the band gap, back electron transfer is restricted which results in the trapping of charge carriers. Trapping of charge carriers into the gap states is a diffusion limited process [15-18]. Electrons generated in the semiconductor are

trapped at surface site within 30 ps and on the other hand valance band hole requires 250 ns. An adsorbed species having appropriate redox potential can sometimes trap one of the charge carriers faster than electron-hole recombination so that beautiful photoinduced chemistry will be observed on the surface Fig.1.4.

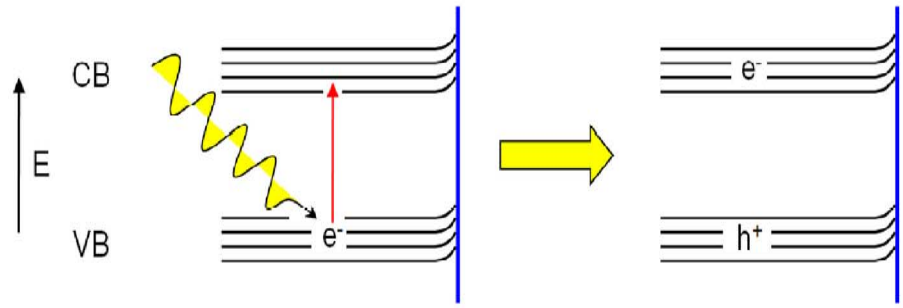

Fig.1.3. Generation of excitons in a semiconductor

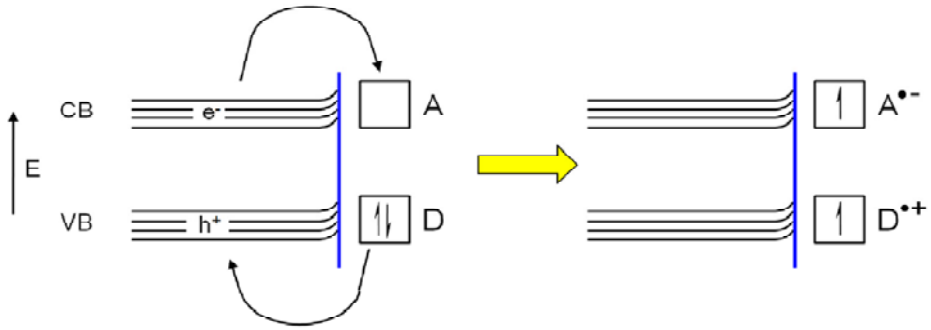

Fig. 1.4. Interfacial electron transfer on Semiconductor Interface

That is, there is a competition between recombination and charge carrier trapping. At very low concentration of charge carriers, the recombination follows first order kinetics [14]. In photocatalysis, only a fraction of the charge carriers reach the surface of the semiconductor nanoparticle to react with adsorbed donor and acceptor molecules.

Upon band gap excitation, the intermediate species 'electron-hole' pair is formed. Some surface defects and suitable scavengers of charge carriers play an important role to improve the redox reactions by decreasing the intensity of electron-hole recombination. Valence band holes are powerful oxidants while the conduction band electrons are powerful reductants. Oxidation power of the holes either directly or indirectly influences the photodegradation process while conduction band electrons are also responsible to produce some reactive oxygen species necessary for degradation. If an acceptor molecule is present at the surface, then the semiconductor donates electrons to this species to reduce it, in turn a hole migrate to the surface and receives an electron from the donor species to facilitate its oxidation. On the other hand if the molecules are not preadsorbed on the surface, then the excited electron may combine with molecular oxygen to form superoxide anion ($O_2^{-\cdot}$). Holes from the valance band migrate to the surface and scavenge H_2O and surface hydroxyl groups to generate hydroxyl radical ($OH^{\cdot}$) which strongly oxidize the adsorbed pollutant molecule [2]. Ultimately in semiconductor photocatalysis, generated elctrons, holes, reactive oxygen species including hydroxyl radical ($OH^{\cdot}$), super oxide anion ($O_2^{-\cdot}$) and singlet oxygen may take part in redox reactions [19]. The overall redox reaction pathway is shown in Fig.1.5 and the possible degradation mechanistic pathways of pollutants may be represented by the following equations.

$$TiO_2 \xrightarrow{h\nu} h^+_{vb} + e^-_{cb} \quad \text{----------} \quad (1.2)$$

$$h^+_{vb} + OH^- \longrightarrow OH^{\bullet} \quad \text{----------} \quad (1.3)$$

$$O_2 + e^-_{cb} \longrightarrow O_2^{\bullet -} \text{ ---------- (1.4)}$$

$$\text{Pollutant} \xrightarrow{h\nu} \text{Pollutant}^{\bullet} \text{ ---------- (1.5)}$$

$$\text{Pollutant} + TiO_2 \longrightarrow \text{Pollutant}^{\bullet +} + TiO_2\,(e) \text{ ---------- (1.6)}$$

$$\text{Pollutant}^{\bullet +} + O_2^{\bullet -} \text{ or } (OH^{\bullet}) \longrightarrow \text{Intermediates} \rightarrow CO_2 + H_2O \text{ -- (1.7)}$$

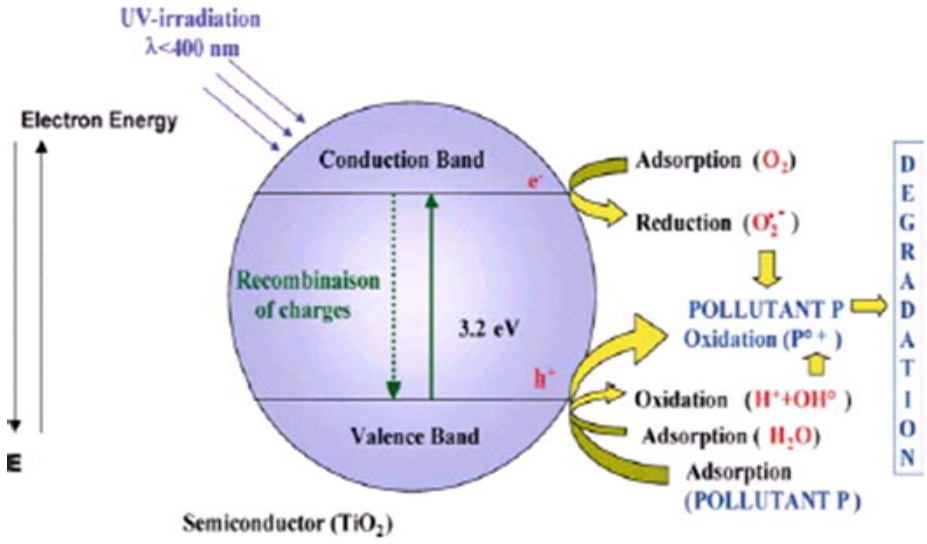

Fig.1.5. General mechanism of photodegradation

1.1.3. Structure of TiO_2

TiO_2 can exist in variety of forms such as anatase, rutile, brookite, α- PbO_2 type, high pressure monoclinic type etc. Photocatalytic activities of amorphous forms are poor due to structural defects. TiO_2 exists in three crystalline habits; anatase, rutile and brookite [20] (Fig.1.6), among which anatase and rutile can be considered as the principal catalytic forms. The

application of brookite is less in the area of photocatalysis because synthesis of pure brookite without anatase and rutile is a difficult process.

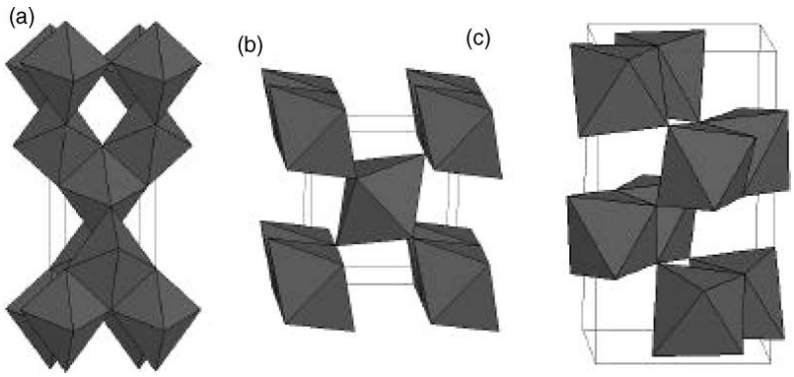

Fig.1.6. Structures of a) anatase b) rutile c) brookite.

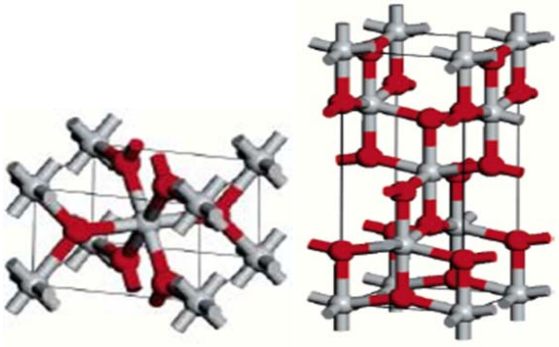

Fig. 1.7. The unit cell structure of anatase and rutile [21-23]

Among the crystalline forms, anatase and rutile belong to tetragonal while brookite belongs to orthorhombic crystal system. Anatase and rutile structures are characterized by chains of TiO_6^{2-} octahedral units. Both structures differ by the distortion and assembly patterns of octahedral chains. Here each Ti^{4+} ion is surrounded by an octahedron of six O^{2-} ions. The irregular octahedron in rutile gives rise to a slight orthorhombic distortion. But in anatase, the symmetry is lower than orthorhombic due to the significant distortion of octahedron. Anatase shows greater Ti-Ti

distances and shorter Ti-O distances than rutile [22]. In anatase, each octahedron is in contact with eight neighbors and the octahedron of rutile is in contact with 10 neighboring octahedral units. These differences cause different mass densities and electronic band structures between the two forms of TiO_2.

Anatase is a metastable phase while rutile can be considered as the thermodynamically more stable phase. Phase transformation of amorphous TiO_2 to anatase takes place around 400°C which is further converted to rutile at a temperature greater than 600°C. The stability and phase transformation of TiO_2 depends on various factors such as particle size, preparation method, morphology etc. According to Hwu et al. crystal structure of TiO_2 nanoparticles depends mainly on the preparation method [24]. Banfield et al. found that the prepared TiO_2 nanoparticles consist of anatase and/or brookite structures which is transformed to rutile after reaching certain particle size [25,26].

The particle size of commercially available anatase is less than 50 nm having a band gap of 3.2 eV corresponding UV wavelength of around 388 nm. But thermodynamically more stable rutile exists as particles larger than 200 nm. Normally anatase can be considered as the photocatalytically more active phase. Lower rates of recombination and higher surface adsorptive capacity make anatase a good candidate for photocatalysis. The phase formation temperature of rutile was found to be greater than 600°C. This high temperature results in aggregation of particles thereby reducing the surface area. The reduction in surface area has a negative impact on photocatalysis.

1.1.4. Limitations and Necessity of modification

Extensive work on TiO_2 has been started after the photodecomposition of water on titania surface by Fujishima and Honda in 1972. This event marked as a new era in heterogeneous photocatalysis. Now TiO_2 is successfully applied in various fields which include photocatalysis, photovoltaic, hydrogen generation via water splitting, antifogging and self-cleaning, photoinduced organic transformations, photo-/electrochromics and sensors.

Even though TiO_2 is known to be a good photocatalyst, it possesses some disadvantages. The major drawbacks of pure TiO_2 are

1) Faster electron-hole recombination
2) Activity is limited in the UV region due to its wide band gap (Anatase, 3.2 eV)

Recombination of charge carriers can be possible in a number of ways. Recombination process reduces the concentration of charge carriers generated upon irradiation with a photon. No methods adopted for the synthesis of any material is perfect in nature. Sometimes surface and bulk irregularities may be produced and these irregularities can act as the site for electron-hole recombination. On the other hand, the defect states or irregularities present on the surface can facilitate the trapping of charge carriers thereby curtail the recombination of charge carriers. Use of electron or hole scavenger is another method to reduce the recombination. The adsorbed molecular oxygen on the surface readily accepts an electron to generate superoxide anion which is detected by IR and EPR measurements [27-29]. The commonly used scavenger molecules for holes are propanol [30], ethanol [31], glycerol [32] and surface hydroxyl groups [33].

Various modifications employed to change the spectral response of TiO_2 are 1) Coupling with other semicondcutors having lower band gap 2) dye sensitization 3) doping with metals and 4) doping with non-metals.

Generation of photocurrent with energy less than the semiconductor band gap is known as sensitization and the light absorbing materials are generally regarded as sensitizers [34,35]. Materials with narrower band gap or those having light response in the visible or infrared region can be used as sensitizers for TiO_2 materials. The interaction of sensitized TiO_2 with light depends mainly on how efficiently the sensitizer interacts with the light. Effective charge transfer from the sensitizer to TiO_2 and the resulting charge separation are the major events of photosensitization of TiO_2. Compatible electronic structures of sensitizer and TiO_2 are very necessary to avoid the charge carrier trapping and recombination which adversely affects the performance of the sensitized system [34-36]. Sensitization can be broadly divided into two depending on the nature of the sensitizers. They are 1) Inorganic sensitization using some low band gap semiconductors 2) Organic sensitization using some dyes.

Optical absorption and charge separation properties of TiO_2 can be improved by sensitization with a narrow band gap semiconductor material. Hole produced in the narrow gap semiconductor material during excitation remains in the material while the electron is transferred to the conduction band of TiO_2 particles (Fig. 1.8). This process improves the charge separation as well as photocatalytic efficiency. The electrons and holes are then free to react with the adsorbents on the surface of the material [3]. Modification of nanocrystalline TiO_2 matrix by PbS nanoparticles results in a strong photoconductance in the visible region [37].

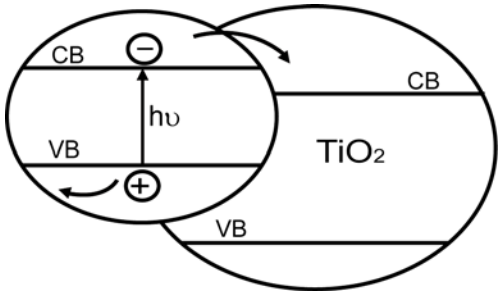

Fig 1.8. Inorganic Sensitization of TiO_2 Material

Sant and Kamat proposed that in CdS-TiO_2 semiconductor system electron transfer from the photoexcited CdS to TiO_2 depends on the size of the TiO_2 nanoparticle [38]. In CdSe-sensitized TiO_2 nanostructure electrode, photoelectrochemical currents in the visible region depend on the structure and electron diffusion coefficient of TiO_2 electrode [39]. So the photocatalytic efficiency of coupled semiconductor material depends on different factors. Organic dyes are another class of compounds used as sensitizers for TiO_2 nanomaterials inorder to improve its optical properties [40-43]. Metal centers of organic dyes generally include Ru(II), Zn(II), Mg(II), Fe(II), and Al(III), while the ligands are nitrogen heterocyclics with delocalized π or aromatic ring systems. The dyes are linked to TiO_2 nanoparticle surface via functional groups through various interactions such as a) covalent attachment by directly linking groups of interest or via linking agents (b) electrostatic interactions via ion exchange, ion-pairing, or donor-acceptor interactions (c) hydrogen bonding and (d) van der Waals forces [7]. On the other hand some functional groups are also responsible to form some stable linkages with surface hydroxyl groups on TiO_2 substrate [44]. The most successful functional groups are based on carboxylic acids which react with the surface titanol groups dehydratively to form ester linkages [45].

That is, sensitization of a wide band gap semiconductor with a dye which is chemisorbed or physisorbed on the surface increases the overall efficiency of the excitation process by expanding the wavelength response of the photocatalyst through excitation followed by charge transfer to the semiconductor material [46].

The optical properties of any material largely depend on its electronic structure. Doping process can alter the chemical composition of the TiO_2 material. Among various materials, metals and non-metals are found to be effective candidates for doping. Substitution of Ti^{4+} cation in TiO_2 with other transition metals are easier than the replacement of O^{2-} anion with other anions due to the difference in potential and ionic radii. The mechanism of photocatalysis by pure TiO_2, metal doped TiO_2 and non-metal doped TiO_2 are shown in Fig.1.9.

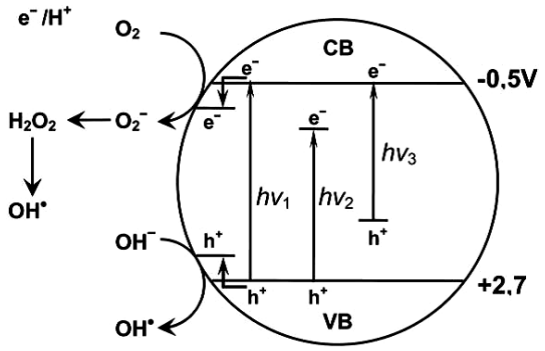

Fig. 1.9. Mechanism of Photocatalysis by Pure and Doped TiO_2 System

In metal doped titania, a new energy level produced in the band gap of TiO_2 due to the dispersion of metal nanoparticles is responsible for the improved visible light activity and it can also tune the redox potential of the photo excited species [47]. In metal doped TiO_2, electrons can be excited

from the defect state to the TiO_2 conduction band by photon of energy equal to $h\nu_2$ as shown in Fig. 1.9. If the doped metal is having a work function greater than the semiconductor material, it can act as the trap for electrons thereby reducing the electron hole recombination (Fig.1.10). Decrease of carrier recombination results in an enhanced photocatalytic activity.

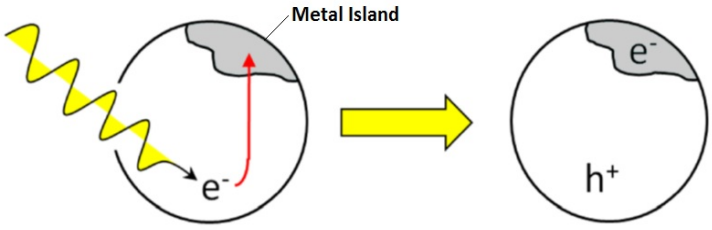

Fig. 1.10. Metalized Semiconductor Particle

A lot of reports are available in the literature regarding the positive and negative effects of TiO_2 modified with various metal ions such as Cu, Co, Ni, Cr, Mn, Mo, Nb, V, Fe, Ru, Au, Ag, Pt etc. [48,49]. The main disadvantage of metal doped TiO_2 is the instability of doped metal against photo corrosion and sometimes the doped metal centre can act as an electron-hole recombination site.

TiO_2 doped with some non-metals such as C, N, S, halogens etc. are called third generation photocatalysts. Nowadays, they have got better attention due to their high activity in the visible region. Sato et al. is the first group reported the N doped TiO_2 in 1986 [50]. Successful photocatalytic activity of N-TiO_2 compelled the researchers to concentrate on other non-metals such as S [51,52], B[53,54], P[55,56] etc. Asashi et al. [57] reported the high visible light response of N-TiO_2 due to band gap narrowing caused by the mixing of N2p state with O2p states. Substitution of oxygen sites by

nitrogen atoms form some isolated impurity energy level above the valance band makes it compatible for visible light absorption [58] (Fig.1.11).

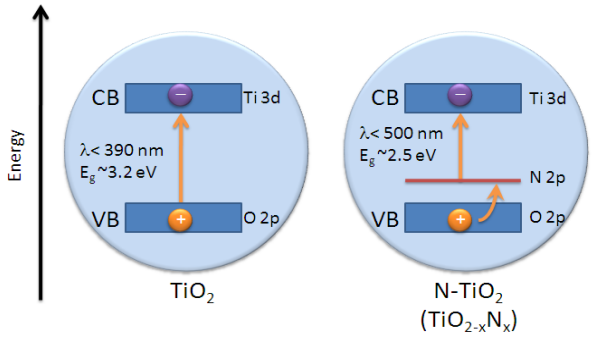

Fig.1.11. TiO_2 doped with non-metals

Another thing that improves the visible light response of N-TiO_2 is the presence of oxygen deficient sites and nitrogen doping in the oxygen vacancies prevents the reoxidation process [59].

1.2. Semiconductor Mediated Organic Transformations

TiO_2 photochemistry has been extensively investigated as a method for the catalytic conversion of organic compounds [60]. Irradiated semiconductor catalysis in the presence of molecular oxygen can be admitted as an innovative and economical process for the conversion of harmful aromatics to less harmful products. Generally, organic synthesis requires a tedious synthetic procedure, use of expensive and toxic chemicals which are harmful to the environment. Electronically excited states of irradiated photocatalyst induce electron or energy transfer reactions used to design specified chemical reactions. Apart from thermal reactions, it needs milder reaction conditions and also we can curtail undesirable side reactions. Light and molecular oxygen can be considered as two reagents in oxidative semiconductor catalysis. Molecular oxygen

can be considered as oxidizing agent although its role is not known unambiguously [4]. But oxygen acts as the source of highly reactive intermediates which are the engine of photocatalyzed reaction. Reaction sequence and the role of molecular oxygen for the oxidation of an organic compound are shown below.

$$TiO_2 \xrightarrow{h\nu} (e^-/h^+) \text{ ----------} (1.8)$$

$$O_2 + e^- \longrightarrow O_2^{\bullet -} \text{ ----------} (1.9)$$

$$2O_2^{\bullet -} + H_2O \longrightarrow H_2O_2 + 2OH^{\bullet} + O_2 \text{ ----------} (1.10)$$

$$H_2O_2 + e^- \longrightarrow {\bullet}OH + OH^- \text{ ----------} (1.11)$$

$$RH_2 + h^+ \longrightarrow {\bullet}RH + H^+ \text{ ----------} (1.12)$$

$$(OH^-)_S + h^+ \longrightarrow ({\bullet}OH)_S \text{ ----------} (1.13)$$

$${\bullet}RH + O_2 \longrightarrow HROO{\bullet} \text{ ----------} (1.14)$$

$$HROO{\bullet} + RH_2 \longrightarrow {\bullet}RH + HROOH \text{ ----------} (1.15)$$

$$HROO{\bullet} + e^- \longrightarrow RO + OH^- \text{ ----------} (1.16)$$

$${\bullet}RH + O_2^{\bullet -} \longrightarrow RO + OH^- \text{ ----------} (1.17)$$

$${\bullet}RH + HOO{\bullet} \longrightarrow RO{\bullet} + H_2O \text{ ----------} (1.18)$$

$$HROO{\bullet} + HOO{\bullet} \longrightarrow HROOH + O_2 \text{ ----------} (1.19)$$

Oxo functionalization of hydrocarbons with environmentally benign and cheap reagent represents a major target from the synthetic and industrial points of view. As per thermodynamic results, most of the organic compounds are least stable to oxidation by O_2. But differences in the spin multiplicities of ground state oxygen and excited state organic

compound show some kinetic limitations towards the feasibility of reaction. Efficiency and selectivity towards a particular product in semiconductor mediated reactions depend mainly on the physical and chemical properties of the photocatalytic system such as light absorption, generation of redox intermediates, the rate of competitive chemical steps, the adsorption-desorption equilibria of substrates etc.

Functional group transformations of organic compounds by semiconductor mediated photocatalysis have been reported by several groups [6]. Generally photo-oxidation means the oxidation reactions induced by light. The main advantage of semiconductor mediated reactions is the high chemical yields of the products and sometimes with quantum yields of few percent less [61]. Photogenerated electrons and holes play an important role in photoinduced oxidation reactions through the formation of some reactive oxygen species. Some research groups revealed that oxidative reaction on TiO_2 nanoparticles in solution state occur via photogenerated hole [62-64] which shows some opposition against hydroxyl radicals as suggested in other studies [65]. Generally, species generated during irradiation of TiO_2 film in liquids are trapped holes, trapped electrons and free electrons [66]. There were so many reports on photo-oxidation of organic compounds by doped titania systems. Some researchers demonstrated the high activity of carbon doped TiO_2 for the photocatalytic oxidation of compounds such as 2-propanol [67,68], salicylic acid [69], formic acid [70] etc. under visible light irradiation. Kisch et al. also reported the high activity of C-TiO_2 for the photodegradation of 4-chlorophenol under visible light. The mechanism of photo-oxidation of organic compounds has been studied mainly in non-metal

doped titania systems [71-76]. Direct and indirect paths have been proposed in the case of non-metal doped titania. In direct path, holes generated in the valance band directly interact with the organic compound while in indirect path the reaction is favored by the interaction of compound with radical intermediates on the surface which are formed either by the reaction of dissolved oxygen with conduction band electrons or by the interaction of surface hydroxyl groups with holes. But these methods are not sufficient to determine the exact mechanism behind the oxidation of compounds of interest. Apart from doping, grafting of metal complexes or cations on TiO_2 surface enhances the visible light absorption thereby carry out organic transformations using renewable energy sources [77,78]. Visible light activity is not the only scope of surface modification and in fact it changes the interfacial reactivity of substrates [79]. Also surface functionalization sometimes improves the selectivity towards a particular product. So the research is more concentrated in the field of electrocatalysis with modified electrodes [80]. That is, surface functionalization is very useful to tune the surface to introduce some new surface sites which improves the selectivity towards a particular product [81]. Majima et al. reported the one electron oxidation of several aromatic compounds on TiO_2 surface in CH_3CN using nanosecond time resolved diffuse reflectance spectroscopy and observed that OH groups play an important role in the adsorption and the efficiency of the one-electron oxidation of the substrates [82-85]. Various reactive oxygen species or the as generated charge carriers either directly or indirectly influence the semiconductor mediated organic transformations. But the exact mechanism and the involvement of radical intermediates and the charge carriers are not known obviously yet.

1.3. Thermal Reactions Based on TiO_2

TiO_2, like other solid acid catalysts such as clays and alumina cannot effectively favor thermal reactions. Acidic/basic properties and oxidation/reduction properties associated with the surface sites present on TiO_2 are not so prominent. But on the other hand it can act as a better support. Higher surface area, better dispersion of active component, strong metal support interactions (SMSI), high thermal and mechanical stability are the key requirements for a good support. Presence of acidic, basic, redox sites, ionic conductivity, strong metal support interactions and chemical inertness makes titania a good catalyst or catalytic support. Processes like vacuum annealing, Ar^+sputtering or chemical reduction using H_2 or CO are responsible to produce coordinatively unsaturated Ti cations [86-89]. Defect sites produced on the surface of TiO_2 exhibit oxidation-reduction properties along with acid-base properties and also these defects facilitate the adsorption of oxygen containing organic molecules which commonly undergo dehydration, dehydrogenation and self-disproportionation reactions. There are so many reports on the deoxygenation of alcohols [90,91], carboxylic acids [92], ketones [93] on reduced TiO_2(100) and TiO_2 powder surfaces. Generally, metal oxides have the ability to exchange electrons, protons or oxide ions which can carry out redox as well as acid–base catalysis [94]. Metals dispersed on various supports can be applicable in various thermal reactions. Transition metals supported on zeolite or oxide catalysts are good candidates to carry out the hydrogenation of acetophenone in liquid phase at low hydrogen pressure [95-100]. Titania catalysts are very effective in photo-oxidation, reduction and decomposition reactions. Group 8-10 metals dispersed on TiO_2 enhances the selectivity towards a particular

product in some reactions [101]. Oxide supports containing a reducible metal ion such as Ti^{4+} possesses strong metal support interaction (SMSI) and they also act as a promoter in CO hydrogenation through SMSI. Bartholomew et al. reported the raft-like structures of Ni/TiO_2 due to strong interactions of metal and the support [102]. Chen et al. observed the effect of cacination and reduction temperatures on Ni/TiO_2 in the hydrogenation of chloronitrobenzene [103]. The supported bimetallic catalysts have been proven to be good candidates for catalytic applications than monometallic catalytic systems. Wildschut et al. used Ru catalysts on various supports (C, Al_2O_3, TiO_2) for the hydrotreatment of fast pyrolysis oil at 350°C for 4h [104]. But Ni-Cu supported on TiO_2 showed better performance for the catalytic hydrotreatment of fast pyrolysis oil which is a combined measure of catalytic activity and stability [105]. Hydrogenation of cinnamaldehyde, an industrially important intermediate for pharmaceuticals can be carried out in a number of ways. But depending on the nature of the metals and supports, the selectivity towards the products is found to be different. Certain catalysts such as Ru[106], Pd[107,108], Au[109] etc. are responsible for the selective hydrogenation of cinnamaldehyde to hydrocinnamaldehyde.

Bimetallic Ir-Ni on TiO_2 was found to be effective for the hydrogenation at mild reaction conditions. The strong interaction between Ir and Ni and the better dispersion of Ir on Ni in $Ir\text{-}Ni/TiO_2$ are the main reasons for enhanced activity [110]. Venzia et al. firstly used Au catalyst in the hydrodesulphurization of thiophene and investigated Au-Pd bimetallic catalysts on various supports [111,112]. Catalytic supports played an important role in enhancing the performance of Au catalyst for hydrodesulphurization of thiophene. Carbon, simple oxides like TiO_2, binary

oxides and acidic materials are the commonly used supports. The main drawback of TiO_2 support is the lower surface area and thermal stability compared to other supports that makes it unsuitable for industrial applications [113]. But a heterogeneous mixture of two oxides possesses higher specific surface area that in turn positively influences some catalytic conversions [114]. For example Au/Pd supported on TiO_2/Al_2O_3 calcined at 773K showed higher catalytic activity in the hydrodesulphurization of thiophene compared to other systems due to stronger interaction between Au-Pd and TiO_2/Al_2O_3 support, larger dispersion, more acidic sites and low apparent activation energy [115]. Gao et al. reported the efficient reduction of nitrate in drinking water using Cu-Pd/TiO_2 system [116]. That is, the addition or presence of second metal has a lot of advantages compared to a monometallic system. It can improve the selectivity towards a particular product; alter the rate of the reaction and also decrease the deactivation rate.

Suzuki cross coupling is an effective method for making new C-C bonds, which have got immense importance in the field of organic chemistry. Pd(0) complexes catalyzed Suzuki coupling reaction is one of the most useful coupling reactions between aryl or vinyl boronic acid with aryl or vinyl halides to give new C-C bond [117-119]. Generally, these kinds of reactions are carried out at a temperature range of 60-80°C which results the products in excellent yields. Most of the coupling reactions are done in homogeneous way. The main drawbacks of traditional Suzuki cross coupling reactions are catalyst decomposition, poor regeneration and poor reagent solubility. In order to overcome these difficulties, researchers are now concentrating to carry out the coupling reactions in heterogeneous way. Polar aprotic solvents are normally employed for Suzuki cross coupling reactions

in the presence of Pd(0) or Pd(II) catalysts which are soluble in these solvents. The most commonly used base in Suzuki cross coupling is Na_2CO_3 which is ineffective towards some sterically demanding substrates. Apart from thermal reactions, some research groups proved the feasibility of C-C bond forming reaction photochemically. A heterogeneous UV-visible light irradiated Heck reaction of various aryl iodides with olefins over $PdCl_2/TiO_2$ as a catalyst was carried out at ambient reaction conditions [120]. Three major processes involved in Suzuki coupling reactions are 1) Oxidative addition 2) transmetalation and 3) reductive elimination. The general scheme of Suzuki coupling reaction is shown in Fig. 1.12.

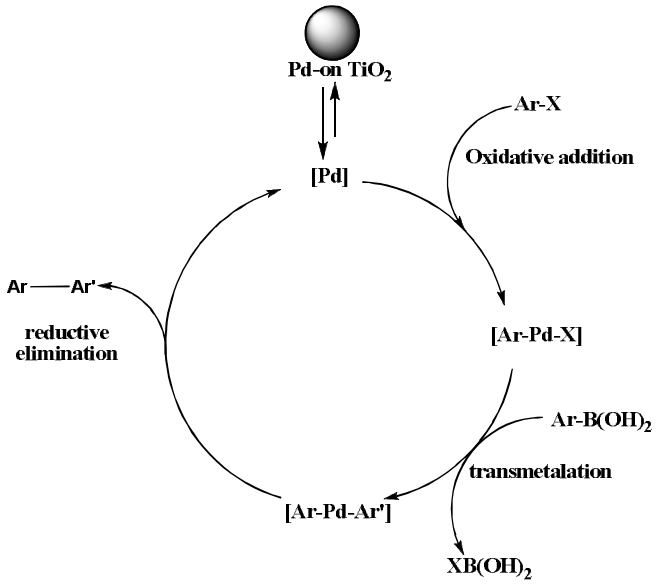

Fig.1.12. Various Steps Involved in Suzuki Coupling Reaction

1.4. Photovoltaic Application of TiO_2

The whole world is nowadays suffering from global warming because of using fossil fuels such as coal and oil. Now the studies are more concentrated to produce clean, sustainable and low-cost energy

due to the scarcity of fossil fuel resources. For this purpose, solar cells which convert solar energy to usable energy have become the centre of attraction. Generally, solar cells or photovoltaic cells are the devices which convert solar energy to electrical energy by using photovoltaic effect of semiconductors. Different varieties of solar cells have been developed to obtain good power conversion efficiency. All of them have got their own advantages and disadvantages. Different kinds of organic and inorganic materials are responsible for the fabrication of solar cells. Power conversion efficiency depends on the materials used for the fabrication. Conducting polymers, dyes, pigments and liquid crystals are the organic compounds normally used in a solar cell. Compatible band gap, easy reproducibility, good power conversion efficiency, high absorption coefficient and good stability are the major characteristics of a solar cell material. Lack of chemical stability is the biggest problem in all kinds of solar cells. Different types of modifications are adopted nowadays for improving the chemical stability and power conversion efficiency of solar cells.

Dye sensitized solar cell (DSSC) is a device that generates electric power from light without undergoing any permanent chemical transformation. DSSCs can be considered as the new technology in the category of solar cells. It was invented in 1991 by Gratzel. DSSCs have got immense importance due to their easy processing and low cost of production. TiO_2 is the most commonly used semiconducting material in dye sensitized solar cells due to its low cost and high power conversion efficiency [121-126]. In almost all the DSSC systems, central part is nanocrystalline TiO_2 semiconducting material with a

monolayer of charge transfer dye attached to its surface. Here the photoexcited dye releases an electron into the conduction band of TiO_2. This process continues and the continuous circulation of electrons creates electric power. The initial state of the dye is restored by electron donation from the electrolyte which is usually an organic compound containing a redox system. The latest reported efficiency of DSSCs based on nanoparticulate TiO_2 is 11.2% [127]. Loss in the nanoparticulate DSSCs are found to be large due to high charge recombination and long carrier diffusion paths through the TiO_2 nanoparticle network [128]. Highly ordered vertically oriented TiO_2 nanotube arrays provide higher internal surface area but reduces the carrier recombination probabilities compared to TiO_2 nanoparticles [129,130]. Graphene has got considerable interest for application in photovoltaic devices due to its superior physical and chemical properties [131]. Wang et al. reported the electrophoretic deposition (EPD) of reduced graphene oxide nanosheets onto TiO_2 nanotube array for application as photoelectrode in DSSCs [132]. Structure of a dye sensitized solar cell is shown in Fig. 1.13.

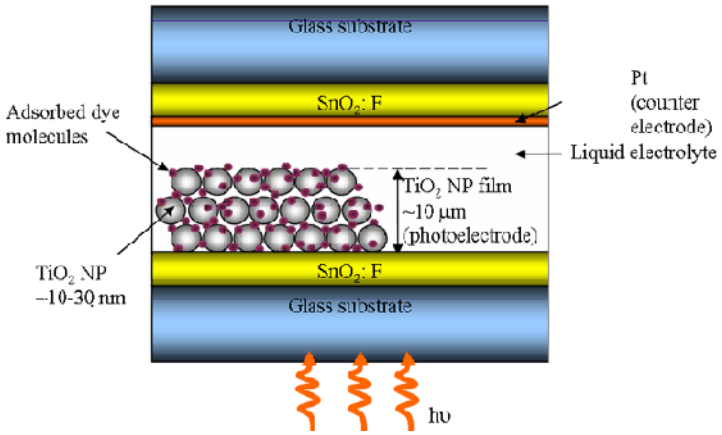

Fig. 1.13. Pictorial representation of a Dye Sensitized Solar Cell

A device which absorbs sun light with a layer of organic molecule and directly converts it to electric energy is known as organic solar cells. Recently most of the inorganic based solar cells are replaced by organic solar cells. Photovoltaic effect was recognized in 1839 by Becquerel. He observed a light induced voltage when shined light on AgCl electrode in an electrolyte solution [133]. The commonly used solar cells are based on Si. In 1954, Bell Laboratories reported an efficiency of about 6% for a Si based solar cell [134]. High fabrication cost and low power conversion efficiencies limited their popularization. So it became very important to find an alternative for these kinds of solar cells. The first organic thin film solar cell with a power conversion efficiency of about 1.2% was reported by Tang in 1986 [135]. The major advantages of organic solar cells over conventional solar cells are

1) Various synthetic strategies are available for the production of organic materials
2) Broad absorption spectra, suitable energy levels and self - organization abilities make organic materials as suitable candidates for photovoltaic applications.
3) Solubility of organic compounds is high in common organic solvents. So they can be processed easily by low-cost technologies such as drop-casting, spin coating, dip coating etc.
4) Solar cells based on organic materials are structurally flexible and these are applicable on large surfaces.

1.4.1. Operating Principle of Organic Solar Cell

Basic requirement for the efficient working of a solar cell is the formation of a p-n junction through the interaction of a donor and an

acceptor species. First step is the generation of electron-hole pair by the absorption of a photon of energy equal to greater than the band gap energy. In the second step, these excitons migrate towards the donor-acceptor interface where they get dissociated into free charges. Final step is the generation of photocurrent and photovoltage due to the movement of free charges towards respective electrodes with the aid of an internal electric field [136]. Schematic representation of the working of a solar cell is shown in Fig. 1.14.

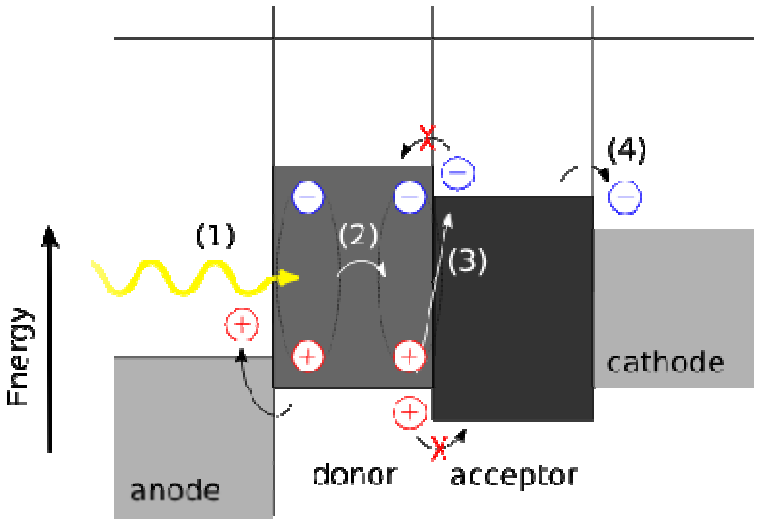

Fig. 1.14. Working principle of an organic solar cell. (1) Generation of excitons by photoabsorption (2) Diffusion of the excitons to the donor-acceptor heterojunction (3) Separation of the excitons into free charge carriers (4) Extraction to the electrical contacts.

1.4.2. Characterization of a Heterojunction

The I-V characteristics of a solar cell in dark and under illumination are shown in Fig. 1.15. Here no current flow was observed in the dark but under irradiation the device generates power. At maximum power point (MPP), the product of current and voltage is found to be higher.

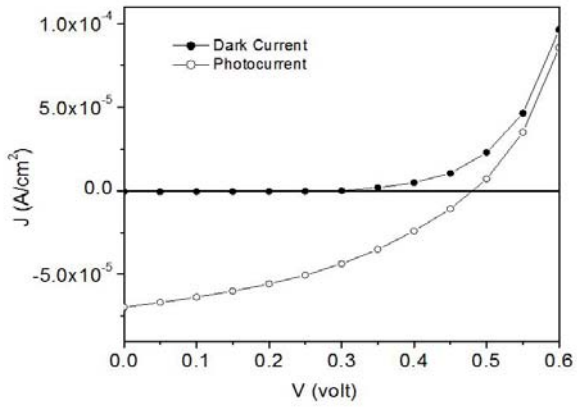

Fig.1.15. I-V Characteristics of an Organic Solar Cell

Power conversion efficiency of a solar cell is determined by the formula given below [137]

$$\eta = \frac{V_{oc} \times I_{sc} \times FF}{P_{in}} \text{ ----------} (1.20)$$

$$FF = \frac{V_{mpp} \times I_{mpp}}{V_{oc} \times I_{sc}} \text{ ----------} (1.21)$$

Where V_{oc} is the open circuit voltage, I_{sc} is the short circuit current, FF is the fill factor and P_{in} is the incident light power density. V_{mpp} and I_{mpp} are the voltage and current at the maximum power point. Brief descriptions of the parameters are as follows.

Open circuit voltage (Voc) is the maximum voltage obtained from a solar cell when no current is flowing. The photovoltage (or open-circuit voltage, V_{OC}) is directly related to the energy difference between the LUMO level of the acceptor and the HOMO level of the donor, which provides the primary driving force for charge separation. Short circuit

current density (J_{sc}) is directly linked to the product of the cell responsivity and incident solar spectrum irradiance. Basically a polymer molecule having a lower HOMO level enhances the 'V_{oc}'. Short circuit current (I_{sc}) is the maximum current obtained from a solar cell when the voltage across the device is zero. Under an external load, the current will always be less than I_{sc}. Short circuit current density (J_{sc}) is another important parameter determining the performance of a solar cell [138]. Band gap narrowing is the better way to improve the J_{sc} for the broader coverage of solar spectrum [139-141]. Simultaneous improvement of V_{oc} and J_{sc} is a very difficult process and structural fine-tuning is an alternative for this drawback [142-145]. Fill factor (FF) is another important factor responsible for achieving high power conversion efficiency. It is the ratio of power obtainable to the product of V_{oc} and J_{sc}. It is affected by many factors such as charge carrier mobility, interface recombination, series and shunt resistances, film morphology and miscibility between the donor and acceptor [146]. But the exact understanding of this parameter is not yet clear. The maximum power point (MPP) is the point on I-V curve where the power produced is found to be higher. At this point, the area of resulting rectangle is largest.

Depending on the device structure, organic polymer based solar cells can be divided into three main categories. They are **1)** bilayer heterojunction **2)** bulk heterojunction and **3)** inverted heterojunction devices. In the case of a bilayer heterostructure, the active layer is located between the ITO and metal electrode. Here the Donor and acceptor species are deposited on ITO layer by layer. Vacuum evaporation technique was adopted for depositing metal electrode on the top of the

active layer. The main drawback of this kinds of devices is the small interfacial area between the donor and acceptor that reduces the concentration of absorbers which in turn affects the photocurrent. This type of device structure is firstly introduced by Tang in 1979 with power conversion efficiency (PCE) of 1% [147,148].

Bulk heterojunction was introduced to improve the efficiency of bilayer heterojunction devices. In this case, interfacial area between the donor and acceptor was increased compared to bilayer heterojunction devices. Here the donor and acceptor species are mixed together which allows the easy transport of the generated excitons to the interface where they dissociate to free charges [149]. The concept of bulk heterojunction was introduced firstly by Hiramoto et al. through the co-evaporation of donor and acceptor molecule under vacuum conditions [150]. The first efficient bulk heterojunction device was fabricated by Heeger and Friend in 1995 using polymer–fullerene and polymer–polymer blends [151,152]. High efficiency polymer photovoltaic devices are almost based on polymer-fullerene systems and approaching an efficiency of around 10%. 'PCE' of bulk heterojunction devices purely depends on the morphology of the device. Bicontinuous interpenetrating network is the more suitable morphology for bulk heterojunction devices [153]. Materials design, morphology and manipulation and interface engineering are the three major things under consideration while fabricating polymer photovoltaic devices. Side-chain tuning is a very important factor responsible for the improvement of Fill factor. Frechet et al. reported the side-chain tuning of N-alkylthieno[3,4-c]pyrrole-4,6-dione (TPD) based polymers. Side-chain tuning helped to optimize π-stacking, polymer

crystallinity and material miscibility thereby improving the Fill factor [154]. Nowadays an efficiency of about 7% was achieved for a TPD-silole copolymer [155].

Inverted heterojunction device is another class of bulk heterojunction devices. In both bilayer and bulk heterojunction devices, electron flow takes place from acceptor to metal electrode and hole movement form donor to Indium doped tin oxide (ITO). ITO can act as electron and hole trap because the work function of ITO is 4.5 eV- 4.7 eV which is in between the HOMO and LUMO of the conjugated polymers. Interface layers have a lot of functions in Organic photovoltaic devices [156]. Reduction of energy barrier between photoactive layer and the electrode is very much necessary to make an ohmic contact for effective charge extraction. The bottom layer of organic photovoltaic device is conventionally ITO. A p-type interface layer of PEDOT:PSS having work function greater than that of ITO applied can act as a hole extraction layer and also smoothens the ITO surface to remove potential pinholes. But the acidic nature of PEDOT:PSS sometimes affects the device's long term stability. In order to remove this difficulty, various transition metal oxides have been introduced in the place of PEDOT:PSS [157-159]. If ITO is coated by electron transporting materials such as ZnO, TiO_2 or In_2S_3 [160-163], the structure is known as inverted heterojunction where ITO can collect electrons. When compared to the normal bulk heterojunction device, the stability of inverted structure was found to be higher [164]. Generally in organic photovoltaics, low work function metals such as calcium, barium and magnesium are used as cathode to provide some ohmic contact at the cathode-polymer interface. But these metals are reactive and destabilize the

device structure. Replacement of these metals by inorganic compounds or low work function metals is very effective to curtail this problem. In inverted heterojunction devices, certain inorganic materials such as nanostructures of zinc oxide, titanium oxide and cadmium selenide can function as acceptors for polymer donors, for which efficiencies of about 3% have been demonstrated [165-167]. Various research groups have demonstrated the use of semiconductor materials in the fabrication of inverted heterojunction devices. The model structure of an inverted heterojunction device is shown in Fig. 1.16.

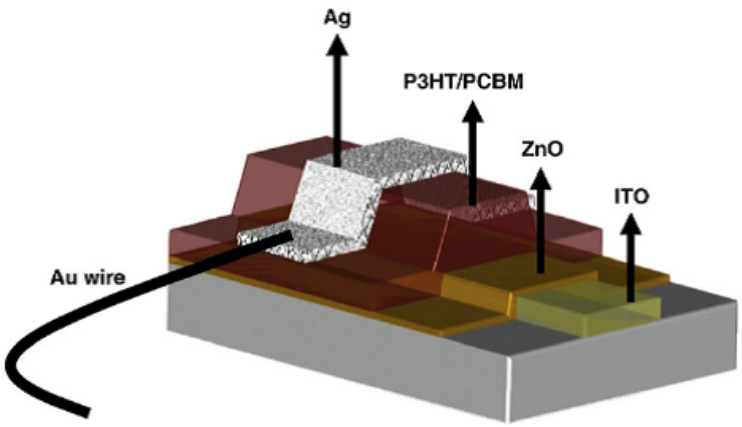

Fig. 1.16. Schematic representation of an inverted heterojunction device

1.5. Non-Linear Optical Properties of Semiconducting Materials

Nonlinear optics means the behavior of light in a nonlinear media. Here the dielectric polarization 'P' responds nonlinearly to the electric field of the light employed [168]. It also deals with the variation of frequency, phase or other physical properties of the material due to the impact of an applied electric field [169]. Nonlinear optics is the basis of all photonic technologies where photons are used for signal transmission

and processing [170]. Very intense electromagnetic fields are responsible to produce nonlinear optical phenomena. So this phenomenon was systematically studied with the help of lasers because the intensity of laser is sufficient to change the optical properties of the system under consideration. But at moderate field strength, the induced polarization responds linearly with the applied field. If the electric field employed is strong, then the polarization can be written as a Taylor series expansion which is shown below.

$$P = \alpha E+\beta EE+\gamma EEE+ \text{----------} (1.22)$$

Where 'α' is the linear polarizibility , while 'β' and 'γ' are referred as first and second hyperpolarizabilities.

Second harmonic generation (SHG) or frequency doubling is the major and extensively investigated nonlinear optical phenomenon. Lack of inversion symmetry is the basic requirement for a medium to show second harmonic generation. Second harmonic generation was first observed in quartz material with the help of ruby laser having a wavelength of 694 nm. In this phenomenon, two photons having same frequency are consumed to produce a new photon with twice frequency or energy [171]. The formulation of SHG by Bloembergen and Pershan is a breakthrough to the development of nonlinear optics. Now the nonlinear optical phenomenon is well established and recognized [172]. In this thesis we are dealing only with the third order nonlinear optical behavior of semiconductor materials. Nonlinearity is often represented by a power series expansion of total applied optical field which is given by

$$P = \chi^{(1)}E + \chi^{(2)}EE + \chi^{(3)}EEE \text{ ----------} (1.23)$$

Here $\chi^{(1)}$ represents the linear susceptibility representing the linear response. $\chi^{(2)}$ and $\chi^{(3)}$ are the second and third order nonlinear susceptibilities. Third order nonlinearities cover a vast and diverse area in nonlinear optics. Linear absorption is a mechanism used to couple laser light with the system. Effective third order nonlinearity occurs when linear absorption affects the refractive index [173]. A thermal nonlinearity is resulting from linear absorption and heating change the refractive index of the material. THG is a special case of sum frequency generation (SFG) involving one, two or three different frequencies giving $\omega_4=\omega_i+\omega_j+\omega_k$, where i,j,k=1,2,3. The third order response of a material contains only four terms in three fields when it is driven by a single beam. Generally, the nature of the coefficients associated with each term is different due to the distribution of susceptibilities. Tensor nature is an important property associated with nonlinear susceptibilities. Due to molecular or lattice structure of the materials, the nonlinear response depends on the polarization of optical fields. Various inorganic materials such as Lithium Niobate ($LiNbO_3$), Potassium titanyl phosphate (KTH), Potassium dihydrogen phosphate (KDP) are known to be good nonlinear active materials. The main drawback of these kinds of material includes difficulty to produce single crystals, high expense and difficulty to incorporate them into electronic devices [174]. So the researchers are looking for a less expensive, user friendly material for nonlinear applications. Both pristine and modified semiconductor materials are found to be better choice for nonlinear studies. Most of the optical integrated devices such as optical switching devices will be developed to achieve

faster response time. Strong nonlinear optical materials are responsible to develop these kinds of devices. Changes in optical properties such as absorption coefficient or refractive index due to the impact of high intense light are the basis of nonlinear optical phenomenon [175]. Among various semiconductor materials, ZnO has got much attention due to wide band gap and large exciton binding energy [176,177]. But compared to linear optical properties, the understanding of nonlinear response of ZnO material is under progress [178]. Second order and third order nonlinearity of ZnO have been reported elsewhere [179-182]. Large third order nonlinear optical susceptibility and faster response time of noble metal nanoparticles are used extensively for optical device fabrication [183]. Zhoe et al. reported the higher third order nonlinearity of Au embedded ZnO nanoparticle array using Z-Scan technique. Here the large nonlinear response was attributed to the surface plasmon resonance (SPR) effect of Au nanoparticles [184]. Morphology of the semiconductor material plays an important role in nonlinear optical response. The effect of polarization on the SHG of ZnO film, SHG and THG of the ZnO nanowire and Raman effect of ZnO nanorods are studied previously [185-187]. Zhou et al. studied the anisotropic third order optical nonlinear response of a single ZnO micro/nanowire by Z-Scan technique with a femtosecond laser [188]. L. Irimpan et al. reported the effect of ZnO and TiO_2 in the nonlinear response of ZnO-TiO_2-SiO_2 nanocomposites prepared by colloidal chemical synthesis [189]. Yumin et al. published the third order nonlinear optical properties of highly ordered chitosan CdSe quantum dots (QDs) and chitosan CdSe-ZnS core-shell QDs films by using Z-Scan with a femtosecond laser having a wavelength of 790 nm [190]. Quantum dots and metal nanoparticles are better candidates to show nonlinear optical

responses. Demir et al. evaluated the third order nonlinear optical phenomenon of colloidal InP/ZnS core-shell quantum dots (QDs) using Z-Scan technique with femtosecond pulses [191]. TiO_2 is another promising material showing very good nonlinear optical response. Among various NLO behaviors, optical limiting is one of the most important properties for practical applications. Rahulan et al. observed the nonlinear optical properties of Pt doped TiO_2 particles and also monitored the effect of Pt concentration on the optical limiting properties of nanoparticles [192]. Very recently Divya et al. reported the third order nonlinearity of amorphous TiO_2 and its common polymorphs, anatase and rutile. Among the three forms anatase was found to show better nonlinearity which depends on the nature of excitons [193]. Long time back Kyoung et al. published the effect of surface plasmon resonance on the third order optical nonlinearity of Au embedded TiO_2 matrices [194]. Here in this thesis, we have evaluated the NLO of modified TiO_2 thin films, which will be discussed in later sections.

1.6. Scope of the Thesis

Among various semiconductor materials, TiO_2 has got better attention due to its superior physical and chemical properties. Different modifications of TiO_2 extends its application to various fields such as photocatalysis, photo induced organic transformations, thermal reactions, photovoltaics, nonlinear optics etc. In the current work, we prepared visible light active metal, non-metal co-doped TiO_2 by hydrothermal technique. The photocatalytic efficiency of the prepared systems was measured by monitoring the degradation of some dyes, pesticides and also measured the photoinduced organic transformation of some anthracene

derivatives in visible region. The prepared systems were characterized by various physico-chemical techniques. TiO_2 is thermally inactive in nature. In order to makes it active for thermal reactions, we have modified it with Pd and Cu. Pd-Cu bimetallic supported on TiO_2 was successfully employed for the synthetically important Suzuki coupling reaction. The as prepared Cu-Pd/TiO_2 system was characterized by different techniques. Thin films of TiO_2 is the most prominent modification due to its heavy application in device fabrication, nonlinear optics etc. Here TiO_2 thin film was applied as an n-type material in the fabrication of photovoltaic device. TiO_2 thin films modified with some noble metals were employed for nonlinear optical studies using Z-Scan technique.

1.7. Major Objectives of the Present Study

1) Prepare Metal (Transition and rare earth) and non-metal co-doped TiO_2 via hydrothermal route.
2) Characterization of the prepared catalysts by various physico-chemical techniques such as XRD, UV-DRS, FT-IR, Raman Spectroscopy, TG-DTG, SEM-EDX, BET Surface Area, XPS etc.
3) Photocatalytic activity of the prepared systems to be evaluated by monitoring the degradation of some dyes, herbicides etc.
4) Photo-oxidation of anthracene derivatives to be evaluated in visible region using the co-doped TiO_2 systems.
5) Prepare Cu-Pd bimetallic supported on TiO_2 for synthetically important Suzuki coupling reactions.
6) Characterization of Cu-Pd/TiO_2 by various physico-chemical techniques.

7) Prepare TiO_2 thin films by Spin Coating technique for photovoltaic applications.

8) Fabricate Inverted heterojuction devices using conjugated polymer as hole transporting layer and TiO_2 as the electron transport layer.

9) Prepare pristine TiO_2 thin films and thin films of TiO_2 modified with some noble metals for nonlinear optical applications.

10) Characterize the prepared thin films by physico-chemical techniques such as XRD, SEM-EDX, AFM, optical absorption etc.

11) NLO properties of the prepared films were measured by Z-Scan technique using 532 nm Nd/YAG laser.

References

[1]. D. Chatterjee, S. Dasgupta, J. Photochem. Photobiol. C: Photochem. Rev. 6 (2005) 186.

[2]. A. T. Kuvarega, R. W. M. Krause, B. B. Mamba, J. Phys. Chem. C. 115 (2011) 22110.

[3]. A. L. Linsebigler, G. Lu, J. T. Yates, Jr., Chem. Rev. 95 (1995) 735.

[4]. M. A. Fox, M. T. Dulay, Chem. Rev. 93 (1993) 341.

[5]. N. Serpone, E. Pelizzetti, Eds. Photocatalysis-Fundamentals and Applications; Wiley Interscience: New York, (1989).

[6]. M. A. Fox, Top. Curr. Chem. 142 (1991) 172.

[7]. X. Chen, S. S. Mao, Chem. Rev. 107 (2007) 2891.

[8]. B. Tryba, A. W. Phenolrawski, M. I. Nagaki, Appl. Catal. B. 46 (2003) 203.

[9]. M. Bissen, B. M. Vieillard, A. J. Schindelin, F. H. Frimmel, Chemosphere. 44 (2001) 751.

[10]. G. Guillard, S. Horikoshi, N. P. Watanabc, H. Hidaka, P. Pichat, J. Photochem. Photobiol. A. 149 (2002) 155.

[11]. Ed. D. F. Ollis, H. Al-Ekabi, Photocatalytic Purification and Treatment of Water and Air, Elsevier, Amsterdam, (1993).

[12]. J. Ryu, W. Choi, Environ. Sci. Technol. 38 (2004) 2928.

[13]. Z. Shi, S. Yao, C. Sui, Catal. Sci. Technol. 1 (2011) 817.

[14]. D. A. Panayotov, S. P. Burrows, J. R. Morris, J. Phys. Chem. C. 116 (2012) 6623.

[15]. D. E. Skinner, D. Philip Colombo, J. J. Cavaleri, R. M. Bowman, J. Phys. Chem. 99 (1995) 7853.

[16]. Y. Tamaki, A. Furube, M. Murai, K. Hara, R. Katoh, M. Tachiya, Phys. Chem. Chem. Phys. 9 (2007) 1453.

[17]. Y. Tamaki, K. Hara, R. Katoh, M. Tachiya, A. Furube, J. Phys. Chem. C. 113 (2009) 11741.

[18]. I. A. Shkrob, M. C. Sauer, J. Phys. Chem. B. 108 (2004) 12497.

[19]. M. M. Haque, M. Muneer, J. Hazard. Mater. 145 (2007) 51.

[20]. A. D. Paola, M. Bellardita, L. Palmisano, Catalysts. 3 (2013) 36.

[21]. J. K. Burdett, Inorg. Chem. 24 (1985) 2244.

[22]. J. K. Burdett, T. Hughbands, J. M. Gordon, J. W. Richardson, Jr., J. V. Smith, J. Am. Chem. Soc. 109 (1987) 3639.

[23]. A. Fahmi, C. Minot, B. Silvi, M. Causa, Phys. Rev. B. 47 (1993) 11717.

[24]. Y. Hwu, Y. D. Yao, N. F. Cheng, C. Y. Tung, H. M. Lin, Nanostruct. Mater. 9 (1997) 355.

[25]. H. Zhang, J. F. Banfield, J. Mater. Chem. 8 (1998) 2073.

[26]. A. A. Gribb, J. F. Banfield, Am. Mineral. 82 (1997) 717.

[27]. T. Berger, M. Sterrer, O. Diwald, E. Knozinger, D. Panayatov, T. L. Thompson, J.T. Yates, Jr. J. Phys. Chem. B. 109 (2005) 6061.

[28]. S. H. Szczepankiewicz, A. J. Colussi, M. R. Hoffmann, J. Phys. Chem. B. 104 (2000) 9842.

[29]. L. Xiao-e, A. N. M. Green, S. A. Haque, A. Mills, J. R. Durrant, J. Photochem. Photobiol. A. 162 (2004) 253.

[30]. H. Goto, Y. Hanada, T. Ohno, M. Matsumura, J. Catal. 225 (2004) 223.

[31]. T. Tan, D. Beydoun, R. Amal, J. Photochem. Photobiol. A. 159 (2003) 273.

[32]. I. A. Shkrob, M. C. Sauer, J. Phys. Chem. B. 108 (2004) 12497.

[33]. T. Lana-Villarreal, J. Bisquert, I. Mora-Sero, P. Salvador, J. Phys. Chem. B. 109 (2005) 10355.

[34]. M. Gratzel, Nature. 414 (2001) 338.

[35]. A. Hagfeldt, M. Gratzel, Chem. Rev. 95(1995) 49.

[36]. G. Meyer, J. Inorg. Chem. 44 (2005) 6852.

[37]. P. Hoyer, R. Koenenkamp, Appl. Phys. Lett. 66 (1995) 349.

[38]. P. A. Sant, P. V. Kamat, Phys. Chem. Chem. Phys. 4 (2002) 198.

[39]. Q. Shen, D. Arae, T. Toyoda, J. Photochem. Photobiol. A. 164 (2004) 75.

[40]. D. M. Adams, L. Brus, C. E. D. Chidsey, S. Creager, C. Creutz, C. R. Kagan, P. V. Kamat, M. Lieberman, S. Lindsay, R. A. Marcus, R. M. Metzger, M. E. Michel-Beyerle, J. R. Miller, M. D. Newton, D. R. Rolison, O. Sankey, K. S. Schanze, J. Yardley, X. Zhu, J. Phys. Chem. B. 107 (2003) 6668.

[41]. X. H. Wang, J. G. Li, H. Kamiyama, M. Katada, N. Ohashi, Y. Moriyoshi, T. Ishigaki, J. Am. Chem. Soc. 127 (2005) 10982.

[42]. M. Zukalova, A. Zukal, L. Kavan, M. K. Nazeeruddin, P. Liska, M. Gratzel, Nano Lett. 5 (2005) 1789.

[43]. M. Adachi, Y. Murata, J. Takao, J. Jiu, M. Sakamoto, F. Wang, J. Am. Chem. Soc. 126 (2004) 14943.

[44]. K. Kalyanasundaram, M. Gratzel, Coord. Chem. Rev. 177 (1998) 347.

[45]. P. Qu, G. J. Meyer, Langmuir. 17 (2001) 6720.

[46]. H. Gerischer, F. Willig, Top. Curr. Chem. 61 (1976) 31.

[47]. A. Zaleska, Recent Patents on Engineering, 2 (2008) 157.

[48]. M. Anpo, Pure Appl. Chem. 72 (2000) 1787.

[49]. H. Yamashita, M. Harada, J. Misaka, J. Synchrotron Rad. 8 (2001) 569.

[50]. S. Sato, Chem. Phys. Lett. 123 (1986) 126.

[51]. T. Umebabayashi, T. Yamaki, H. Itoh, K. Asai, Appl. Phys. Lett. 81 (2002) 454.

[52]. T. Ohno, T. Mitsui, M. Matsumura, Chem. Lett. 32 (2003) 364.

[53]. A. Zaleska, J. W. Sobczak, E. Grabowska, J. Hupka, Appl. Catal. B. 78 (2007) 92.

[54]. S. C. Moon, H. Mametsuka, S. Tabata, E. Suzuki, Catal. Today. 58 (2000) 125.

[55]. J. C. Yu, L. Zhang, Z. Zheng, J. Zhao, Chem. Mater. 15 (2003) 2280.

[56]. L. Korosi, I. Dekany, Colloids Surf. A. 280 (2006) 146.

[57]. R. Asahi, T. Morikawa, T. Ohwaki, K. Aoki, Y. Taga, Science. 293 (2001) 269.

[58]. H. Irie, Y. Watanabe, K. Hashimoto, J. Phys. Chem. B. (2003) 5483.

[59]. T. Ihara, M. Miyoshi, Y. Triyama, O. Marsumato, S. Sugihara, Appl. Catal. B. 42 (2003) 403.

[60]. D. A. Panayotov, S. P. Burrows, J. R. Morris, J. Phys. Chem. C. 116 (2012) 6623.

[61]. F. Sabin, T. Turk, A. Vogler, J. Photochem. Photobiol. A. 63 (1992) 99.

[62]. Y. Tamaki, A. Furube, M. Murai, K. Hara, R. Katoh, M. Tachiya, J. Am. Chem. Soc. 128 (2006) 416.

[63]. T. Tachikawa, S. Tojo, K. Kawai, M. Endo, M. Fujitsuka, T. Ohno, K. Nishijima, Z. Miyamoto, T. Majima, J. Phys. Chem. B. 108 (2004) 19299.

[64]. K-i. Ishibashi, A. Fujishima, T. Watanabe, K. Hashimoto, J. Photochem. Photobiol. A.134 (2000) 139.

[65]. G. Riegel, J. R. Bolton, J. Phys. Chem. 99 (1995) 4215.

[66]. T. Yoshihara, R. Katoh, A. Furube, Y. Tamaki, M. Murai, K. Hara, S. Murata, H. Arakawa, M. Tachiya, J. Phys. Chem. B. 108 (2004) 3817.

[67]. H. Irie, Y. Watanabe, K. Hashimoto, Chem. Lett. 32 (2003) 772.

[68]. H. Irie, S.Washizuka, K. Hashimoto, Thin Solid Films. 510 (2006) 21.

[69]. S. Sakthivel, H. Kisch, Angew. Chem. Int. Ed. 42 (2003) 4908.

[70]. B. Neumann, P. Bogdanoff, H. Tributsch, S. Sakthivel, H. Kisch, J. Phys. Chem. B. 109 (2005) 16579.

[71]. J. Yang, C. Chen, H. Ji, W. Ma, J. Zhao, J. Phys. Chem. B. 109 (2005) 21900.

[72]. J. Zhao, C. Chen, W. Ma, Top. Catal. 35 (2005) 269.

[73]. C. Chen, X. Li, W. Ma, J. Zhao, J. Phys. Chem. B. 106 (2002) 318.

[74]. T. L. Villarreal, R. Gomez, M. Neumann-Spallart, N. Alonso-Vante, P. Salvador, J. Phys. Chem. B. 108 (2004) 15172.

[75]. C. Y. Wang, J. Rabani, D. W. Bahnemann, J. K. Dohrman, J. Photochem. Photobiol. A. 148 (2002) 169.

[76]. M. E. Calvo, R. Candal, S. Bilmes, Environ. Sci. Technol. 35 (2001) 4132.

[77]. H. Yu, H. Irie, K. Hashimoto, J. Am. Chem. Soc. 132 (2010) 6898.

[78]. H. Irie, T. Shibanuma, K. Kamiya, S. Miura, T. Yokoyama, K. Hashimoto, Appl. Catal. B. 96 (2010) 142.

[79]. G. Colon, M. C. Hidalgo, J. A. Navıo, A. Kubacka, M. Fernandez-Garcıa, Appl. Catal. B. 90 (2009) 633.

[80]. R. Murray, Molecular Design of Electrode Surface, JohnWiley & Sons, New York, NY, USA, (1992).

[81]. R. Amadelli, L. Samiolo, A. Maldotti, A. Molinari, D. Gazzoli, Int. J. Photoenergy. 2011 (2011) 259453.

[82]. T. Tachikawa, S. Tojo, M. Fujitsuka, T. Majima, Chem. Phys. Lett. 382 (2003) 618.

[83]. T. Tachikawa, S. Tojo, M. Fujitsuka, T. Majima, J. Phys. Chem. B. 108 (2004) 5859.

[84]. T. Tachikawa, S. Tojo, M. Fujitsuka, T. Majima, Langmuir. 20 (2004) 2753.

[85]. T. Tachikawa, S. Tojo, M. Fujitsuka, T. Majima, Langmuir. 20 (2004) 4327.

[86]. R. L. Kurtz, R. Stockbauer, T. E. Madey, E. Roman, J. L. de Segovia, Surf. Sci. 218 (1989) 178.

[87]. J. M. Pan, B. L. Maschhoff, U. Diebold, T. E. Madey, J. Vac. Sci. Technol. A. 10 (1992) 2470.

[88]. W. Gopel, G. Rocker, R. Feierabend, Phys. Reu. E. 28 (1983) 3427.

[89]. H. Idriss, K. S. Kim, M. A. Barteau, Surf. Sci. 262(1992) 113.

[90]. K. S. Kim, M. A. Barteau, W. E. Farneth, Langmuir. 4 (1988) 533.

[91]. K. S. Kim, M. A. Barteau, Surf. Sci. 233 (1989) 13.

[92]. J. M. Vohs, M. A. Barteau, Surf. Sci. 201 (1990) 481.

[93]. A. Kiennemann, H. Idriss, R. Kieffer, P. Chaumette, D. Durand, Ind. Eng. Chem. Res. 30 (1991) 1130.

[94]. J. Haber, Perspectives in Catalysis, Blackwell scientific publications. 371 (1992).

[95]. M. A. Aramendia, V. Borau, C. Jimenez, J. M. Marinas, M. E. Sempere, P. Urbano, Appl. Catal. 43 (1988) 41.

[96]. P. S. Kumbhar, Appl. Catal. A. 96 (1993) 241.

[97]. I. Bergault, P. Fouilloux, C. Joly-Vuillemin, H. Delmas, J. Catal. 175 (1998) 328.

[98]. N. Lavaud, P. Magnoux, F. Alvarez, L. Melo, G. Giannetto, M. Guisnet, J. Mol. Catal. A. 142 (1999) 223.

[99]. M. V. Rajashekharam, I. Bergault, P. Foilloux, D. Schweich, H. Delmas, R. V. Chaudhari, Catal. Today. 48 (1999) 83.

[100]. I. Bergault, C. Joly-Vuillemin, P. Fouilloux, H. Delmas, Catal. Today. 48 (1999) 161.

[101]. K. Joseph Antony Raj, M. G. Prakash, R. Mahalakshmy, T. Elangovana and B. Viswanathan, Catal. Sci. Technol. 2 (2012) 1429.

[102]. C. H. Bartholomew, R. B. Pannell, J. L. Butler, D. G. Mustard, Ind. Eng. Chem. Prod. Res. Dev. 20 (1981) 296.

[103]. J. Chen, N. Yao, R. Wang, J. Zhang, Chem. Eng. J. 148 (2009) 164.

[104]. J. Wildschut, F. H. Mahfud, R. H. Venderbosch, H. J. Heeres, Ind. Eng. Chem. Res. 48 (2009) 10324.

[105]. A. R. Ardiyantia, S. A. Khromovab, R. H. Venderboschc, V. A. Yakovlevb, I. V. Melián-Cabreraa, H. J. Heeresa, Appl. Catal. A: Gen. 449 (2012) 121.

[106]. M. Lashdaf, M. Tiitta, T. Venalainen, H. Osterholm, A. O. I. Krause, Catal. Lett. 94 (2004) 7.

[107]. F. Zhao, Y. Ikushima, M. Chatterjee, M. Shirai, M. Arai, Green Chem. 5 (2003) 76.

[108]. A. Cabiac, T. Cacciaguerra, P. Trens, R. Durand, G. Delahay, A. Medevielle, D. Plee, B. Coq, Appl. Catal. A: Gen. 340 (2008) 229.

[109]. H. Shi, N. Xu, D. Zhao, B. Q. Xu, Catal. Commun. 9 (2008) 1949.

[110]. W. Lin, H. Cheng, L. He, Y. Yu, F. Zhao, J. Catal. 303 (2013) 110.

[111]. A. M. Venezia, L.V. Parola, G. B. Deganello, J. Catal. 215 (2003) 317.

[112]. B. Pawelec, A. M. Venezia, L. V. Parola, Appl. Surf. Sci. 242 (2005) 380.

[113]. S. Yoshinaka, K. Segawa, Catal. Today. 45 (1998) 293.

[114]. M. Breysse, P. Afanasiev, C. Geantet, M. Vrinat, Catal. Today. 86 (2003) 5.

[115]. Z. Gu, L. Luo, S. Chen, Ind. J. Chem. Technol. 16 (2009) 175.

[116]. W. Gao, N. Guan, J. Chen, X. Guan, R. Jin, H. Zeng, Z. Liu, F. Zhang, Appl. Catal. B: Environ. 46 (2003) 341.

[117]. N. Miyaura, T. Yanagi, A. Suzuki, Synth. Commun. 11 (1981) 513.

[118]. A. Suzuki, Pure Appl. Chem. 57 (1985) 1749.

[119]. M. Sato, N. Miyaura, A. Suzuki, Chem. Lett. 1405 (1989).

[120]. S. B. Waghmode, S. S. Arbuja, B. N. Wanib, New J. Chem. 37 (2013) 2911.

[121]. M. Gratzel, Nature. 414 (2001) 338.

[122]. M. Gratzel, Prog. PhotoVolt. 8 (2000) 171.

[123]. M. Gratzel, J. Sol-Gel Sci. Technol. 22 (2001) 7.

[124]. M. Gratzel, J. Photochem. Photobiol. C. 4 (2003) 145.

[125]. M. Gratzel, J. Photochem. Photobiol. A. 164 (2004) 3.

[126]. M. Gratzel, MRS. Bull. 30 (2005) 23.

[127]. M. A. Green, K. Emery, Y. Hishikawa, W. Warta, Progress in Photovoltaics: Research and Applications. 19 (2011) 84.

[128]. P. Roy, S. Berger, P. Schmuki, Angew. Chem. Int. Ed. 50 (2011) 2904.

[129]. P. Roy, D. Kim, K. Lee, E. Spiecker, P. Schmuki, Nanoscale. 2 (2010) 45.

[130]. J. Lin, J. Chen, X. Chen, Nanoscale Research Letters. 6 (2011) 475.

[131]. A. K. Geim, K. S. Novoselov, Nat. Mater. 6 (2007) 183.

[132]. X. Luana, L. Chenb, J. Zhangb, G. Quc, J. C. Flakec, Y. Wanga, Electrochimica Acta. 111 (2013) 216.

[133]. A. E. Becquerel, Comptes Rendus. 9 (1839) 561.

[134]. D. M. Chapin, C. S. Fuller, G. L. Pearson, J. Appl. Phys. 25 (1954) 676.

[135]. C. W. Tang, Appl. Phys. Lett. 48 (1986) 183.

[136]. M. V. Maheshkumar, "Design and Synthesis of conjugated polymers for Photovoltaic and Chemosensor applications" Ph.D thesis (2012).

[137]. H. Hoppe, N. S. Sariciftci, J. Mater. Chem. 19 (2004) 1924.

[138]. G. Li, R. Zhu, Y. Yang, Nature Photonics. 6 (2012) 153.

[139]. Y. J. Cheng, S. H. Yang, C. S. Hsu, Chem. Rev. 109 (2009) 5868.

[140]. Y. Y. Liang, L. P. Yu, Polym. Rev. 50 (2010) 454.

[141]. Y. Y. Liang, L. P. Yu, Acc. Chem. Res. 43 (2010) 1227.

[142]. Y. Y. Liang, J. Am. Chem. Soc. 131 (2009) 7792.

[143]. H. Y. Chen, Nature Photon. 3 (2009) 649.

[144]. S. C. Price, A. C. Stuart, L. Q. Yang, H. X. Zhou, W. You, J. Am. Chem. Soc. 133 (2011) 4625.

[145]. H. X. Zhou, Angew. Chem. Int. Ed. 50 (2011) 2995.

[146]. D. Chen, F. Liu, C. Wang, A. Nakahara, T. P. Russell, Nano Lett. 11 (2011) 2071.

[147]. C. W. Tang, US patent 4, 164 (1979) 431.

[148]. C. W. Tang, Appl. Phys. Lett. 48 (1986) 183.

[149]. T. Taima, M. Chikamatsu, Y. Yoshida, K. Saito, K. Yase, Appl. Phys. Lett. 85 (2004) 6412.

[150]. M. Hiramoto, H. Fujiwara, M. Yokoyama, J. Appl. Phys. 72 (1992) 3781.

[151]. G. Yu, J. Gao, J. C. Hummelen, F. Wudl, A. Heeger, Science. 270 (1995) 1789.

[152]. J. J. M. Halls, Nature. 376 (1995) 498.

[153]. X. Yang, J. Loos, Macromolecules. 40 (2007) 1353.

[154]. C. Piliego, J. Am. Chem. Soc.132 (2010) 7595.

[155]. T. Y. Chu, J. Am. Chem. Soc. 133 (2011) 4250.

[156]. L. M. Chen, Z. Xu, Z. R. Hong, Y. Yang, J. Mater. Chem. 20 (2010) 2575.

[157]. Y. M. Sun, Adv. Mater. 23 (2011) 2226.

[158]. V. Shrotriya, G. Li, Y. Yao, C. W. Chu, Y. Yang, Appl. Phys. Lett. 88 (2006) 0735080.

[159]. M. D. Irwin, B. Buchholz, A. W. Hains, R. P. H. Chang, T. J. Marks, Proc. Natl Acad. Sci. USA. 105 (2008) 2783.

[160]. J. Gilot, I. Barbu, M. M. Wienk, R. A. Janssen, J. Appl. Phys. Lett. 91 (2007) 113520.

[161]. J. Y. Kim, Adv. Mater.18 (2006) 572.

[162]. M. R. Rajesh Menon, M. V. Maheshkumar, K. Sreekumar, C. Sudha Kartha, K. P. Vijayakumar, Physica status solidi. 209 (2012) 199.

[163]. M. R. Rajesh Menon, M. V. Maheshkumar, K. Sreekumar, C. Sudha Kartha, K. P. Vijayakumar, Solar Energy Materials and Solar Cells. 94 (2010) 12212.

[164]. F. C. Krebs, S. A. Gevorgyan, J. Alstrup, J. Mater. Chem. 19 (2009) 5442.

[165]. M. D. McGehee, MRS. Bull. 34 (2009) 95.

[166]. S. Dayal, N. Kopidakis, D. C. Olson, D. S. Ginley, G. Rumbles, Nano Lett. 10 (2010) 239.

[167]. J. Weickert, R. B. Dunbar, H. C. Hesse, W. Wiedemann, L. Schmidt-Mende, Adv. Mater. 23 (2011) 1810.

[168]. http://en.wikipedia.org.

[169]. D. R. Kanis, M. A. Ratner, T. Marks, Chem. Rev. 94 (1994) 195.

[170]. M. G. Kuzyk, C. W. Disk, (Eds), Marcell Dekker Inc. New York (1998).

[171]. C. Wang, T. Zhang, W. Lin, Chem. Rev. 112 (2012) 1084.

[172]. N. Bloembergen, P. S. Pershan, Phys. Rev. 128 (1962) 606.

[173]. M. Sheik-Bahae, M. P. Hasselbeck, OSA Handbook of Optics, Vol. IV, Chapter.17 (2000).

[174]. T. Verbiest, S. Houbrechts, M. Kauranen, K. Clays, A. Persoons, J. Mater. Chem. 7 (1997) 2175.

[175]. B. W. Nie, Adv. Mater. 5 (1993) 520.

[176]. C. Klingshirn, Phys. Status Solidi B. 9 (2007) 3027.

[177]. S. Y. Kim, I. S. Lee, Y. S. Yeon, S. M. Park, J. K. Song, Bull. Korean Chem. Soc. 29 (2008) 1960.

[178]. H. S. Shim, N. S. Han, J. H. Seo, S. M. Park, J. K. Song, Bull. Korean Chem. Soc. 31 (2010) 2675.

[179]. J. H. Lin, Y. J. Chen, H. Y. Lin, W. F. Hsieh, J. Appl. Phys. 97 (2005) 033526.

[180]. G. Wang, G. T. Kiehne, G. K. L. Wong, J. B. Ketterson, Z. Liu, R. H. P. Chang, Appl. Phys. Lett. 80 (2002) 401.

[181]. N. S. Han, H. S. Shim, S. M. Park, J. K. Song, Bull. Korean Chem. Soc. 30 (2009) 2199.

[182]. C. F. Zhang, Z. W. Dong, G. J. You, R. Y. Zhu, S. X. Qian, H. Deng, H. Cheng, J. C. Wang, Appl. Phys. Lett. 89 (2006) 042117.

[183]. D. Cotter, R. J. Manning, K. J. Blow, A. D. Ellis, A. E. Kelly, D. Nesset, I. D. Phillips, A. J. Poustie, D. C. Rogers, Science. 286 (1999) 1523.

[184]. T. Ning, Y. Zhou, H. Shen, H. Lu, Z. Sun, L. Cao, D. Guan, D. Zhang, G. Yang, Appl. Surf. Sci. 254 (2008) 1900.

[185]. U. Neumann, R. Grunwald, U. Griebner, W. Seeber, Appl. Phys. Lett. 87 (2005) 171108.

[186]. J. C. Johnson, H. Q. Yan, R. D. Schaller, R. J. Saykally, Nano Lett. 2 (2002) 279.

[187]. C. T. Chien, M. C. Wu, C. W. Chen, Y. F. Chen, Appl. Phys. Lett. 92 (2008) 223102.

[188]. K. Wang, J. Zhou, L. Yuan, Y. Tao, J. Chen, P. Lu, Z. L. Wang, Nano Lett. 12 (2012) 833.

[189]. L. Irimpan, B. Krishnan, V.P.N. Nampoori, P. Radhakrishnan, Optical Materials. 31 (2008) 361.

[190]. X. Wang, Y. Du, S. Ding, Q. Wang, G. Xiong, M. Xie, X. Shen, D. Pang, J. Phys. Chem. B. 110 (2006) 1566.

[191]. Y. Wang, X. Yang, T. C. He, Y. Gao, H. V. Demir, X. W. Sun, H. D. Sun, Appl. Phys. Lett. 102 (2013) 021917.

[192]. K. M. Rahulan, N. Padmanathan, G. Vinitha, C. C. Kanakam, Mat. Res. Bull. 48 (2013) 3037.

[193]. S. Divya, I. Sebastian, V. P. N. Nampoori, P. Radhakrishnan, A. Mujeeb, Optics &Laser Technology. 56 (2014) 207.

[194]. M. Kyoung, M. Lee, Bull. Korean Chem. Soc. 21 (2000) 26.

.....ꕥ.....

Chapter 2

Experimental and Characterization Techniques

Contents

Varieties of methods are available for the preparation of materials. None of the methods adopted for the synthesis of the compound is perfect in nature. Every method has its own advantages and disadvantages. Proper caring and tuning of parameters are very important to get high quality materials that possess strong potential for diverse applications. Properties and nature of the materials under investigation can be identified perfectly with the help of suitable characterization tools. Some characterization techniques are qualitative which provide images of the surface of the material and some others are quantitative that gives better insight into the relative concentrations of atoms that comprise the material. Ultimately, suitable characterization technique is very necessary to understand the whole picture of the material that in turn helps the researcher to find out the exact field of its application.

2.1. Introduction

Characterization is an inevitable part of materials scientists. The characteristics and performance of a material depends on the method of

preparation and pretreatment conditions. We can tune the mechanical, thermal, chemical and electrical properties of the material for specific applications. But in order to make a correlation between properties of the materials and its application, suitable characterization techniques are essential. Sensitivity of the characterization techniques are improved perfectly to measure parts per trillion (ppt) concentrations of impurities in a bulk sample. Varieties of techniques are available for the characterization of materials with specific properties and applications. All these techniques aim to determine the crystal structure, defect structure, phase, size, shape, crystal or grain size, composition etc. [1]. Molecular structure, composition and vibration frequencies of a substance can be better understood in terms of spectroscopy. It is also useful to find the concentration of reactants with respect to time and to find the reaction intermediates [2]. Spectroscopy is a widely accepted technique for the elucidation of molecular structure as well as the qualitative and quantitative determination of impurities. Optical microscopy is the simplest characterization technique available for the analysis of solid materials. This chapter describes the preparation of materials and common analysis techniques used to gather information from the prepared materials.

2.2. Catalyst Preparation

Catalytic performance of the system depends mainly on the methods of preparation. Selection of methods, preparation conditions and tuning of parameters are important factors to obtain a catalyst with immense potential for diverse applications. Here pristine and modified (metal, non-metal co-doped) TiO_2 systems were prepared by hydrothermal technique. Hydrothermal synthesis is normally conducted in steel pressure vessels

called autoclaves under controlled temperature and pressure with the reaction in aqueous solution. Temperature and the amount of solution added determine the internal pressure produced within the system [3]. It is a widely accepted method for the synthesis of small particles and so many groups have reported the preparation of TiO_2 nanoparticles [4-8]. In this method, $Ti[OCH(CH_3)_2]_4$ was taken as the source for titania. Metal nitrates and urea were selected as the sources for metals and N respectively. 10 ml of $Ti[OCH(CH_3)_2]_4$ was dissolved in 30mL of ethanol by vigorous stirring at room temperature, which was called as first solution. Desired amount of metal nitrates and urea (urea to $Ti[OCH(CH_3)_2]_4$ ratio was 1:1 molar) were dissolved in 1:1 V/V of ethanol and Millipore water. This was known as second solution. Second solution was added drop wise to the first with vigorous stirring in order to carry out hydrolysis. After ageing of about three days, the mixture was transferred to a stainless steel Teflon lined autoclave and heated at a temperature of 110°C for 12h. Then the final mixture was washed several times with ethanol and Millipore water to remove the impurities completely. The obtained powder was dried at 80°C and calcined at 500°C for 4h. The prepared catalyst was designated as M(X)-N-Ti, where M and X represents the different metals and their concentrations respectively. We have prepared five different co-doped TiO_2 systems for photocatalytic applications. Co-doped systems with various concentrations of metals were prepared to study the effect of dopant concentration on the catalytic performance. But in all these cases the amount of nitrogen was kept constant.

Preparation of Cu/Pd bimetallic supported on TiO_2 for thermal reactions, preparation of TiO_2 and noble metal modified TiO_2 thin films

for photovolataic and nonlinear optical applications will be discussed in the respective chapters.

The systems prepared for various applications and its notations are shown in Table. 2.1.

Table.2.1. Prepared systems and its notations

Systems	Notations
Gadolinium and nitrogen co-doped TiO_2	Gd-N-Ti
Palladium and nitrogen co-doped TiO_2	Pd-N-Ti
Silver and nitrogen co-doped TiO_2	Ag-N-Ti
Cadmium and nitrogen co-doped TiO_2	Cd-N-Ti
Praseodymium and nitrogen co-doped TiO_2	Pr-N-Ti
Copper (1wt%) modified TiO_2	Cu(1wt%)-Ti
Palladium (4wt%) modified TiO_2	Pd(4wt%)-Ti
Copper (1wt%) and palladium (4wt%) modified TiO_2	Cu(1wt%)-Pd(4wt%)-Ti
Copper (2wt%) and palladium (4wt%) modified TiO_2	Cu(2wt%)-Pd(4wt%)-Ti
Gold modified TiO_2 thin films	Au-TiO_2
Silver modified TiO_2 thin film	Ag-TiO_2
Palladium modified TiO_2 thin film	Pd-TiO_2

2.3. Characterization techniques

Characterization techniques can be considered as the backbones of materials chemistry. Clear picture of a material can be better evidenced from the collective use of various techniques. X-ray diffraction, electron microscopy, spectroscopy, thermogravimetric analysis are the common methods used to interpret the structure and properties of the material. A brief description on the purpose and theory of various characterization techniques are discussed below.

2.3.1. X-ray Diffraction (XRD)

X-ray diffraction is the most powerful and successful technique for determining the structure of crystals. It also gives some idea regarding crystallinity, crystal grain size, lattice parameters, phase composition, lattice defects etc. Spectroscopy and photography are the two main classifications of X-ray diffraction methods. The spectroscopic technique known as the X-ray powder diffractometry, is the most widely used diffraction method. On the other hand, photographic techniques are not common but used to determine unknown crystal structures [9]. X-ray diffraction is a nondestructive technique used to analyze polycrystalline aggregate solids rather than powder samples. X-ray crystallography is a commonly used method for determining the arrangement of atoms within a crystal. A beam of X-ray strikes a crystal and diffracts into many specific directions. X-ray striking an electron produces secondary spherical waves emanating from the electron. A regular array of spherical waves can be produced due to the regular array of electrons. These waves cancel out each other in most directions through destructive interference and add constructively in a few specific directions determined by Bragg's law:

$$2d \sin\theta = n\lambda \quad \text{---------- (2.1)}$$

where 'λ' is the wavelength of X-rays, 'n' represents the order of reflections and 'd' is the spacing between the crystallographic planes. A diffraction peak is observed due to the constructive interference of X-rays scattered from the atomic plane in a crystal. The diffraction patterns obtained provide some information regarding phase purity, crystallinity and cell parameters [10,11]. Spacing between atomic planes of a crystal can be determined on the basis of incident angle and the wavelength of

the incident beam. Knowing the spacing of the crystallographic planes by diffraction method is a significant factor to obtain crystal structure of the material. The X-ray diffractogram obtained at 2θ range of 10-70° is known as wide angle spectra and that obtained at 2θ below 10° is known as low angle which gives mesoporous nature of the materials. XRD is also used to determine crystal grain size according to the Scherrer equation

$$D = K\lambda / \beta\cos\theta \quad \text{---------- (2.2)}$$

where K is a dimensionless constant, 2θ is the diffraction angle, λ is the wavelength of the X-ray radiation, and β is the full width at half-maximum (FWHM) of the diffraction peak [12]. Crystallite size is inversely related to the FWHM of an individual peak. That is, narrower the peak larger the particle size. Ultimately, the size of the nanomaterials purely depends on the FWHM of the diffraction peak. Phase identification is another important task of XRD. In powder X-ray diffraction, the phase corresponding to a particular plane can be identified by comparing it with reference spectra from JCPDS.

The powder X-ray diffraction of the sample was performed using a Bruker AXS D8 diffractometer with Ni filtered Cu Kα radiation source (λ= 1.5406 A) in the range of 10-70° at a scan rate of 0.5°/min.

2.3.2. Raman Spectroscopy

Raman spectroscopy is a powerful method for the investigation of the structural properties of nanoparticles because the variations in particle size can be easily monitored with the help of Raman spectra [13]. Generally, it is used to determine the vibrational, rotational and other low

frequency modes in a system. Maximum of the low frequency Raman band is very useful to understand the size of nanoparticles. The positions and widths of Raman bands of materials are useful to study the vibrational and structural properties. Local structure and electronic environment of constituent atoms of a material are very significant for the better understanding of a Raman spectrum [14,15]. The interaction of light with the electron cloud and the bonds of the molecule are the basis of Raman spectra. The interaction of laser light with molecular vibrations, phonons or some other excitations in the system improves the energy of laser photons. This shift in energy gives information about the vibrational modes in the system. Amount of deformation of electron cloud or molecular polarizability changes with respect to the vibrational coordinates is required for a molecule to show Raman effect. The Raman scattering intensity is directly related to the amount of polarizability. Raman scattering by an anisotropic crystal gives information about crystal orientation. Raman spectra are also suitable for the microscopic examination of minerals, materials, cells and proteins. It also gives information regarding the presence of impurities, defects etc. In crystalline solids, Raman effect deals with phonons instead of molecular vibration. A phonon is Raman active only if the first derivative of polarizability with respect to the vibrational coordinate has a non-zero value which depends on the crystal symmetry.

Raman spectra measurements were done using a micro Raman system from Jobin Yvon Horibra LABRAM-HR with a He-Ne Laser Source (633 nm) and Argon (488 nm).

2.3.3. Scanning Electron Microscopy (SEM)

Scanning electron microscopy is a widely accepted technique to extract structural and chemical information point-by-point from a region of interest in the sample. It is generally employed to examine the surface morphologies of the material at higher magnifications. It is an inevitable tool in heterogeneous catalysis because most of the reactions are taking place on the surface. Due to higher spatial resolution, it is used to characterize a wide range of materials at nanometer to micrometer length scales [16]. Accelerated electrons in a scanning electron microscope possess enormous amount of kinetic energy and this energy is dissipated as a variety of signals due to its interaction with the sample under consideration. Secondary electrons, backscattered electrons, diffracted backscattered electrons, photons, visible light and heat are the major constituents of the signals produced from the SEM instrument. Among these, secondary electrons are responsible to produce the surface image of the sample. Scattered and backscattered electrons give information regarding crystal structures and orientation of minerals. That is, backscattered electrons are most valuable for illustrating contrasts in composition in multiphase samples [17]. Elemental analysis of the sample was done with the help of photons emerging from the system due to electron impact. SEM can be considered as a nondestructive technique because the X-rays generated by electron interactions do not lead to volume loss of the sample. So by using SEM, we can analyze the same sample repeatedly [18]. Ultimately, SEM images the surface structure of bulk materials with high magnifications. The images produced from SEM have greater resolution than optical micrographs making it suitable for the analysis of rough specimens such as fractured surfaces and particulate materials.

Scanning electron micrographs were taken using JEOL Model JSM-6390LV with a resolution of 1.38 eV.

2.3.4. Transmission Electron Microscope (TEM)

Transmission electron microscopy is a powerful tool that provides information about the morphology, crystallography and elemental composition for advanced materials. It is also an electron microscopic technique with high resolution to extract structural information. A combination of topographic and crystallographic information gives particle size distribution in the material. TEM is a microscopy technique where an electron source emits a stream of electrons with the help of electromagnetic lance. These electrons are focused into a very thin beam which are transmitted through the specimen and finally projected on a fluorescent screen giving a "shadow image" of the specimen. The contrast of the image depends on the density of the material. Here the magnified images are recorded by hitting a fluorescent screen, photographic plate or light sensitive sensor such as a CCD camera and displayed in real time on a computer. From the high resolution TEM images, we can understand the ordered nature of the material and selective area electron diffraction gives information about the crystalline nature. TEM has a better resolution than light microscopy due to the lower wavelength of electrons [19]. TEM finds applications in cancer research, virology, materials science as well as pollution, nanotechnology and semiconductor research [20]. It also provides information about the various morphological phases such as cubic, hexagonal etc.

TEM analysis was performed in an ultrahigh resolution analytical electron microscope JEOL 3010.

2.3.5. Thermogravimetric Analysis

Thermal analysis is an analytical technique used to investigate the behavior of a sample as a function of temperature [21]. Commonly used thermal analysis techniques include differential thermal analysis, differential scanning calorimetry, thermogravimetry, thermomechanical analysis etc. Thermogravimetry (TG) is the branch of thermal analysis which examines the mass change of a sample as a function of temperature in the scanning mode or as a function of time in the isothermal mode [22]. All the thermal events may not bring about a change in mass of the sample. Desorption, absorption, sublimation, vaporization, oxidation, reduction and decomposition are some thermal events that change the mass of the sample during analysis. TG is used to characterize the decomposition and thermal stability of materials under a variety of conditions and also used to examine the kinetics of the physico-chemical processes occurring in the sample. In TG analysis, the sample is placed in a thermal microbalance and heated at a predetermined rate, then change in weight of the sample is detected. Mass changes occur in a variety of ways and this produces steps in thermogravimetric analysis (TGA) or peaks in the differential thermogravimetric (DTG) curve.

Thermo gravimetric analysis is normally carried out in air or an inert atmosphere such as Helium or Argon. The analyzer consists of a balance with a platinum pan where we can load the sample. The pan is placed in an electrically heated oven with a thermocouple to measure the temperature accurately. The reaction atmosphere is purged with an inert gas to prevent oxidation or other undesired reactions.

Thermal analysis was done with the help of a Perkin Elmer Pyris Diamond thermo gravimetric/differential thermal analyzer under nitrogen atmosphere at a heating rate of 10°C/min from room temperature to 800°C in which samples were mounted on a Platinum sample holder.

2.3.6. X-ray Photoelectron Spectroscopy (XPS)

Elemental composition of the material under investigation can be better understood in terms of XPS. X-ray photoelectron spectroscopy determines the qualitative and quantitative identification of chemical elements by detecting characteristic X-rays that are emitted from atoms irradiated by a high-energy beam.

Generally electrons are bound to atom with different energies. Different stimuli such as monochromatic photon beam or electron beam interact with the atoms and bound electrons may be ejected with different kinetic energies. XPS is purely based on photoelectric effect where kinetic energy of the ejected electron is measured and reported in terms of binding energy. In photoelectron spectroscopy, intensity is measured as a function of kinetic energy of the electrons [23]. In X-ray photoelectron spectroscopy, soft X-ray beam is used as the stimulant. But UV radiation can eject electrons with low binding energy and this method is known as Ultraviolet photoelectron spectroscopy (UPS). Atoms can eject some core level electrons upon high energy stimulation. This excited atom may relax by dropping an outer electron to the core level and the difference in energy is emitted as X-ray photon. This is known as X-ray fluorescence. But on the other hand, if the energy is transferred to an outer electron instead of being emitted as X-ray, that electron comes out with a certain kinetic energy which may be studied by β-spectrometer. This is known as

Auger electron. Electrons emitted from the bulk of the atoms undergo multiple scattering due to collision with other atoms. Only those electrons that are emitted from atoms at the surface escape without energy loss. Hence it is a surface specific technique and used for studying the surface. Along with main binding energy peaks, several other peaks are also present in the XPS spectra. Thorough identification of these secondary peaks is necessary for the correct interpretation. XPS spectra always have some additional kinetic energy peaks due to Auger emission. The identification of Auger peaks is very easy because the position of Auger peaks remain unchanged by changing the X-ray energy. Additional peaks appear in the lower kinetic energy side of XPS spectrum is known as satellite peaks. Spin orbital splitting and peak area ratios are the two main factors used for elemental identification. It is a quantitative technique used to determine the percentage of elements present in the sample [24].

Surface composition and electronic structures were analyzed by X-ray photoelectron spectroscopy using an Omicron Nanotechnology XPS system with a monochromatic Al Kα radiation (hυ = 1486.6 eV) of source voltage 15 kV and emission current of 20 mA. All scans were carried out at ultrahigh vacuum of 2×10^{-10} mbar. The obtained XPS spectra were deconvoluted using Casa XPS programme (Casa Software Ltd, UK), in which the background was simulated using the Shirley function and the peaks were fitted using a Gaussian Lorentzian function. All binding energies were referenced to C1s for calibration.

2.3.7. Energy Dispersive X-ray Analysis (EDX)

EDX type X-ray spectrometer is commonly associated with SEM and TEM. With the help of X-ray spectrometer in an electron microscope,

we can do elemental analysis while examining the microstructure of materials. The main difference between EDS in an electron microscope and in a stand-alone XRF is the source to excite characteristic X-rays from a specimen. It is often referred to as a microanalysis because; it analyzes the chemical elements in microscopic volume in the specimen [9]. EDX consists of two modes of operations. They are stationary and scanning mode. In the stationary mode, the probe points at one location until the collection of X-ray photons is complete. The dwell time of the probe for EDX is directly proportional to the number of X-ray photon counts received by the detector. Elemental detection purely depends on the signal-to-noise ratio and intensity of the spectra correlates with the concentration of elements present in it. Low concentration of impurities (<1 wt%) requires longer dwell times for their detection. In the scanning mode, the electron probe moves over the specimen surface similar to the way in which the probe moves for obtaining an electron image in the SEM. The intensity of specific characteristic X-rays can be recorded and superimposed on the corresponding electron image. The line scans of elements help to identify the elemental distribution and also we can use the scanning mode to make composition maps in which the distributions of elements are clearly revealed.

Compositional information about the sample was analyzed by EDX using JEOL Model JED-2300 [25].

2.3.8. Atomic Force Microscopy (AFM)

Atomic force microscopy is another technique used to understand the surface morphology, surface roughness etc. The AFM operates like a record player except that it is associated with flexible cantilevers, sharp

tips, and a force feedback system. It is a quantitative technique used to measure nano scale surface roughness and surface nano-texture of different type of material surface including polymers and nanocomposites [26]. In atomic force microscope, a probe consisting of a sharp tip located near the end of cantilever beam is scanned across the surface of the specimen using piezoelectric scanners. Material interactions are often monitored using an optical lever detection system in which laser is reflected off of the cantilever and onto a position sensitive photodiode. In the scanning time, operating parameter is at constant level and images are generated through a feedback loop between the optional detection system and the piezoelectric scanners. AFM operation is of two types a) contact mode b) non-contact mode. In Contact Mode, the sample-tip distance is so small that the important force is the core-core repulsive one. In non-contact mode, the force is the van der Walls and it can achieve a resolution of nearly 1 nm. AFM can scan both hard and soft samples in ambient air or in a fluid environment.

Morphology of the film was monitored using a BT 02218 Nano surfeasy Scan 2AFM/STM package with single controller.

2.3.9. UV-Visible Diffuse Reflectance Spectroscopy

Diffuse reflectance spectroscopy is a sensitive technique which uses the interaction of light, absorption and scattering to produce characteristic spectrum providing information regarding the structure and composition of the material. Electronic transition in materials can be observed in liquid state using UV-Visible spectroscopy. But in the case of insoluble solids, UV-Visible diffuse reflectance is used. It is used to study the electronic transitions between orbitals or bands in the case of atoms, ions and

molecules in gas, liquid or solid state. This technique is performed on the basis of electronic excitation by the absorption of light. Electronic transitions of transition metals are two types, a) metal centered transitions b) charge transfer transitions (CT). d-d transition give information about the oxidation state and coordination environment of the metal ions. But 'CT' transitions are very intense and are sensitive to the nature of donor and acceptor atoms [27]. The surface of the sample is responsible for the reflection and absorption of employed radiation and hence is used in the study of surfaces. The band gap of the semiconductor materials can be calculated from UV-Vis DRS spectrum using the equation

$$E = hc/\lambda = 1239.8/\lambda \text{ (nm)} \quad \text{---------- (2.3)}$$

This is one of the simple versions of Kubelka-Munk equation where λ is the wavelength from which reflection has taken place [28].

Light response of the catalysts were recorded by UV-Vis-NIR spectrometer in the range of 200-900 nm on Labomed UV-Vis double beam UVD-500 spectrophotometer using $BaSO_4$ as reflectance standard with a CCD detector.

2.3.10. Surface Area Analysis

In heterogeneous catalysis, most of the reactions occur at the surfaces. So knowing surface area is very significant to predict the catalyst properties. Surface area measurements are commonly carried out by gas physisorption method and nitrogen physisorption measurements are performed at liquid nitrogen temperature. Out of several methods, BET method is the widely accepted one for the estimation of surface area

[29]. This method is based on the extension of Langmuir theory to multilayer adsorption. A simple form BET equation can be written as

$$P/[V(P_0-P)] = [1/V_m C] + [(C-1)/V_m C] [P/P_0] \text{ ------- (2.4)}$$

Here 'C' is a constant at a given temperature and is related to the heat of adsorption, 'V' is the volume adsorbed at equilibrium pressure P, V_m is the volume of adsorbate required for monolayer coverage and P_0 is the saturation vapour pressure of the adsorbate. According to BET theory, a plot of $P/ [V(P_0-P)]$ Vs P/P_0 is a straight line with slope $S= (C-1)/ Vm C$ and intercept $I= 1/V_m C$. Knowing slope and intercept, V_m can be calculated which is used for the calculation of specific surface area using the following equation

$$S = (V_m N_A A_m) / (22414 \times Wt) \text{ ---------- (2.5)}$$

Where V_m is the monolayer volume in mL at STP, N_A is the Avogadro number, W_t is the weight of the sample and A_m is the cross sectional area occupied by adsorbate molecule.

Surface area of the catalyst was determined by Micromeritics Tristar 3000 surface area analyzer.

2.4. Applications of Prepared Systems

Photocatalytic reactions were carried out in an Oriel Arc lamp system designed to produce uniform illumination. The diameter of the collimated beam is around 1 inch (2.54 cm) and the work plane is 2.6 inches (6.65 cm) from the lower end of the beam tuning assembly. In order to control the temperature for the lamp environment, uniform

illuminator was equipped with fan cooled lamp housing. The light source of the system was 150 W Xe ozone free lamps with an average life of 1500 hours. The filter used in this study was 420-630 nm dichoric mirrors (cold mirror) with an irradiance of 96.8 mW/cm^2 in order to get visible radiation.

Here we monitored the degradation of some water pollutants such as herbicides using visible region of electromagnetic spectrum. The percentage of degradation was studied using the equation $(C_0\text{-}C) \times 100/ C_0$, where C_0 and C represent the initial and final concentrations of the samples. Degradation of herbicides was analyzed by HPLC (Dionex Ultimate 3000) with photo diode array UV detector and a 5μm Thermo Hypersil ODS-2 C-18 reverse phase column (150 × 4.6mm). The experiments were repeated and its average value was reported.

We have also studied the photo induced organic transformations of some anthracene derivatives by visible light responsive metal/non-metal co-doped TiO_2 systems. These compounds were synthesized in the organic laboratory of Department of Applied Chemistry, CUSAT. Here we have used column chromatographic techniques for the separation of products. All the resultant products were characterized by various physico-chemical techniques such as ^1H NMR, melting point(MP) measurement, FT-IR, and GCMS analysis. The details of reaction conditions and different parameters will be discussed later. We have carried out Suzuki coupling reaction using Cu/Pd bimetallic on TiO_2 in order to find out the practical application of TiO_2 in thermal reactions. Various parameters such as effect of solvents, effect of bases and effect of catalysts were monitored in more detail. Preparation procedure of the

catalyst and reaction conditions will be discussed in the respected section. With the help of thin films of TiO_2, we have fabricated an inverted heterojunction solar cell using two different acceptors. Here TiO_2 acts as an n-type semiconductor material and conjugated polymer was selected as the p-type material. Characterization of the TiO_2 thin films and details of the photovoltaic applications will be discussed. Nowadays almost all photonic devices are based on nonlinear optical properties where photons are used for signal processing and transmission. Investigation of third order nonlinearity of semiconductor material is a newly emerging field. In our work we have measured the nonlinear optical properties of pristine TiO_2 and TiO_2 modified with noble metals such as Pd, Ag and Au using Z-Scan technique. The nonlinear optical properties of noble metal doped TiO_2 was found to be higher than that of bare TiO_2.

References

[1]. R. Bhardwaj, V. Gupta, 2nd International Conference on Role of Technology in Nation Building (ICRTNB-2013) ISBN: 97881925922-1-3.

[2]. J. M. Hollas, Modern Spectroscopy, Fourth Edition by John Wiley & Sons, Ltd, (2004).

[3]. X. Chen, S. S. Mao, Chem. Rev. 107 (2007) 2891.

[4]. M. Andersson, L. Oesterlund, S. Ljungstroem, A. Palmqvist, J. Phys. Chem. B. 106 (2002) 10674.

[5]. S. Y. Chae, M. K. Park, S. K. Lee, T. Y. Kim, S. K. Kim, W. I. Lee, Chem. Mater. 15 (2003) 3326.

[6]. J. Yang, S. Mei, J. M. F. Ferreira, J. Am. Ceram. Soc. 83 (2000) 1361.

[7]. J. Yang, S. Mei, J. M. F. Ferreira, J. Mater. Res. 17 (2002) 2197.

[8]. J. Liu, R. Han, Y. Zhao, H. Wang, W. Lu, T. Yu, Y. Zhang, J. Phys. Chem. C. 115 (2011) 4507.

[9]. Y. Leng, Materials Characterization: Introduction to Microscopic and Spectroscopic Methods, John Wiley &Sons(Asia) Pte Ltd, (2008).

[10]. W. H. Bragg, W. L. Bragg, "The crystalline State, McMillan", New York, Vol.1, (1949).

[11]. S. Biz, M. Occelli, Catal. Rev. Sci. Eng. 40 (1998) 329.

[12]. T. Lindgren, J. M. Mwabora, E. Avendano, J. Jonsson, A. Hoel, C. G. Granqvist, S. E. Lindquist, J. Phys. Chem. B. 107 (2003) 5709.

[13]. H. C. Choi, Y. M. Jung, S. B. Kim, Vibrational Spectroscopy. 37 (2005) 33.

[14]. A. Turkovic, M. Ivanda, S. Popovic, A. Tonejc, M. Gotic, P. Dubcek, S. Music, J. Mol. Struct. 271 (1997) 410.

[15]. S. Music, M. Gotic, M. Ivanda, S. Popovic, A. Turkovic, R. Trojko, A. Sekulic, K. Furic, Mater. Sci. Eng. B. 47 (1997) 33.

[16]. J. Goldstein, Scanning electron microscopy and x-ray microanalysis. Kluwer Adacemic/Plenum Pulbishers, (2003) 689.

[17]. L. Reimer, (1998) Scanning electron microscopy: physics of image formation and microanalysis. Springer, (1998) 527.

[18]. R. F. Egerton, Physical principles of electron microscopy: an introduction to TEM, SEM, and AEM. Springer, (2005) 202.

[19]. R. F. Egerton, Physical principles of electron microscopy: Springer, ISBN 0387258000, (2005).

[20]. H. H. Rose, "Optics of high-performance electron Microscopes" Science and Technology of Advanced Materials. 9 (2008).

[21]. T. Hatakeyama, F. X. Quinn, Thermal analysis: fundamentals and applications to polymerscience. 2. ed Chichester: John Wiley & Sons, (1999) p.180 ISBN 0471983624.

[22]. W. J. D. Santos, Scientia Plena. 5 (2009) 064402.

[23]. T. A. Carlson, Photoelectron and Auger Spectroscopy, Plenum Press. (1975).

[24]. P. M. A. Sherwood, D. Briggs, M. P. Seah, Practical surface analysis, Wiley, Newyork (1990).

[25]. J. Matta, D. Courcot, E. Abiaad, A. Aboukais, Chem. Mater. 14 (2002) 411.

[26]. R. A. Wilson, H. A. Bullen,Y. Sugimoto, P. Pou, M. Abe, P. Jelinek, R. Pérez, S. Morita, O. Custance, Nature. 446 (2007) 7131.

[27]. G. Ertl, H. Koninger, J. Weitkamp, Handbook of Heterogeneous Catalysis, Vol. 2, VCH, Weinheim (1997) 646.

[28]. P. Kubelka, F. Munk, Tech. Phys. 12 (1931) 593.

[29]. S. Brunauer, P. H. Emmette, E. Teller, J. Am. Chem. Soc. 60 (1938) 309.

.....ഇ൦ര.....

Chapter 3

Physico – Chemical Characterization

Contents

3.1. Introduction

Characterization is an inevitable part of materials research. Determination of physico-chemical properties of the prepared materials using suitable characterization techniques is very crucial to find its exact field of application. Characterization of solid surface requires the use of analytical techniques which are useful to detect low quantity of the material and to differentiate between the information from the surface and that originating from the bulk. Usually information is searched on the roughness of the surface, its structure, chemical composition and quantitative distribution of the elements. In heterogeneous catalysis, most of the reactions take place on the surface. Surface compositions of most materials are differing from that of the bulk. In catalytic reactions, activity and selectivity are two important parameters that determine how good a catalyst is. Research on catalyst composition, structure of the framework of the solid and nature of its porosity are essential parameters to correlate with catalyst performance. Understanding of structure-property for existing catalyst is very useful in the design of more

efficient ones. The above goals can be achieved with the help of powerful characterization techniques. Ultimately, characterization (diagnostic) techniques are now useful for measuring the shape, chemical, physical, micromechanical properties, composition and chemical states of any solid surface [1-6]. Understanding of catalysts structure and texture is of vital significance for optimizing catalysts with respect to performance and life time. This chapter gives an account of the most relevant methods employed to characterize the size, shape, structure and composition of the materials prepared. Various types of spectroscopy, diffraction and imaging techniques were used to achieve the goal of determining and understanding quantitative structure/composition-activity/ selectivity relationships. These detailed investigations are necessary to design new and efficient catalysts for the sustainable production of chemicals as well as for the effective removal of the harmful compounds in industrial processes.

Here we have prepared different metal/non-metal modified TiO_2 systems via hydrothermal route for photocatalytic applications. During synthesis, Titanium isopropoxide to urea were taken in a 1:1 molar ratio in all the catalysts and varied the amount of metal content. We have applied all these catalysts for photocatalytic applications and studied various parameters affecting its efficiency. Before that the prepared systems were characterized thoroughly by various physico-chemical techniques and these results will be discussed in this chapter.

3.2. Physical Characterization

3.2.1. X-ray Diffraction Analysis (XRD)

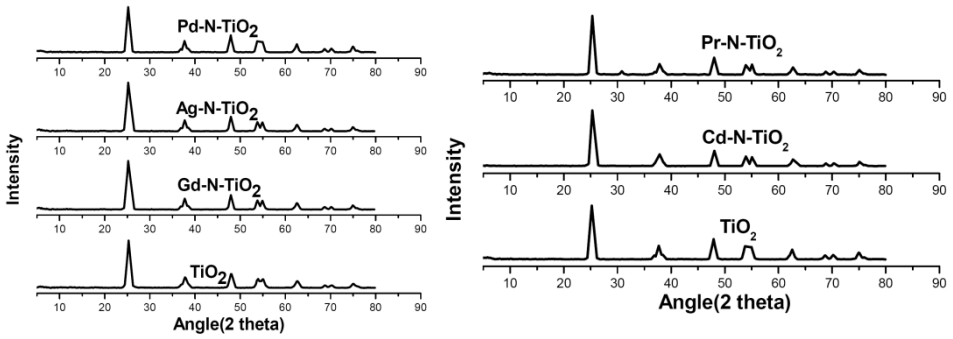

Fig. 3.1. XRD spectra of pure and co-doped TiO_2

XRD is the most widely used nondestructive technique for determining the crystallographic phases present in the sample. It also gives information regarding phase purity, crystallite size, defects, presence of impurities etc. Fig. 3.1 represents the XRD patterns of pure TiO_2 and the co-doped TiO_2 systems calcined at 500°C. It is clear from the pattern that photocatalytically active anatase phase dominates in the calcined samples with peaks at 2θ values around 25.4°, 38°, 48.1°, 55.2° and 62.7° corresponding to (101), (004), (200), (211) and (204) crystal planes (JCPDS 21-1272) respectively [7]. But in the case of Pr-N-Ti sample, a new peak was observed at 2θ = 30.8° corresponding to the (121) plane of the polymorph brookite. There are no visible peaks corresponding to dopants which may be due to their low concentration or it is an indication of the better dispersion of impurities in the TiO_2 [8]. Calcination of the samples resulted in sharp and intense peaks of anatase. This is an indicative of the highly crystalline nature of the prepared catalysts. The influence of low concentration of impurities on the crystal structure of

TiO_2 is marginal. But higher concentration sometimes changes the crystallite size, width and position of the diffraction peaks. Crystallite size is a measure of the size of a coherently diffracting domain. Crystallite size of the sample was calculated from Scherrer equation by using full width at half maximum (FWHM) of the (101) peak of the anatase phase. It is related inversely to the FWHM of an individual peak. Crystallite size cannot be affected by small concentration of impurities but higher concentration sometimes decreases the crystallite size. The average crystallite size was calculated by Scherrer equation which is given by

$$D_{hkl} = \frac{0.9\lambda}{\beta Cos\theta} \quad \text{---------- (3.1)}$$

Where D_{hkl} is the crystallite size, θ and λ are the Bragg angle and wavelength of X-ray used. 'β' is the full width at half maximum (FWHM) of the individual peak. But the crystallite size of all the co-doped TiO_2 was found to be lower than that of bare TiO_2 which indicates that the doping of metal ions having higher ionic radius into the lattice of TiO_2 causes some lattice distortion which suppresses the growth of TiO_2 nanoparticles. Strain energy accumulated in the crystal due to the introduction of larger metal ions also inhibits the phase transition from anatase to rutile. The crystallite size of all the prepared co-doped samples is about 11-14 nm which is lower than that of pure TiO_2. Compared to pure TiO_2, the peak width of all the co-doped samples are somewhat broadened. Lower crystallite size shows a random arrangement having low degree of periodicity which results in the peak broadening. The crystallite size calculated is tabulated in Table 3.1.

Table. 3.1. Crystallite Size, Band Gap and Surface Area of the Prepared Systems

Catalyst	Crystallite Size (nm)	Band Gap (eV)	$S.A_{BET}$ (m^2/g)
TiO_2	16	3.2	59.0
Gd-N-Ti	11.5	2.1	90.0
Pd-N-Ti	12.4	2.2	82.7
Ag-N-Ti	12.9	2.53	76.1
Pr-N-Ti	13.6	2.63	70.0
Cd-N-Ti	14.0	2.71	68.5

3.2.2. Raman Spectroscopy

Raman spectroscopy is a sensitive technique employed to investigate the surface homogeneity and the nature of the crystallographic phases. Fig.3.2 represents the Raman spectra of pure TiO_2 and the prepared co-doped catalysts. The structural identity of the prepared systems obtained from XRD pattern is further confirmed by Raman spectra measurements. Anatase has six Raman active modes. Well resolved Raman peaks at 143 cm^{-1} (E_{1g}), 197 cm^{-1} (E_{2g}), 399 cm^{-1} (B_{1g}), 540 cm^{-1} (combination of A_{1g} and B_{1g}) and 639 cm^{-1} (E_g) in the spectra of calcined samples point to the presence of anatase phase [10]. Absence of Raman peaks corresponding to metal ions and N indicates the homogeneous structure of the prepared samples with minor lattice distortion, since a severe lattice distortion generally leads to the splitting of Raman modes. Sharp and intense peaks at low wave numbers confirmed the presence of nanoparticles in the crystalline state. Raman peak at about 145 cm^{-1} is observed for all the samples which is attributed to the main E_g anatase vibration mode. Maximum of the lowest vibrational Raman mode is used to understand the nanoparticle size since the location of Raman peaks and their widths are affected by particle size, known as quantum size confinement effect

[10,11]. The intensity of the lowest vibration peak at 145 cm^{-1} was found to be increased and its width broadened after the addition of dopants [12-14]. This suggests an enhanced crystallite property and a reduction in particle size.

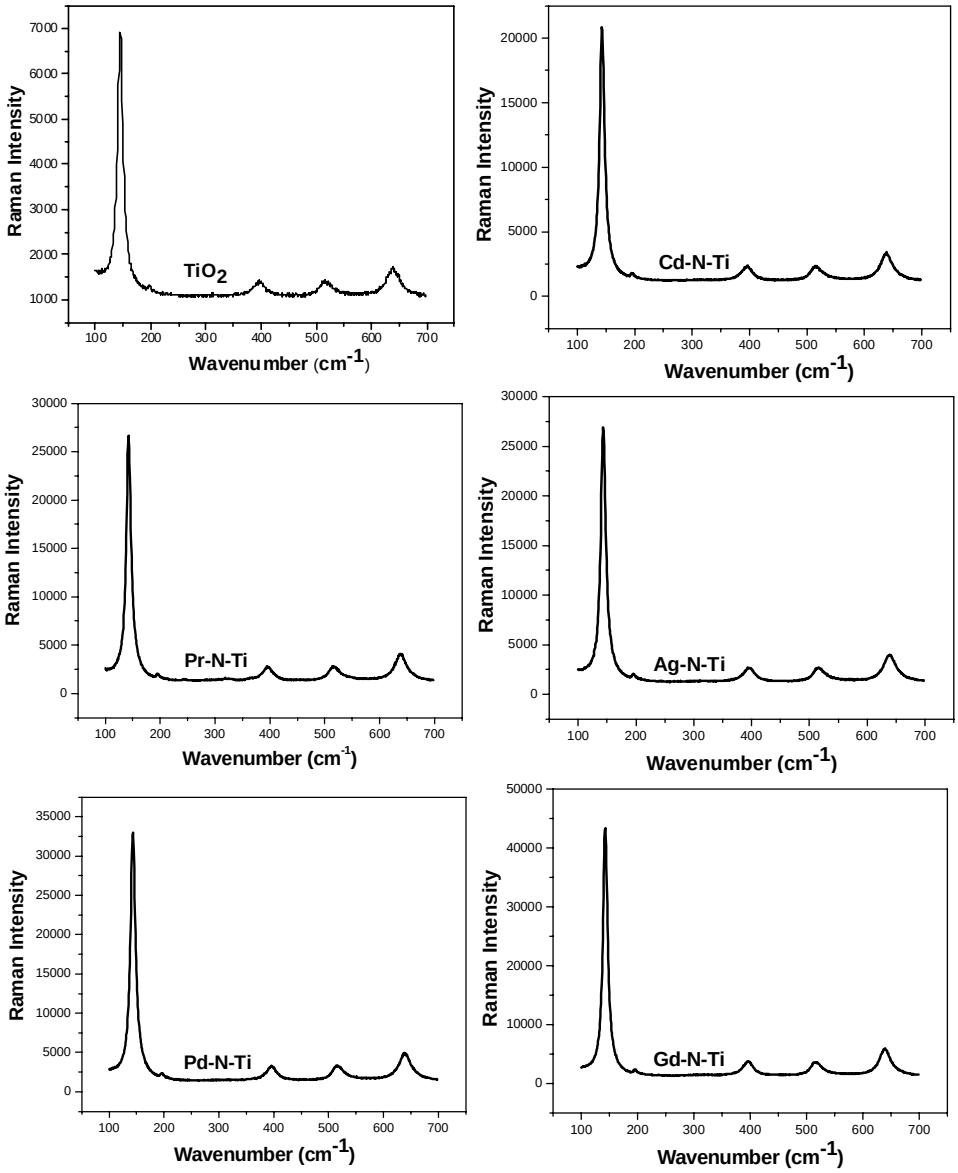

Fig. 3.2. Raman Spectra of Pure TiO_2 and co-doped Catalysts

3.2.3. UV-Visible Diffuse Reflectance Spectroscopy (UV-Vis.DRS)

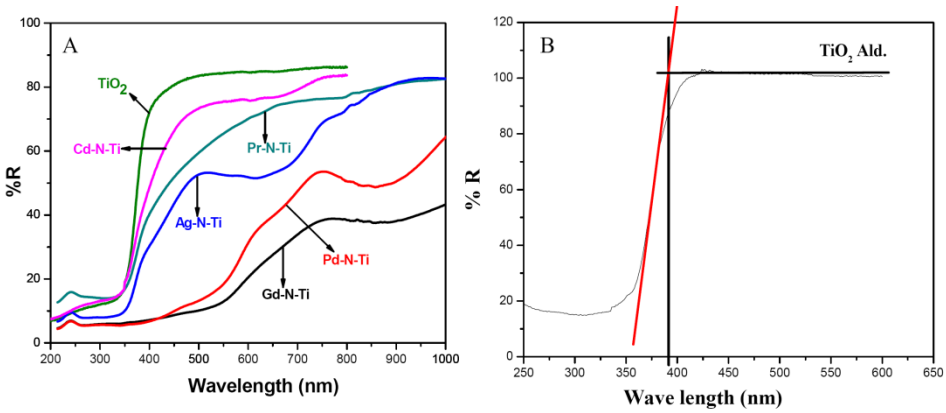

Fig. 3.3. (A) UV-Vis. DRS Spectra of TiO_2 and co-doped catalysts (B) slope method for the determination of band gap

UV-Vis. Diffuse reflectance spectroscopy is a widely used technique to study the light response of the insoluble solid materials. It also gives information regarding active phase-support interactions, chemical changes during modification etc. Metal centered d-d transitions and charge transfer transitions can be perfectly differentiated by UV-DRS. The most appropriate theory behind diffuse reflections and transmission of light scattering layers is developed by Kubelka and Munk [15,16]. For a thick, opaque layer the Kubelka-Munk equation can be written as

$$F(R\alpha) = (1-R\alpha)^2 / 2R\alpha = k/s \text{----------} \quad (3.2)$$

Where 'Rα' is the diffuse reflectance of the layer relative to a non-absorbing standard such as $BaSO_4$, 'k' is the molar absorption coefficient and 's' is the scattering coefficient.

Fig. 3.3.(A) represents the UV-Vis. DRS of pure TiO_2 and the co-doped systems. Spectral response of pure titania is in the UV region but all the co-doped samples have exhibited a red shift and increased absorbance in the visible region. A strong and broad absorption observed below 400 nm in pure TiO_2 is associated with charge transfer from the valance band to the conduction band of TiO_2 [17]. It has been reported that metal could form a new energy level within the band gap of TiO_2. The electronic transition from valance band to impurity level or from the newly formed level to conduction band can effectively extend the band edge absorption threshold [18]. In the co-doped system, nitrogen may be present in the substitutional and interstitial position of the semiconductor which leads to a reduced band gap by mixing with O2p states and generating an isolated impurity level above the valance band. The presence of some surface nitrogen species creates oxygen vacancies which are also responsible for the visible light absorption [19-22]. The higher red shift for the co-doped samples shows that the co-doping of metal and non-metal exhibits distinct synergistic effects. The band gaps of the co-doped systems were calculated by the equation, $E_g = 1240 / \lambda$ [23]. This is one of the simple versions of Kubelka- Munk equation where 'λ' is the wavelength from which reflection has taken place. The band gaps of the co-doped systems were calculated using this equation and are tabulated in Table 3.1. The band gap reduction indicates the successive incorporation of dopants into the lattice of the semiconductor material. Lower or somewhat similar ionic radii of the dopants facilitate substitutional doping at cationic as well as anionic sites which is responsible for the better reduction of the band gap. Fig.3.3. (B) shows the pictorial representation of slope method used for the determination of band gap.

3.2.4. Thermal Analysis

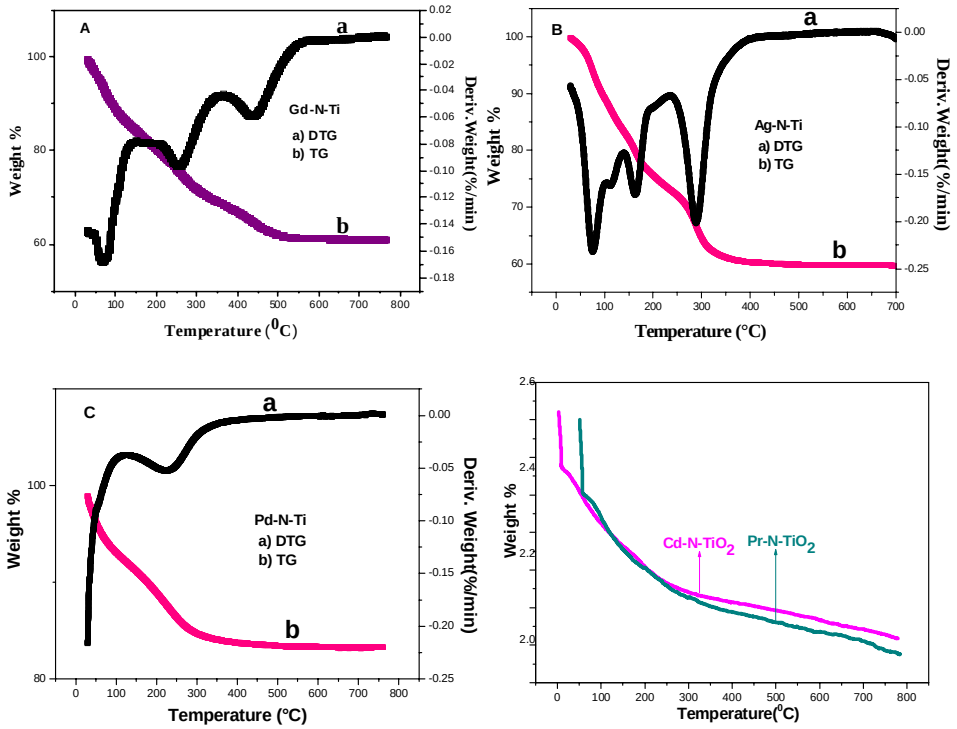

Fig. 3.4. TG/DTG curves of co-doped catalytic systems

Thermo gravimetric analysis is a well-known technique for determining the thermal stability of the prepared systems.

Fig. 3.4. represents the TG-DTG curves of pure and co-doped systems. Thermo gravimetric analysis was carried out to study the thermal decomposition process of the precursor and stability of the prepared systems. This also gives information regarding phase change, hydration etc. Mass changes occur in a variety of ways and this produces steps in thermo gravimetric analysis (TGA) or peaks in the differential thermo gravimetric (DTG) curve (Fig.3.4). Fig. 3.4. (A) represents the TG/DTG curves of Gd-N-Ti system. A weight loss in the range of 76-110°C is assigned to the loss of adsorbed water. Another weight loss in the range of 144-190°C

represents the initial decomposition of urea. A very sharp and narrow weight loss located around 244-320°C indicates the complete decomposition of gadolinium nitrate and urea. After 400°C there is no noticeable weight loss on TG which indicates the stability of the catalyst and hence the calcination temperature was fixed at 500°C. Fig. 3.4. (B) represents the TG/DTG of Ag-N-Ti system. Three major weight losses located below 350°C is due to the decomposition of the adsorbed water and precursor molecules. After that the compound was found to be stable so that we fixed again the calcination temperature as 500°C. Pd-N-Ti system also shows some weight losses below 350°C and there is no major weight loss above that temperature. TG curves of Pr-N-Ti and Cd-N-Ti also show some weight losses below 400°C which indicates the stability of these systems above that particular temperature.

3.2.5. FT-IR Spectra

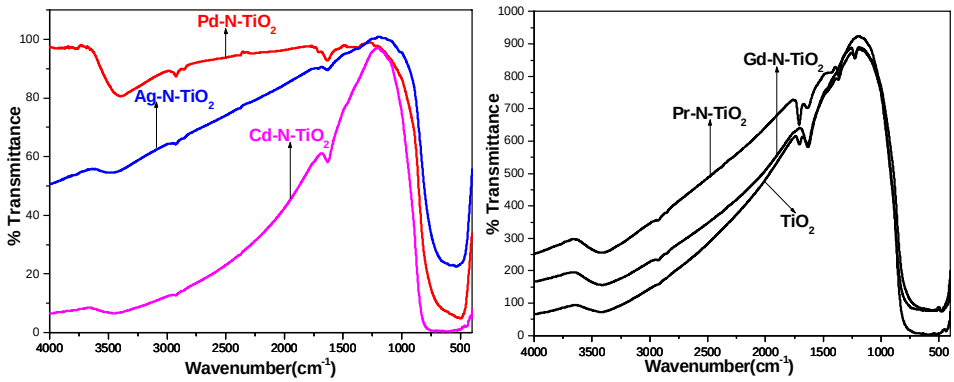

Fig. 3.5. FT-IR Spectra of co-doped Catalytic Systems

FT-IR spectra were performed to understand the functional groups as well as to study the surface changes occurred during modification.

The presence of adsorbed water and surface hydroxyl groups were identified from IR spectroscopy results. The band around 3390-3415 cm^{-1} was attributed to the stretching vibrations of the O-H group and the bands

appearing at 1630 cm^{-1} were the bending vibrations of O-H group which are mainly due to the adsorbed water [24,25]. After modification with metals, a clear increase of the intensity of O-H bands is observed showing an increase in the surface O-H groups. This surface hydroxylation enhances the photocatalytic ability of titania because it improves the oxygen adsorption capacity [26,27]. Molecular oxygen on the surface sometimes acts as the scavenger for conduction band electrons and facilitates the formation of superoxide anion. The photoexcited holes react with water or surface hydroxyl groups to form hydroxyl radical which could be considered as one of the reactive species in photocatalytic reactions. The main band around 590 cm^{-1} is due to the Ti-O and O-Ti-O stretching vibrations of titania [28]. No absorption corresponding to the dopant species were observed due to their low concentration.

3.2.6. Energy Dispersive X-ray Analysis

EDX is a qualitative technique used to estimate the elemental composition of various samples. It is also useful to detect the traces of other materials such as dopants or adducts. Here metals and non-metals were added as the impurities in order to change the spectral response of TiO_2 systems. The intensity of the peaks correlates with the amount of elements present in the sample. The EDX spectra of all the co-doped samples show signals directly related to the dopants. Spectra of all the co-doped systems contain O and Ti as the major components with low concentrations of doped elements. Atom percentage of the impurities such as metals and non-metals present in the co-doped samples were calculated and are tabulated in Table 3.2. This confirmed the successive incorporation of both the dopants into the TiO_2 system. In these systems, the percentage of

all the metal dopants was 1wt%. But depending on the nature of dispersion of metals, the percentage of incorporation may also vary and that in turn affects the incorporation of the second impurity (Table 3.2).

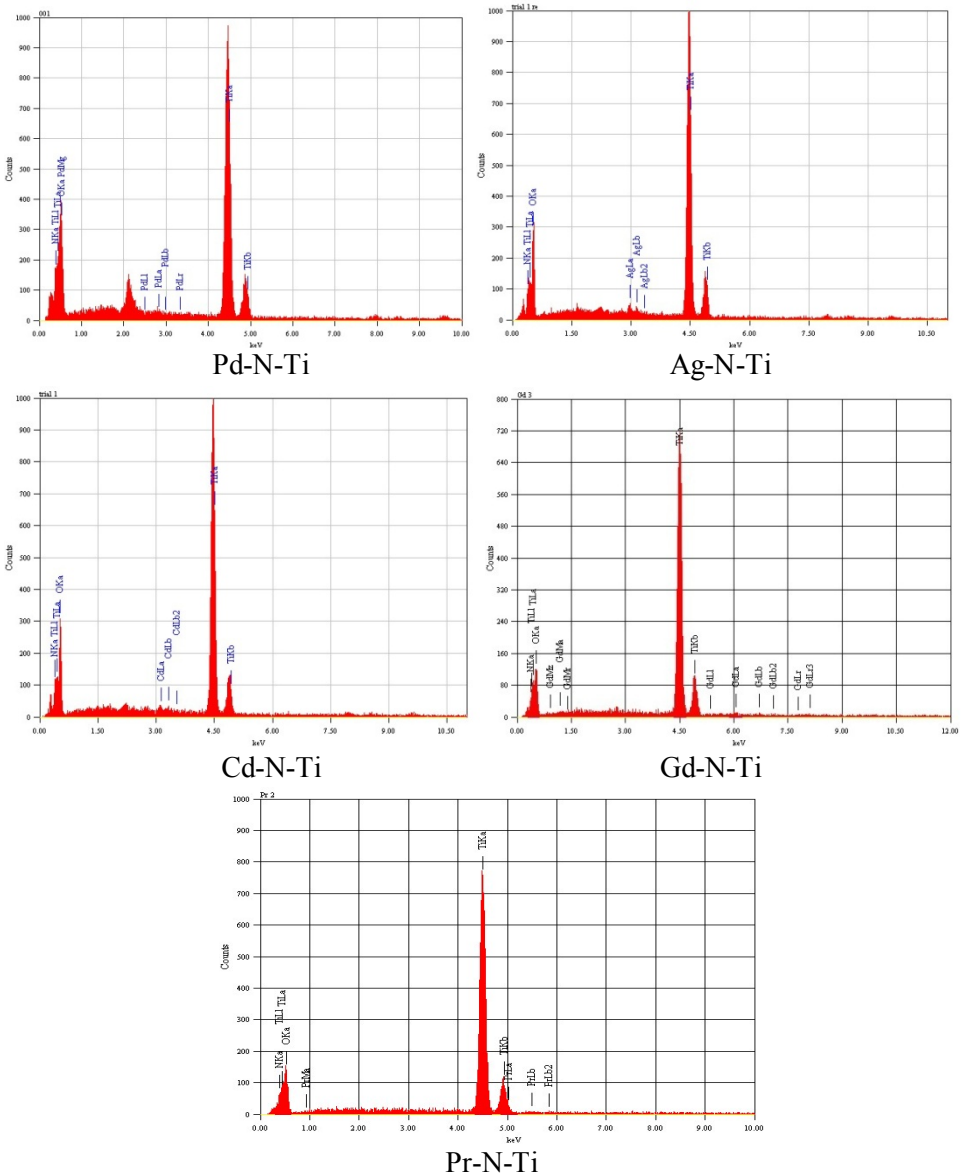

Fig. 3.6. EDX Patterns of co-doped Systems

Table 3.2. Percentage of incorporation of doped species

Name of the Catalyst	% of Dopants	
Pd-N-Ti	N- 2.74	Pd- 0.70
Ag-N-Ti	N- 0.60	Ag- 2.48
Cd-N-Ti	N- 0.74	Cd- 1.00
Gd-N-Ti	N- 0.84	Gd- 1.10
Pr-N-Ti	N- 0.54	Pr- 0.76

3.2.7. Scanning Electron Microscopy

Surface morphology of the co-doped catalysts was evidenced from SEM images (Fig. 3.7). Knowledge of surface morphology helps in interpreting photocatalytic reactions because in heterogeneous catalysis almost all reactions take place on the surface of the catalyst. Catalyst morphology can sometimes affect the light absorption ability and generation of excitons which in turn gets reflected in its efficiency. Preparation procedure and composition may change the surface morphology. The prepared samples (Fig.3.7) consist of nearly spherical particles with some degree of aggregation. The shapeless structures in the image are mainly due to aggregation which may occur during hydrothermal synthesis. Particle aggregation results in an increase of particle size thereby decreasing the surface area. However these aggregates cannot negatively influence the catalytic activity because photocatalysis depends on various other factors.

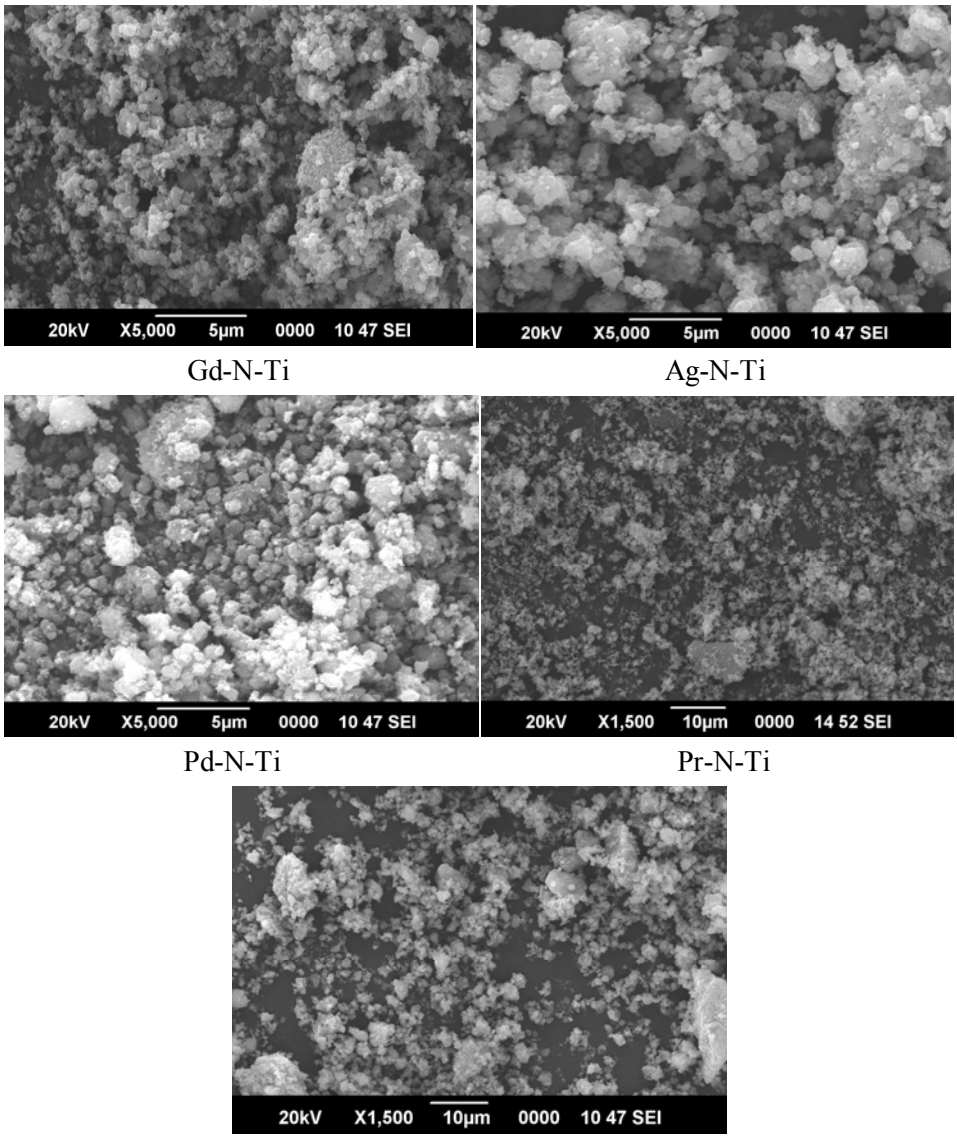

Gd-N-Ti Ag-N-Ti

Pd-N-Ti Pr-N-Ti

Cd-N-Ti

Fig. 3.7. SEM Micrographs of the co-doped Systems

3.2.8. Transmission Electron Microscopy

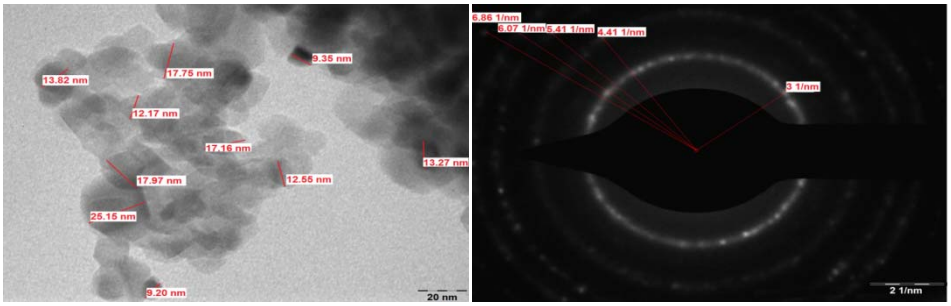

Gd-N-Ti

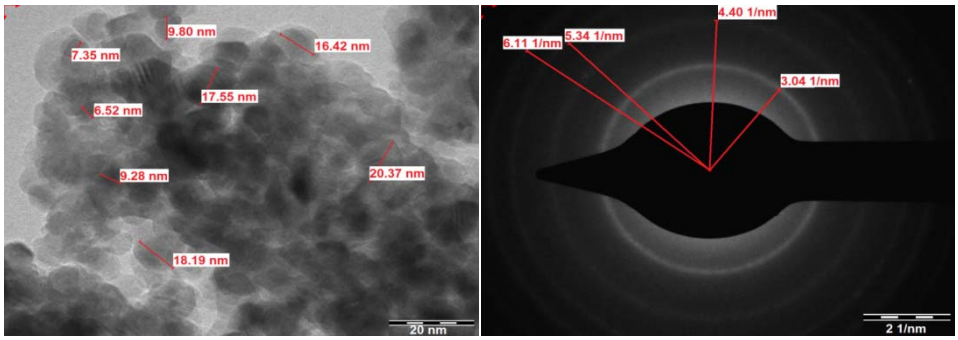

Pd-N-Ti

Fig. 3.8. TEM Images of Gd-N-Ti and Pd-N-Ti Systems

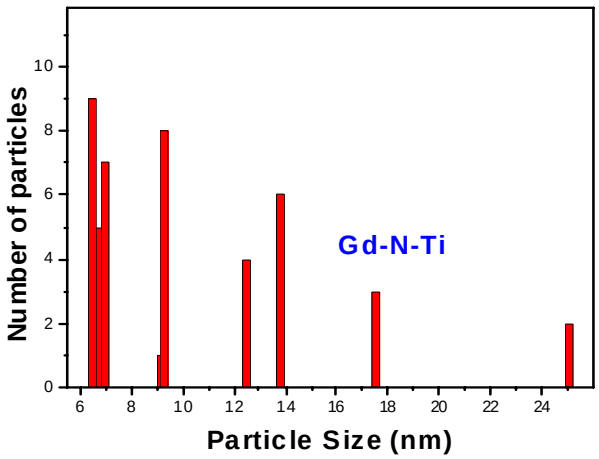

Fig.3.9. Particle Size Histogram of Gd-N-Ti

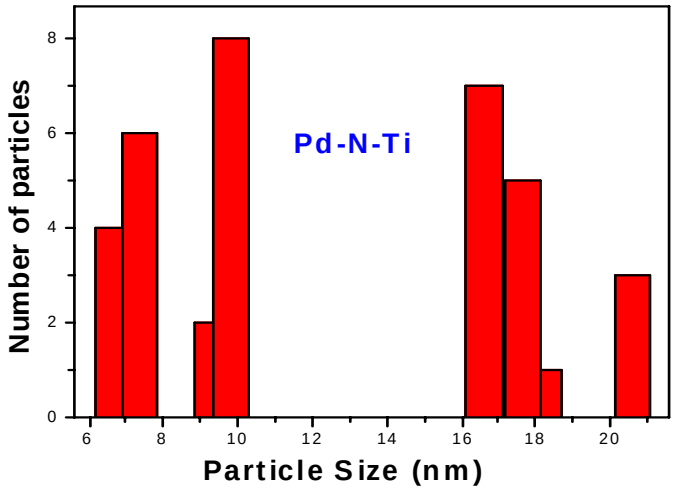

Fig.3.10. Particle Size Histogram of Pd-N-Ti

Fig.3.8 shows the TEM images of Gd-N-Ti and Pd-N-Ti systems. Figure showed irregularly shaped structures due to the agglomeration of particles during hydrothermal synthesis. These results are in good agreement with the results of SEM micrographs. Adsorption of reactants takes place effectively on modified TiO_2 due to its surface roughness and high surface area. Fig.3.9 represents the particle size histogram of Gd-N-Ti system. Particles having size ranging from 6.5 nm to 25 nm was observed from the image. Non-uniform nature of the sample was evidenced from this histogram data. The average particle size was calculated to be around 12 nm, well in accordance with the crystallite size obtained from XRD results. Selected area electron diffraction (SAED) also supported the crystalline nature of the co-doped system. Fig.3.10 represents the histogram of Pd-N-Ti system. Particle having size ranging from 6.6 nm to 20 nm was observed from the image. Average particle size was calculated based on this histogram and that was found to be 13.3 nm which is also in good agreement with the XRD results.

3.2.9. X-ray Photoelectron Spectroscopy (XPS)

XPS is a commonly and widely used technique for surface analysis due to its simplicity in use and data interpretation. Here spin orbit splitting and peak area ratios are the two factors responsible for determining the elemental composition. Peak area ratio and spin orbit splitting of an element that present in different compounds are the same. Fig.3.11. shows the survey scan of Gd-N-Ti and its high resolution scan over various core levels such as Ti2p, O1s, Gd3d, Gd4d and N1s. Two peaks observed at 458 eV and 464 eV corresponding to the $Ti2p_{3/2}$ and $Ti2p_{1/2}$ levels conformed Ti^{+4} species with stable Ti-O bond in the co-doped system (Fig.3.11a). These two peaks are mainly due to the spin-orbit splitting of Ti2p [29]. A small Ti3p peak at 37.2 eV again confirmed the presence of Ti^{4+}as an oxide. There is no evidence for the presence of Ti^{3+} species in the system. Compared to pure TiO_2, the Ti2p peaks of Gd-N-Ti show a small shift in binding energy. Shift of Ti2p core levels suggesting the successful incorporation of dopants in the titania lattice [30]. High resolution spectra of gadolinium show two peaks at binding energy values 1186.3 eV and 1218.7 eV (Fig.3.11b). These spin orbit doublets separated by a binding energy difference of 32 eV represents the $Gd3d_{5/2}$, $Gd3d_{3/2}$ respectively and $3d_{5/2}$ peak has a full-width-half-maximum (FWHM) of 5.6 eV indicative of multiple bonding states. The normal doublet structure observed for other rare earths due to bonding and antibonding states between final state configurations is not well resolved for trivalent Gd [31-33]. The marginal energy difference indicates a higher degree of mixing between these two states and the core-valence intra-atomic exchange is dominated by the 3d core-4f exchange interaction [34]. An additional peak was observed at binding energy of

143 eV which corresponds to the Gd4$d_{5/2}$ core level (Fig.3.11c). Along with this, a shoulder was observed at a binding energy around 148 eV which corresponds to the Gd4$d_{3/2}$ core level (Fig.3.11c). Broad $4d_{5/2,3/2}$ spin-orbit pair manifested the existence of p-f bonding-antibonding states. Multiplet structures produced due to Gd 4d-4f interaction are also included in the spectrum and this 4d-4f interaction is strong as the 4d spin-orbit coupling [35]. N1s signals are observed at binding energy values of 396.3 eV, 399 eV and 402.8 eV as shown in the figure 3.11e. The peak at 396.3 eV (Fig.3.11e) was due to the substitutional doping of Nitrogen atoms at oxygen sites in the titania system [36]. The signal at a binding energy of 399 eV (Fig.3.11e) is attributed to the O-Ti-N linkage in the system [37]. Higher binding energy value of nitrogen around 402.8 eV (Fig.3.11e) represents the presence of some surface nitrogen species [38]. The valence band of titania is constructed with O2p state which is hybridized with the Ti3d states [39]. O1s signal at 530 eV represents the O^{2-} ion ($O1s_{1/2}$) in the lattice of TiO_2 ((Fig.3.11d). Another shoulder peak at 532 eV (Fig.3.11d) indicates the presence of surface hydroxyl groups. So XPS gives strong support for the incorporation of both the dopants in the titania system.

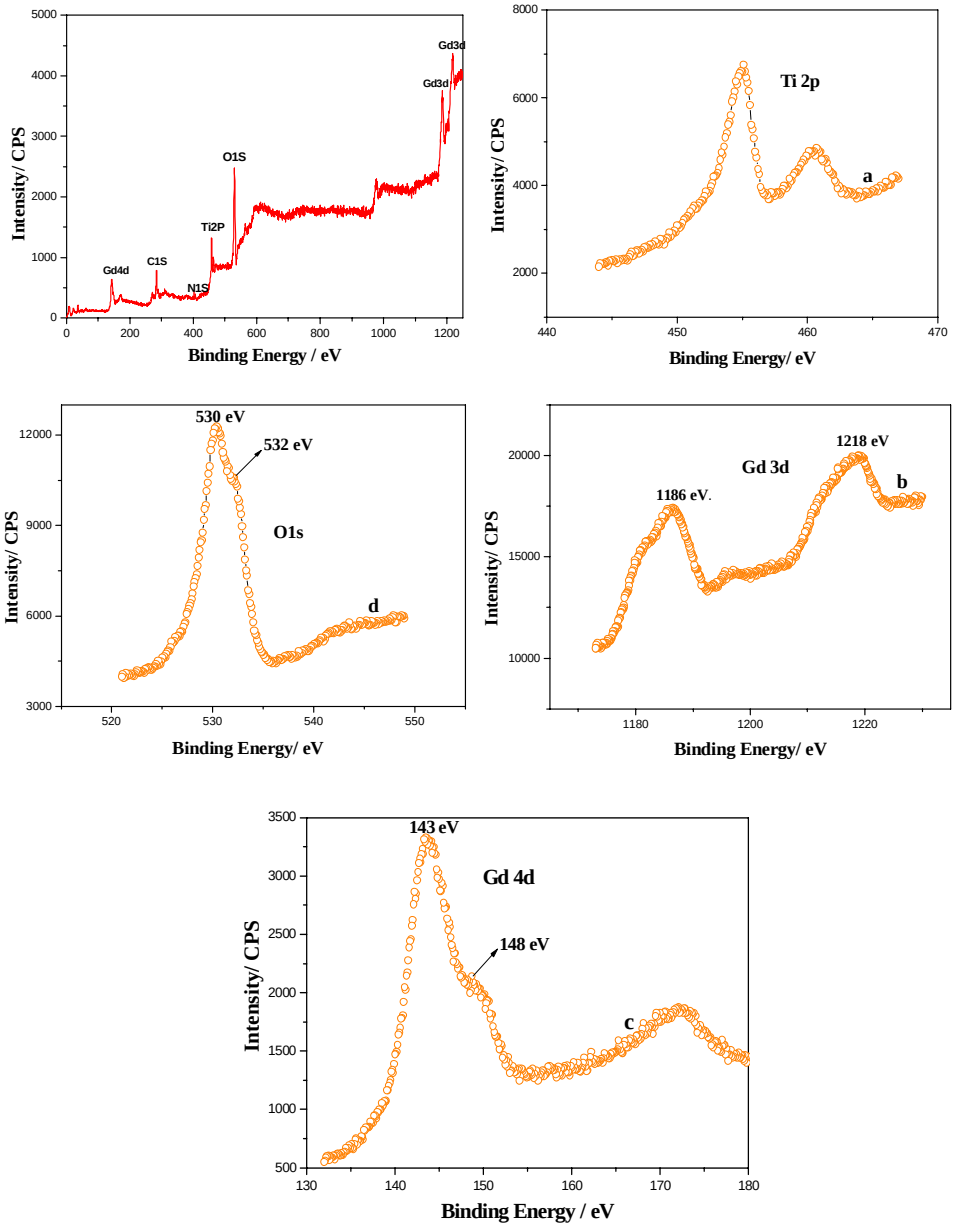

Fig.3.11. XPS Spectra of Gd-N-Ti System

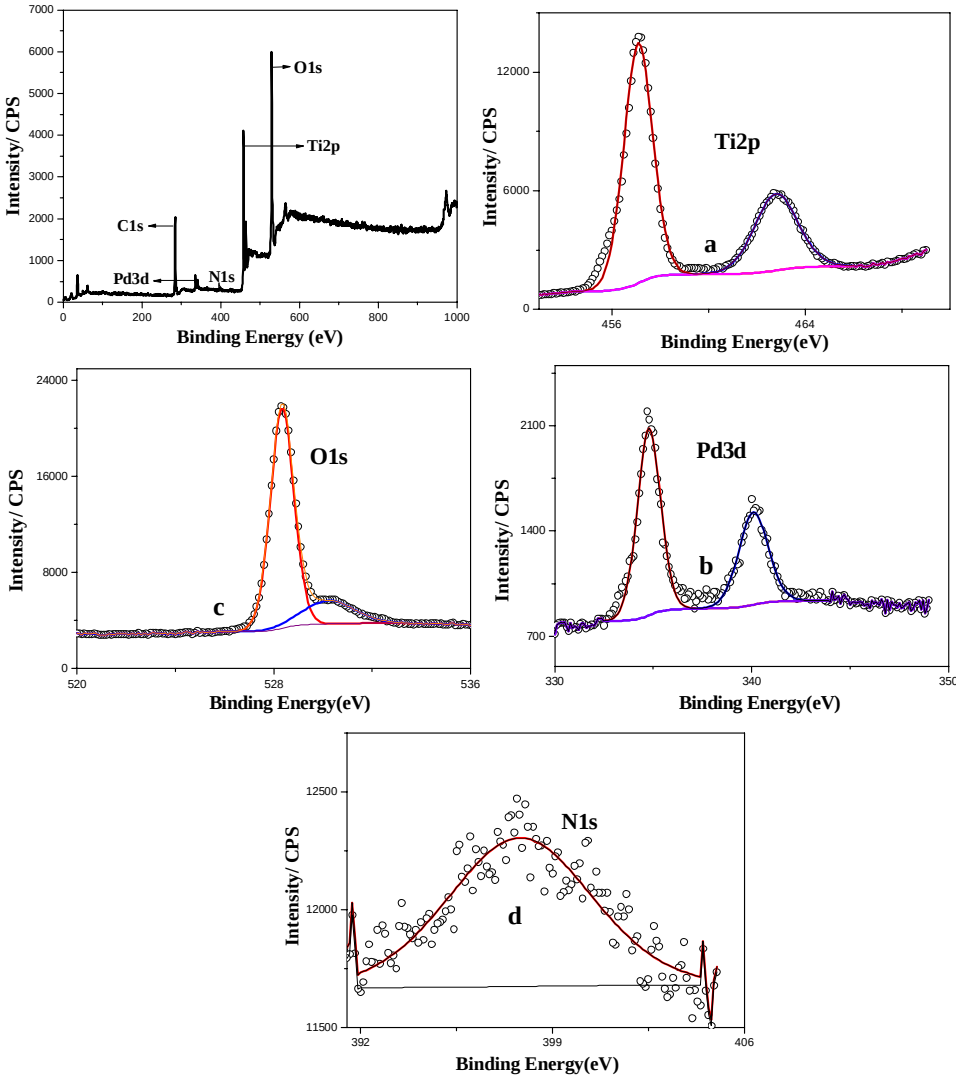

Fig. 3.12. XPS Spectra of Pd-N-Ti System

Fig. 3.12 shows the survey scan and core levels of individual elements present in Pd and N co-doped TiO_2 system. Binding energy corresponding to Ti2p, Pd3d, N1s and O1s core levels can be seen from the survey scan of co-doped system (Fig.3.12). Two intense peaks observed at binding energy values around 456 eV and 464 eV corresponding to the $Ti2p_{3/2}$ and $Ti2p_{1/2}$ levels conformed the Ti^{+4} species in the co-doped

system (Fig.3.12a). Shift of Ti2p core levels suggests the successful incorporation of dopants. The binding energies of $Pd3d_{5/2}$ (334 eV) and $3d_{3/2}$ (341 eV) revealed that palladium was in the form of PdO in the prepared system [40] (Fig. 3.12b). The added Pd was oxidized to PdO in the preparation procedure. The peak at 396.7 eV (Fig.3.12d) was due to the substitutional doping of Nitrogen atoms at oxygen sites in the titania system. O1s signals at 529 eV and 531 eV (Fig.3.12c) indicate the presence of lattice oxygen and surface hydroxyl groups respectively.

Fig. 3.13 represents the survey scan and high resolution peaks of individual elements in Ag-N-Ti system. In pure TiO_2, $Ti2p_{3/2}$ and $Ti2p_{1/2}$ core levels can be observed at binding energies 456 eV and 464 eV with an energy difference of 8 eV confirming the presence of Ti^{+4} species. But the Ag and N co-doped TiO_2 shows $Ti2p_{3/2}$ and $Ti2p_{1/2}$ core levels at 459 eV and 464.8 eV respectively (Fig. 3.13a). The shift of these Ti2p peaks in co-doped TiO_2 suggests the difference in the electronic interaction of Ti with ions and a better incorporation of dopants into the lattice. The binding energies of $Ag3d_{5/2}$ (368 eV) and $3d_{3/2}$ (374 eV) reveals that silver is in the form of AgO in the prepared system (fig. 3.13c). The signal at a binding energy of 399 eV (Fig. 3.13d) is attributed to the O-Ti-N linkage in the system. Higher binding energy of nitrogen around 401.2 eV (Fig. 1.13d) represents the presence of some surface nitrogen species. The major O1s core level at 529 eV and a shoulder at 531 eV (Fig. 3.13b) indicate the presence of lattice oxygen (Ti-O) and oxygen from surface hydroxyl groups respectively.

Fig.3.14. shows the XPS spectra of Pr-N-Ti system. Here also all the binding energies corresponding to Ti2p, O1s, N1s and Pr3d can be seen from the figure 3.14. Here also Ti is in the +4 oxidation state

(Fig.3.14a). Two oxygen species were detected in this system. A peak at binding energy of around 400 eV confirmed the presence of O-Ti-N linkage in the system. $Pr3d_{5/2}$ and $Pr3d_{3/2}$ signals at binding energies of 933 eV and 954 eV confirmed the existence of Pr^{3+} species (Fig. 3.14c).

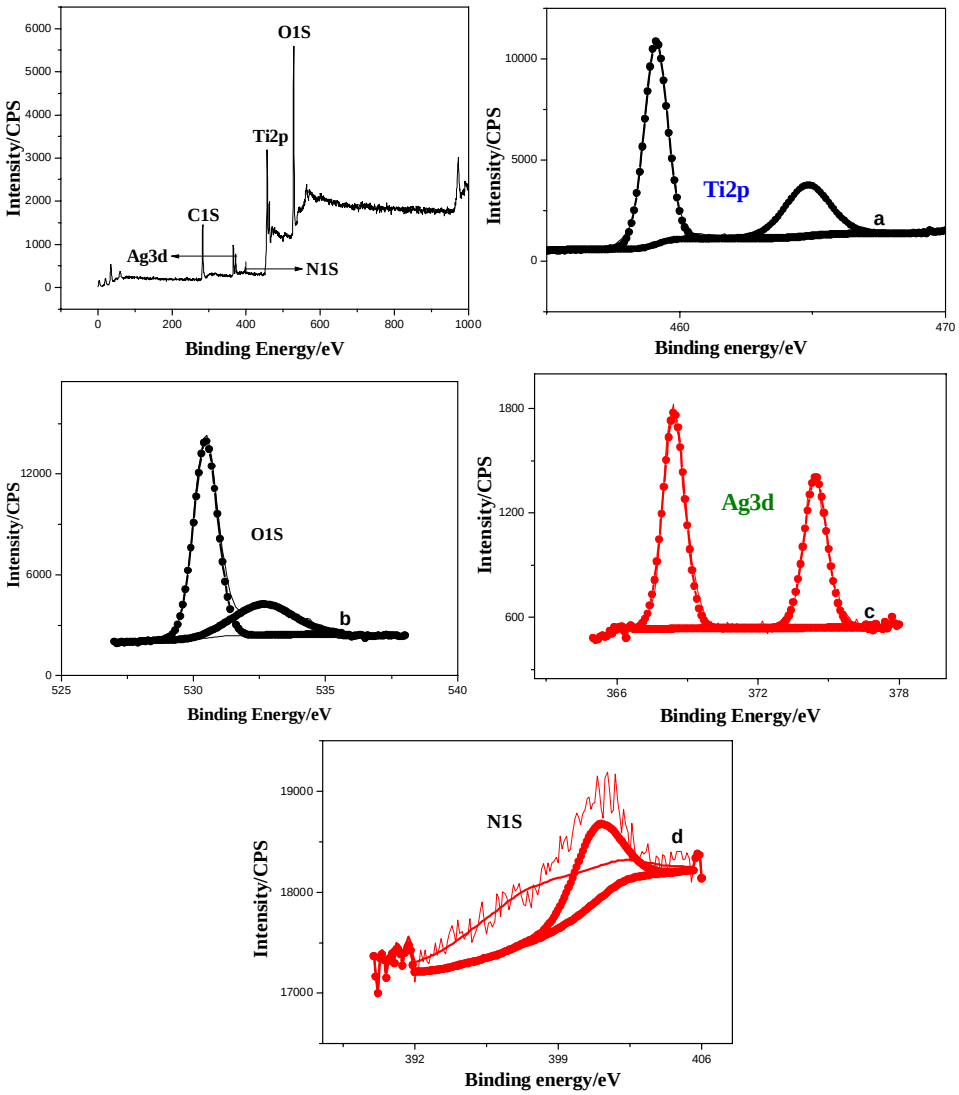

Fig.3.13. XPS Spectra of Ag-N-Ti System

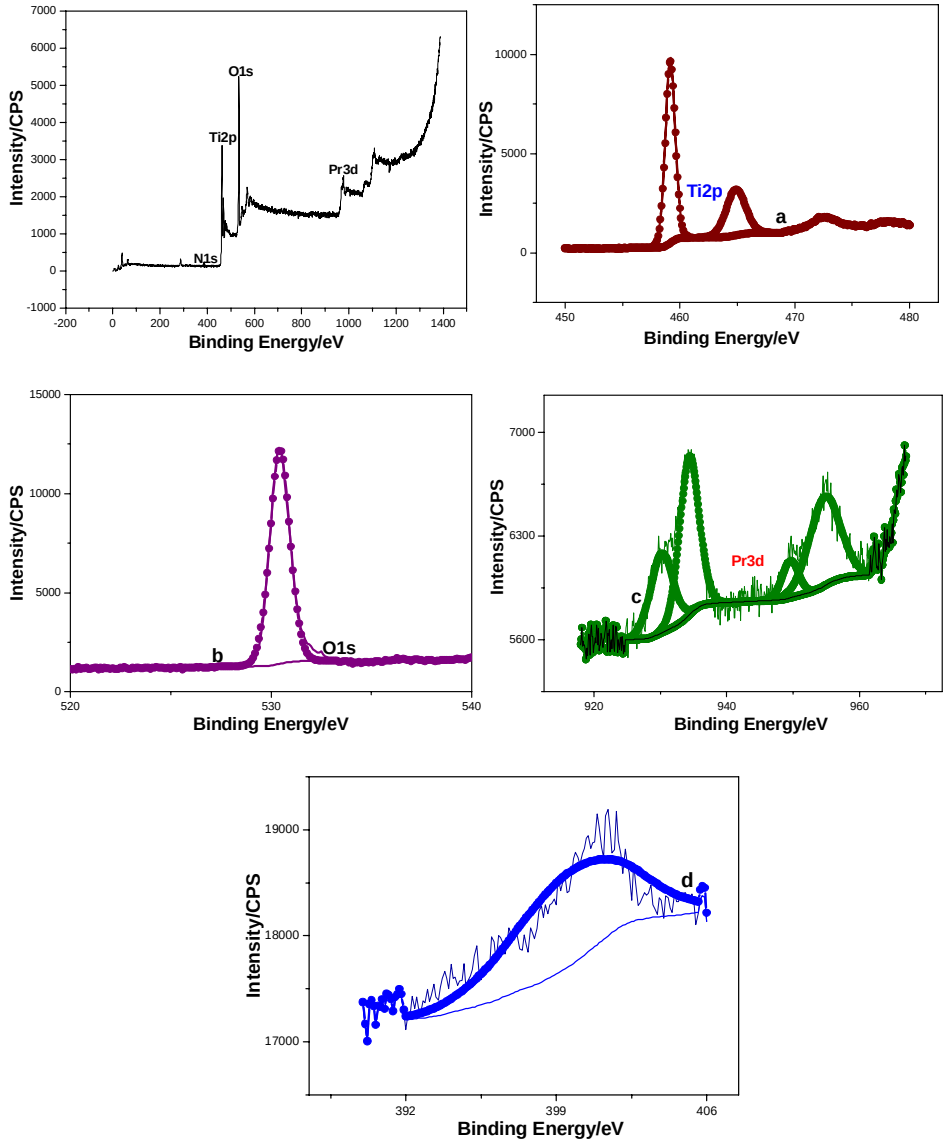

Fig.3.14. XPS Spectra of Pr-N-Ti System

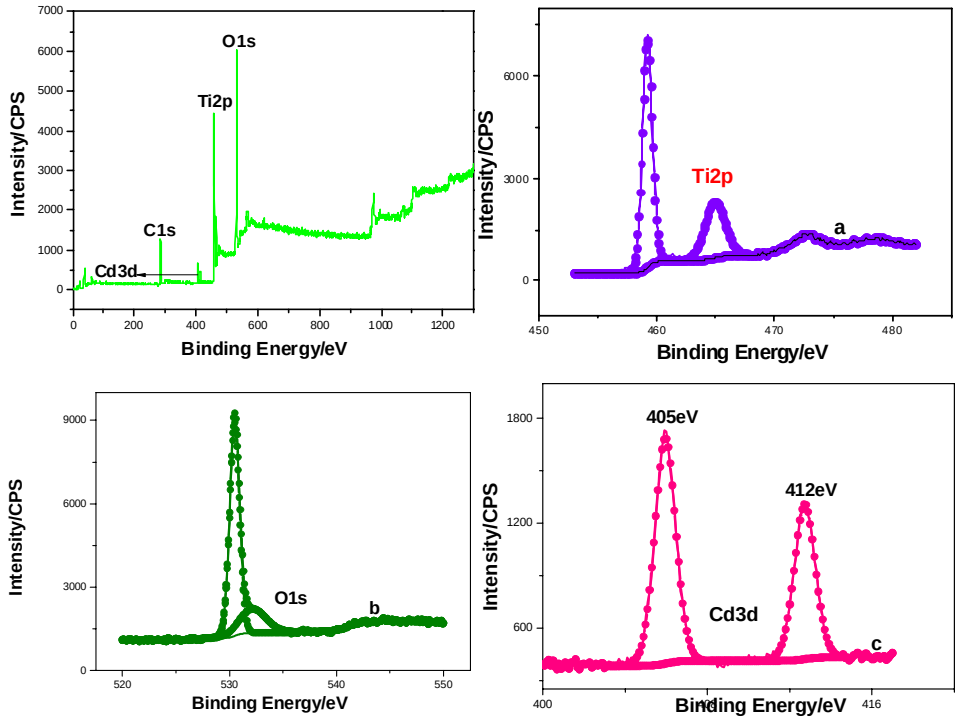

Fig. 3.15. XPS Spectra of Cd-N-Ti System.

Fig.3.15. shows all the high resolution peaks of Ti2p, O1s and Cd3d. Here N was not detected in the survey scan due to the low levels of incorporation of nitrogen after calcination at 500°C or it is below the detection limit of the instrument. Samples were not argon sputtered for surface cleaning prior to analysis. This might have affected the emission from N1s due to superficial contaminants. This does not mean that nitrogen is not there because we have already confirmed the presence of nitrogen by EDX analysis. High resolution peak of Ti2p supported the +4 oxidation state of Ti in the system. O1s spectrum showed two types of oxygen environment. Two signals at binding energy values around 405 eV and 412 eV corresponds to $Cd3d_{5/2}$ and $Cd3d_{3/2}$ respectively (Fig. 3.15c). This result showed that Cd was not incorporated into the TiO_2 crystal

lattice but existed in the form of CdO. This also supported that Cd excluded from the Ti-O framework to the surface and suppressed the crystal growth of anatase phase [41].

3.3. Conclusion

Prepared co-doped systems were characterized by various physico-chemical techniques such as XRD, Raman spectroscopy, TG-DTG, FT-IR, BET, SEM, EDX, TEM and XPS. Structural identity of the systems was observed from XRD and Raman measurements. Thermal stability and functional groups were determined from TG and FT-IR results respectively. Band gap and visible light absorption characteristics of the systems were observed from UV-DRS measurements. Agglomerated nature of the prepared systems was observed from SEM and TEM measurements. Particle size histogram data were used to understand the particle size of the systems and these results were well in accordance with the crystallite size calculated from XRD measurements. Better distribution of the dopants and percentage of dopants were observed from XPS and EDX results respectively.

References

[1]. K. Miyoshi, Y. W. Chung, Surface Diagnostics in Tribology: Fundamental Principles and Applications. River Edge, NJ: World Scientific Publishing Co., (1993).

[2]. T. F. J Quinn, Physical Analysis for Tribology. Cambridge, U.K.: Cambridge University Press, (1991).

[3]. D. H. Buckley, Surface Effects in Adhesion, Friction, Wear, and Lubrication. Tribology Series 5. Amsterdam: Elsevier, (1981).

[4]. W. A. Glaeser, ed. Characterization of Tribological Materials. Stoneham, MA: Butterworth-Heinemann and Manning, (1993).

[5]. C. R. Brundle, C. A. Evans, Jr., S. Wilson, eds. Encyclopedia of Materials Characterization. Stoneham, MA: Butterworth-Heinemann and Manning, (1992).

[6]. D. M. Brewis, ed. Surface Analysis and Pretreatment of Plastics and Metals. New York: Macmillan, (1982).

[7]. S. Song, J. J. Tu, Z. Q. He, F. Y. Hong, W. P. Liu, J. M. Chen, Appl. Catal. A. 378 (2010) 169.

[8]. A. T. Kuvarega, R. W. M. Krause, B. B. Mamba. J. Phys. Chem. C. 115 (2011) 22110.

[9]. A. Golubovic, M. Scepanovic, A. Kremenovic, S. Askrabic, V. Berec, Z. Dohcevic-Mitrovic, Z. V. Popovic, J. Sol-Gel Sci. Technol. 49 (2009) 311.

[10]. A. L. Bassi, D. Cattaneo, V. Russo, C. E. Bottani, E. Bartoriri, T. Mazza, P. Pisen, P. Midani, F. O. Ernst, K. Wegner, S. E. Pratsinis, J. Appl. Phys. 98(7) (2005) 074305.

[11]. D. Bersani, P. P. Lottici, X. Z. Ding, Appl. Phys. Lett. 72 (1998) 73.

[12]. W. Ying, W. Yan, M. Yanling, D. Hanming, S. Yougkui, Z. Xian, T. Xiaozhen, J. Phys. Chem. C. 112 (2008) 6620.

[13]. Y. Shu, A. Yohei, K. Masakazu, W. Jinshu, T. Qing, S. Tsugio, J. Mater. Chem. 15 (2005) 674.

[14]. C. Ye, Z. Jinlong, C. Feng, A. Masakazu, J. Phys. Chem. C. 111 (2007) 6976.

[15]. S. Sakthivel, H. Kisch, Angew. Chem. Int. Ed. 42 (2003) 4908.

[16]. J. E. Herrera, D. E. Resasco, J. Phys. Chem. B. 107 (2003) 3738.

[17]. M. Maicu, M. C. Hidalgo, G. Colon, J. A. Navio, J. Photochem. Photobiol. A. 217 (2011) 275.

[18]. K. Nagaveni, M. S. Hegde, G. Madras, J. Phys. Chem. B. 108 (2004) 20204.

[19]. S. Rehman, R. Ullah, A. M. Butt, N. D. Gohar, J. Hazard. Mater. 170 (2009) 560.

[20]. J. J. Liu, W. Qin, S. L. Zuo, Y. C. Yu, Z. P. Hao, J. Hazard. Mater. 163 (2009) 273.

[21]. R. Asahi, T. Morikawa, Chem. Phys. 339 (2007) 57.

[22]. G. Liu, X. W. Wang, L. Z. Wang, Z. G. Chen, F. Li, G. Q. Lu, H. M. Cheng, J. Colloid Interface Sci. 334 (2009) 171.

[23]. P. Kubelka, F. Munk, Tech. Phys. 12 (1931) 593.

[24]. K. L. Lv, H. S. Zuo, J. Sun, K. J. Deng, S. C. Liu, X. F. Li, D. Y. Wang, J. Hazard. Mater. 161 (2009) 396.

[25]. F. Y. Wei, L. S. Ni, P. Cui, J. Hazard. Mater. 156 (2008) 135.

[26]. B. Ohtani, Y. Ogawa, S. Nishimoto, J. Phys. Chem. 101 (1997) 3746

[27]. C. Anderson, A. J. Bard, J. Phys. Chem. 99 (1995) 9882.

[28]. J. Liu, H. Rong, Y. Zhao, H. Wang, W. Lu, T. Yu, Y. Zhang, J. Phys. Chem. C. 115 (2011) 4507.

[29]. W. Ying, W. Yan, M. Yanling, D. Hanming, S. Yougkui, Z. Xian, T. Xiaozhen, J. Phys. Chem. C. 112 (2008) 6620.

[30]. P. Feng, C. Lingfeng, Y. Hao, W. Hongjuan, Y. Jian, J. Solid state Chem. 181 (2008) 130.

[31]. D. F. Mullica, C. K. C. Lok , H. O. Perkins, G. A. Benesh, V. Young, J. Elect. Spectrosc. Relat. Phenonm. 71 (1995) 1.

[32]. A. Novosselov, E. Talik, A. Pajaczkowska, J. Alloys and Compounds. 351 (2003) 50.

[33]. C. Suzuki, J. Kawai, M. Takahashi, A. M. Vlaicu, H. Adachi, T. Mukoyama, Chem. Phys. 253 (2000) 27.

[34]. A. Nelson, J. Adams, K. Schaffers, Appl. Surf. Sci. UCRL-JRNL-205064, (2004)

[35]. S. P. Kowalczyk, N. Edelstein, F. R. McFeely, L. Ley, D. A. Shirley, Chem. Phys. Lett. 29 (1974) 491.

[36]. R. Asahi, T. Morikawa, T. Ohwaki, K. Aoki, Y. Taga, Science. 293 (2001) 269.

[37]. H. Choi, M. G. Antoniou, M. Pelaez, A. A. De la Cruz, J. A. Shoemaker, D. D. Dionysiou, Environ. Sci. Technol. 41 (2007) 7530.

[38]. S. Sakthivel, H. Kish, Chem. Phys. Chem. 4 (2003) 485.

[39]. Y. Tezuka, S. Shin, A. Agui, M. Fujisawa, T. Ishii, A. Yagishita, J. Elect. Spectrosc. Relat. Phenonm. 79 (1996) 195.

[40]. Q. Li, R. Xie, E. A. Mintz, J. K. Shang, J. Am. Ceram. Soc. 90(12) (2007) 3863.

[41]. H. Gao, B. Lu, F. Liu, Y. Liu, X. Zhao, Int. J. Photoenergy. 2012 (2012) 1.

.....ൠ.....

Chapter 4

Photocatalytic Degradation of Herbicides

Contents

Contamination of the earth's environment by toxic chemicals from various sources to a larger extent is a serious threat to the entire world. Major part of the total environmental pollution is coming from contaminated aquatic environment [1]. Removal of these recalcitrant chemicals for a clean, vivid and salubrious environment is the main aim of Green chemistry. Cost effective, recyclable and environmentally benign materials have got immense significance in environmental pollution control. The present research is pertained to the mineralization of water contaminants by advanced oxidation processes (AOPs) using metal and non-metal co-doped TiO_2 systems. Here we specifically discuss the photodegradation of herbicides, Atrazine and Metolachlor in the visible region. Various parameters are also discussed for the same.

4.1. Introduction

Among the various organic pollutants, herbicides are a major pollution source for both underground and surface waters. Contamination of herbicides in water due to agricultural, non-agricultural and industrial activities is a serious worldwide problem. The environmental fate of these pollutants depends a lot on their mobility in soils and their tendency to

intrude into other environmental compartments such as air and water [2]. Movement of water and dissolved chemicals through soil is known as leaching and the physico-chemical properties of the agrochemicals used as well as soil properties play a decisive role in this process [3, 4]. The transfer of these pollutants from soil to water mainly depends on its life time in soil [5]. Sorption of organic pollutants by soils from aqueous solutions is quantitatively measured in terms of soil organic adsorption coefficient (K_{OC}). K_{OC} is a universally accepted measure of the relative mobility of pesticides in soils and also describing the partitioning of pesticides in soil/water/atmosphere systems [6]. Generally, compounds having higher log K_{OC} values will be less mobile than those with lower values. The extensive use of herbicides in agriculture fields to control weedy plants and to increase the quality and quantity of crop productivity has become an important tool to the detriment of the environment. The herbicides and their degradation products may alter the natural habitats of different plant and animal species depending on how they are transported in the environment [7]. The release of toxic, recalcitrant and persistent organic pollutants such as pesticides, dyes, polychlorinated biphenyls (PCBs), halogenated organic solvents and polycyclic aromatic hydrocarbons (PAHs) into aquatic environment from industrial, wastewater treatment plants, agricultural run-off has drawn much attention and is considered as one of the arduous problems facing environmental scientists today [8]. Due to their chemical stability, resistance to biodegradation and sufficient water solubility, these organic pollutants penetrate deep into the ground water [9, 10]. The chemical properties of the pesticides affect their durability in the soil and their rate of movement from the surface soil to the ground water. Water solubility determines a pesticide's propensity to dissolve in

water making the chemical more amenable to migrate through the soil and into an aquifer.

Once the soil and pesticides begin to interact, their combined chemical properties create molecular reactions forming new molecular bonds. This propensity for soils and pesticides to interact affects the rate of pesticide migration in different types of soils. Once pesticides are introduced onto a field, they have the potential to migrate deep into the soil and into the aquifers below. If the chemical is degraded by biological or chemical processes before it leaches, it never reaches the aquifer. If the chemical has high persistence, it is not degraded, and also does not bind with soil, it is very likely to leach into and contaminate the ground water. Hydrolysis is the rate of degradation of a pesticide in water. If the pesticide leaches below top layers of soil beyond biological activity, hydrolysis becomes the only process available to decompose the pesticide. But this technique is not sufficient for the effective removal of the pollutants.

Ubiquitous use and improper disposal of herbicides cause serious ecological consequences. As a result, if these xenobiotic organic chemicals are introduced into water ecosystems, they can make water quality worse and threaten human health [11]. So it is very mandatory to curtail these recalcitrant and persistent chemicals for a hygienic environment. A lot of methods have been employed for this purpose and some are found to be effective. Conventional waste water treatments such as adsorption onto granular activated carbon, air stripping, incineration, chemical remediation, pyrolysis, reverse osmosis etc. are very slow or non-destructive for these kinds of compounds [12,13]. Degradation of pollutants is also possible through photochemical and biological processes but most of these require

long treatment periods [14]. Among various techniques, Ultrasonic irradiation is an attractive technique as the degradation of contaminants may occur under ultrasonic irradiation without the addition of other chemical substances [15]. Adsorption of these pollutants onto clays or other high surface area materials transfers them but cannot degrade them into harmless substances. Ozonation is also less effective due to its selectivity towards some organic pollutants. So it is very beneficial to apply a highly effective and sophisticated technique in the field of environmental protection. Here comes the importance of advanced oxidation process [16-18].

Heterogeneous semiconductor photocatalysis is a highly effective technique for the degradation and mineralization of pollutants in water and waste water to environmentally harmless compounds. Heterogeneous photocatalysis is a part of a family of techniques called Advanced Oxidation Processes and has got immense attention because of complete oxidation of pollutants, removal of inorganic compounds, heavy metals, bacteria and viruses from water [19-22]. However, in the treatment of bio-refractory compounds such as pesticides, pharmaceuticals and other complex molecules, it is more logical and economical to perform the oxidation process only up to the point at which the intermediate products become biodegradable [23,24]. Among various oxide semiconductor photocatalysts, TiO_2 has proven to be the better choice for widespread environmental applications due to its chemical inertness, strong oxidizing power, lower cost and long-term stability against photo corrosion and chemical corrosion. The photocatalytic degradation of various organic systems using irradiated TiO_2 and its modified forms and the basic principles of photocatalytic oxidation are well established [25-29].

The current chapter discusses the photocatalytic degradation of some herbicides using metal, non-metal co-doped TiO_2 systems. Five different co-doped catalytic systems and for each catalysts, three compositions were prepared by varying the concentration of metal and checked its photocatalytic activity in the degradation of herbicides. The organic pollutants selected are Atrazine and Metolachlor. According to environmental protection agency, these two chemicals are toxic and affect the ecosystem adversely. The selection of these compounds is based on its solubility in aqueous medium and toxicity. Various parameters like effect of time, effect of different catalysts, effect of catalyst amount and reusability were monitored for the degradation. Here we could not identify the by-products obtained after degradation due to lack of instrumental facility and the reports are based on the percentage degradation calculated from the data obtained from HPLC analysis. The light response of our co-doped catalytic systems is purely in the visible region. So we use a dichoric mirror of wavelength between 420-630 nm in order to get visible radiation specifically.

4.2. Activity Studies

4.2.1. Photocatalytic Degradation of Atrazine

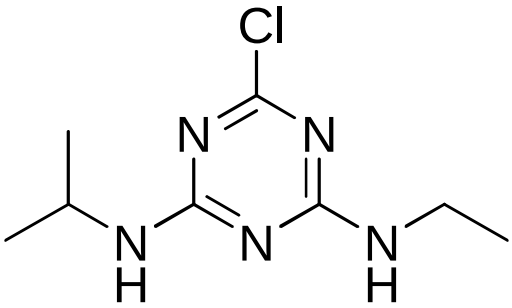

Fig.4.1. Structure of Atrazine

Atrazine is a tri-azine based compound. Chlorinated tri-azines are herbicides widely used for the control of annual and perennial grass and annual broad-leaved weeds and are amongst the most commonly used herbicides all over the world [30,31]. The main compound of this family is the atrazine (2-chloro-4-ethylamino-6-isopropylamino-s-triazine) and it is found in the environment contaminating soil and water reserves [32]. This herbicide belongs to the persistent organic pollutants because of its poor biodegradability and long half-life in water. Atrazine, which has been found in both deep and superficial waters, presents a moderate solubility in water ($1.6x10^{-4}$M at 20 ºC) and it is relatively stable in aqueous environments and soils where it possesses a half-life of one hundred days [33]. Several methods have been employed to remove atrazine from aqueous wastes such as adsorption on activated carbon and its combination with ozone [34,35], adsorption onto carbon nanotubes [36] etc. But all these methods have got a lot of disadvantages. Advanced oxidation process based on semiconductors is found to be better alternative for the conventional methods for the removal of herbicides. During this process, oxidation of the lateral chains and subsequent disappearance of the initial compound is very fast but the formation of the final product (cyanuric acid) may require a long irradiation time [37]. Due to the stability of the s-triazine ring, complete mineralization of atrazine could not be attained at shorter periods of time via oxidation which only affects the lateral chains with 5 of the 8 carbons removed as CO_2. The photocatalytic oxidation of s-triazine herbicides and their pathway of degradation have been scrutinized by various researchers and suggested that the degradation of the s-triazines occurred in a complex way with

cyanuric acid as the end product [37,38]. In this work, metal, non-metal modified TiO_2 were used for the effective degradation of this herbicide.

4.2.1. (a) Effect of Various Catalysts

Table. 4.1. % Degradation of Atrazine against different catalysts

Catalyst	% Degradation
Gd(0.5wt%)-N-Ti	57
Gd(1wt%)-N-Ti	73
Gd(1.5wt%)-N-Ti	68
Pd(0.5wt%)-N-Ti	58
Pd(1wt%)-N-Ti	63
Pd(1.5wt%)-N-Ti	60
Ag(0.5wt%)-N-Ti	49
Ag(1wt%)-N-Ti	62
Ag(1.5wt%)-N-Ti	57
Pr(0.5wt%)-N-Ti	44
Pr(1wt%)-N-Ti	54
Pr(1.5wt%)-N-Ti	47
Cd(0.5wt%)-N-Ti	43
Cd(1wt%)-N-Ti	51
Cd(1.5wt%)-N-Ti	49
TiO_2	31

Here we evaluated the degradation of Atrazine using various co-doped TiO_2 catalysts having different concentration of metal content. In all these cases, the concentration of N is fixed. In this study, around 10 ml of 10^{-4} M aqueous solution of the substrate was taken and 0.1 g (1g/L) of the catalyst was added to it. The irradiation time was limited to 60 minutes based

on the lamp life. Before irradiation, the entire system was magnetically stirred for 30 minutes in order to attain the adsorption/ desorption equilibrium between the catalyst surface and the substrate. Then the suspension was irradiated with a 150 W Xenon ozone free lamps. The dichoric mirror of 420-630 nm was used as the source for visible light which excludes all other radiations. The suspension was centrifuged and filtered after irradiation and the concentration was analyzed using HPLC technique. The mobile phase used was a solution of water/1 mmol ammonium acetate in the ratio 50:50 at flow rate of 1.4 ml/min with UV detection at 226 nm. The percentage of degradation was measured using the relation $(C_0\text{-}C) \times 100/C_0$, where C_0 and C are the initial and final concentrations of the herbicide. Five different co-doped catalytic systems were prepared and compared its activity with pure TiO_2 in the degradation of the herbicide Atrazine. For each catalyst, three different versions were prepared by varying the metal content and observed its activity. From the table it is clear that all the co-doped catalysts showed better activity than pure TiO_2. After irradiation, no huge degradation was observed for pure TiO_2 due to its specified spectral response in the UV region. In these co-doped systems, one element (N) is responsible for changing the light response and metal part reduces the electron-hole recombination. Effective band gap narrowing of TiO_2 can be achieved by using non-metal elements such as 'N' due to its comparable potential with oxygen in the lattice [46]. Liu et al. also observed the reduction in band gap of N-doped TiO_2 by using ammonia as the nitrogen source [47]. Among various catalysts, all the 1wt% metal doped co-doped systems showed superior activity than other systems. It is believed that the metal induces greater enhancements in the photocatalytic activity of TiO_2 by creating a Schottky junction

between metal and semiconductor. The metal particle acts as a sink for photogenerated electrons thereby reducing the rate of their recombination with holes [48]. There is an increase in the degradation efficiency with increasing metal content up to 1wt% then a decrease for the sample having higher metal content. The dosage level is an important factor influencing the enhancement of photo activity in metal doped systems. Below an optimum dosage, the metals can act as charge separation centers and thus enhance the photo activity of modified TiO_2 systems. However, as dosage levels exceed optimum loading they can act as electron-hole recombination centers which adversely affect the photocatalytic activity [46]. This may also be due to the population of the photosensitive surface of TiO_2 by the metal dopant. This observation led to the conclusion that the optimum amount of metal dopant for effective photocatalytic activity is 1wt%. Higher metal levels (1.5wt%) led to lower photodegradation rates as these become recombination centers and thus short circuiting the system. In pure TiO_2, the rate of electron-hole recombination is very high. Nitrogen and metal content have synergistic effects which is also responsible for improving the photocatalytic activity under visible light irradiation. Introduction of substitutional or interstitial nitrogen in the TiO_2 results the formation of new level above the valance band. So upon irradiation with visible light, electrons can be excited from the newly formed level to the conduction band of TiO_2 [49]. Generally, metals can be existed on the surface of the semiconductor material as an island. If the work functions of the metals present are higher than the semiconductor material, the photogenerated electrons are trapped by them leading to electron-hole separation. Then the holes are free to migrate to the surface and react with surface adsorbed water or hydroxyl groups generating highly reactive

hydroxyl radical species. On the other hand, the electrons scavenge the oxygen molecules to form very reactive superoxide radicals [50]. Both these radicals are very reactive and non-specific in nature that results the better degradation of herbicide. The metal content and nature of the metals affect the electron scavenging ability which in turn influence the photocatalytic activity. Here the activity follows as Gd-N-Ti > Pd-N-Ti >Ag-N-Ti > Pr-N-Ti > Cd-N-Ti > TiO_2. Complex formation between titania and f-orbitals of rare earths improve the absorptivity and electronic properties. The resulting Rare Earth-O-Ti bond will cease the transformation from metastable anatase to rutile phase [51, 52]. Among all the co-doped titania sytems, Gd doped system shows lowest band gap and particle size thereby increasing the surface area and pore volume which positively affects the photocatalytic activity [53].

4.2.1. (b)Effect of Catalyst Amount

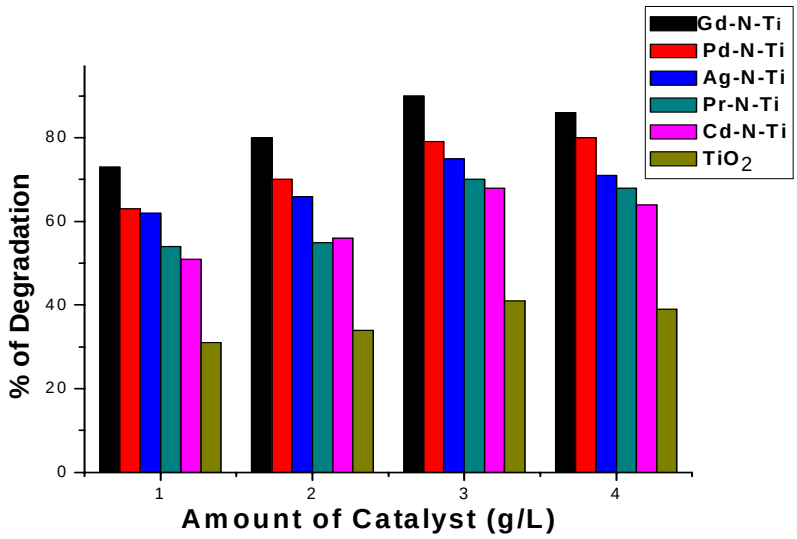

Fig. 4.2. % Degradation of Atrazine against amount of catalysts

The effect of different catalysts revealed that co-doped TiO_2 systems containing 1wt% metal are very good candidates for degradation of Atrazine. So we evaluated the effect of catalyst amount by considering only the 1wt% metal doped catalysts. 10 ml of 10^{-4}M aqueous solution of the herbicide was taken and different catalyst amounts varying from 1 g/L to 4 g/L were added. Before irradiation the suspension was stirred for about 30 minutes in order to attain adsorption/desorption equilibrium and then the time of irradiation was limited to 60 minutes. The dichoric mirror of 420-630 nm was used as the source for visible light. After irradiation, the percentage degradation was analyzed using HPLC technique. Maximum degradation of about 91% was observed with Gd(1wt%)-N-Ti system with a catalyst amount of 3 g/L. From the results it is clear that photocatalytic degradation increases with increase of catalyst amount and reaches a maximum. Further increase of catalyst amount does not have much effect on degradation. Active surface sites increase as the catalyst amount increases which improves the photocatalytic efficiency through the formation of activated photoexcited species. Increase of catalyst concentration beyond the optimum value made the suspension very thick for the light to transmit and resulted in a reduced photocatalytic activity. So catalyst amount is a significant parameter to be determined to avoid the catalyst loss and ensure the effective absorption of photons. Here also the activity follows the same trend as before.

4.2.1. (c) Effect of Time

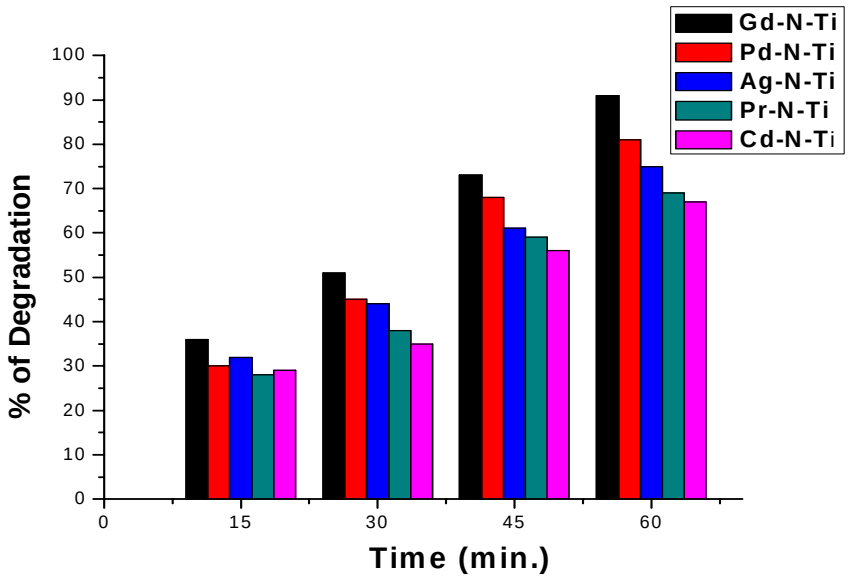

Fig. 4.3. % Degradation of Atrazine against time

In this case a total of 50 ml aqueous solution of Atrazine was taken in a beaker and catalyst amount of 3 g/L was added. The suspension was magnetically stirred for 30 minutes in order to achieve adsorption/ desorption equilibrium. Dichoric mirror of 420-630 nm was used as the light source. After starting the lamp, 10 ml of the suspension was pipetted out from the solution at an interval of 15 minutes up to 60 minutes. The concentrations of the collected samples were monitored by HPLC technique. It is clear from the figure that the percentage of degradation increases with increase of irradiation and reaches above 90% with an irradiation time of 60 minutes. Here also maximum degradation was observed with Gd(1wt%)-N-Ti system. The degradation follows the same pattern as before. Increase of irradiation time allows more light energy to fall on catalyst surface which enhances the generation of photoexcited

species. The formation of these intermediate species facilitates the generation of reactive oxygen species responsible for the degradation of adsorbed substrates.

4.2.1. (d) Recyclability Studies

Recyclability studies were conducted with two of the most active catalysts. The catalysts were removed from the reaction mixture by centrifuging the suspension. Then it was washed with various solvents and calcined at 500°C for 1 hour. The reactivated catalysts were active in the second cycle without appreciable loss in its activity. Here the catalyst amount used was 3 g/L and the time of irradiation was 1h. The catalysts employed were Gd(1wt%)-N-Ti and Pd(1wt%)-N-Ti. The results are shown in the table below.

Table. 4.2. Recyclability Studies

No. of Cycles	Catalysts	% Degradation	
1	Gd(1wt%)-N-Ti	91	83
2	Pd(1wt%)-N-Ti	88	81

4.2.2. Photocatalytic Degradation of Metolachlor

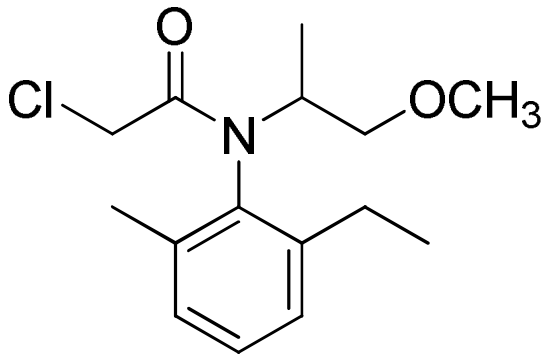

Fig.4.4. Structure of Metolachlor

Metolachlor is an aniline derivative. It is chemically 2-chloro-N-(2-ethyl-6-methylphenyl)-N-(2-methoxy-1-methylethyl)acetamide. It is structurally similar to other herbicides such as Alachlor, Butachlor etc. and the difference is manifested mainly in the methoxyalkyl side chain. This moiety controls selectivity, water solubility and other such herbicidal properties. Metolachlor is a pre-emergent germination inhibitor used to control annual broadleaf weeds, grasses in corn, soybean and other crops and is the most intensively used herbicide belonging to the chemical class of chloroacetamides [39,40]. It inhibits cell growth and induces cytotoxic and genotoxic effects to lymphocytes. Due to its high mobility and persistency in soil, it has a high potential to contaminate ground water. Among the acetanilide herbicides, Metolachlor appears to be the most persistent ($t_{1/2}$=200 d in highly acidic water, 97 d in highly alkaline waters) and has the potential to leach to ground water because of its relatively high water solubility (530 mg L^{-1} at 20ºC) [41]. Concentration of Metolachlor in ground and surface water was found to be in the range of 0.01 to 0.40 µg/L [42-45]. Several studies revealed the persistence of Metolachlor indicating that it is fairly resistant to hydrolysis at a wide pH range. So there is a need of some advanced and sophisticated technique for their removal from the environment. Here also we employed modified TiO_2 systems for the degradation studies.

4.2.2. (a) Effect of Various Catalysts

Table 4.3. % Degradation of Atrazine against different catalysts

Catalyst	% Degradation
Gd(0.5wt%)-N-Ti	60
Gd(1wt%)-N-Ti	81
Gd(1.5wt%)-N-Ti	76
Pd(0.5wt%)-N-Ti	54
Pd(1wt%)-N-Ti	74
Pd(1.5wt%)-N-Ti	69
Ag(0.5wt%)-N-Ti	51
Ag(1wt%)-N-Ti	68
Ag(1.5wt%)-N-Ti	67
Pr(0.5wt%)-N-Ti	47
Pr(1wt%)-N-Ti	62
Pr(1.5wt%)-N-Ti	60
Cd(0.5wt%)-N-Ti	43
Cd(1wt%)-N-Ti	54
Cd(1.5wt%)-N-Ti	51
TiO_2	29

Here we evaluated the degradation of Metolachlor using various co-doped TiO_2 catalysts having varied amount of metal content. In all these cases, the concentration of N is fixed. In this study, around 10 ml of 10^{-4} M aqueous solution of the substrate was taken and 0.1 g (1g/L) of the catalyst was added to it. The irradiation time was limited to 60 minutes based on the lamp life. Before irradiation, the entire system was magnetically stirred for 30 minutes in order to attain the adsorption/desorption equilibrium between the catalyst surface and the substrate. Then the suspension was irradiated with a 150 W Xenon ozone free lamps with an irradiance of 96.8 mW/cm^2. The dichoric mirror of 420-630 nm was used

as the source for visible light. The suspension was centrifuged and filtered after irradiation and the concentration was analyzed using HPLC technique. The mobile phase used was a solution of acetonitrile/water in the ratio 63:37 at a flow rate of 1.4 ml/min with UV detection at 220 nm. The percentage of degradation was measured using the relation $(C_0\text{-}C) \times 100/C_0$, where C_0 and C are the initial and final concentrations of the herbicide respectively. Preparation method, the doping concentration, the dopant energy level within the TiO_2 lattice and the distribution of the dopant in the particle can sometimes affect the photocatalytic performance of the catalysts [54]. The metal ion dopant can act as a mediator of interfacial charge transfer or as combination centre, so there must be an optimum value for the dopant concentration in order to carry out photocatalysis effectively [55]. Compared to pure TiO_2, all the co-doped catalysts showed better activity in the degradation of the substrate in visible region. The optimum concentration of metal content for effective degradation of herbicide was found to be 1wt% in all the cases. Above that concentration, the metal centers facilitate electron-hole recombination thereby reducing the photodegradation rate. Anpo and co-workers have reported that the overlap of the 'd' orbitals of TiO_2 and 'd' orbital of the doped metal ions could decrease the band gap of TiO_2 to absorb the visible light [56]. So upon irradiation of a co-doped system using visible light, the electrons can be excited from the impurity level of N to metal impurity level or from the N impurity level to the conduction band or from valance band to the impurity level of the metal. Therefore, the quantity of excitons is much higher than that of the pure titania which affects the photodecompositon positively. Here also the activity follows as Gd-N-Ti > Pd-N-Ti > Ag-N-Ti > Pr-N-Ti > Cd-N-Ti > TiO_2. The

effect of the dopants, optimum concentration of dopants, the rate of electron-hole recombination and generation of reactive oxygen species have been explained previously.

4.2.2. (b) Effect of Catalyst Amount

In a suspension, the catalyst dosage is an important controlling parameter that can affect degradation rate. The co-doped systems containing 1wt% metal content were employed for finding out the effect of catalyst dosage on degradation because higher activity of these systems has been proved in the earlier study. With a constant concentration of 10 ml of 10^{-4}M aqueous solution of Metolachlor, the optimum catalyst amount was found by varying the catalyst dosage from 1 g/L to 4 g/L. Here 420-630 nm dichoric mirror was used as the visible light source and the time of irradiation was limited to 60 minutes depending on the lamp life. Concentration of the solution after degradation was monitored using HPLC technique. Maximum degradation of about 95% was observed with Gd(1wt%)-N-Ti system with a catalytic amount of 3 g/L. The degradation rate was found to increase with the increase in catalyst concentration which is the characteristic of heterogeneous photocatalysis [57,58]. Up to an optimum concentration, the reaction rates were found to be directly related to the catalyst concentration. But above that concentration the reaction rate decreases and becomes independent of the catalyst concentration. Surface area of the catalyst available for adsorption and degradation increase as the catalyst amount is increased. But increasing of catalyst loading beyond the optimum value increases the solution opacity leading to a decrease in the penetration of the photon flux thereby reducing the photocatalytic degradation. Curtail the use of excess catalyst

and efficient photon absorption can be attained by optimizing the catalyst concentration.

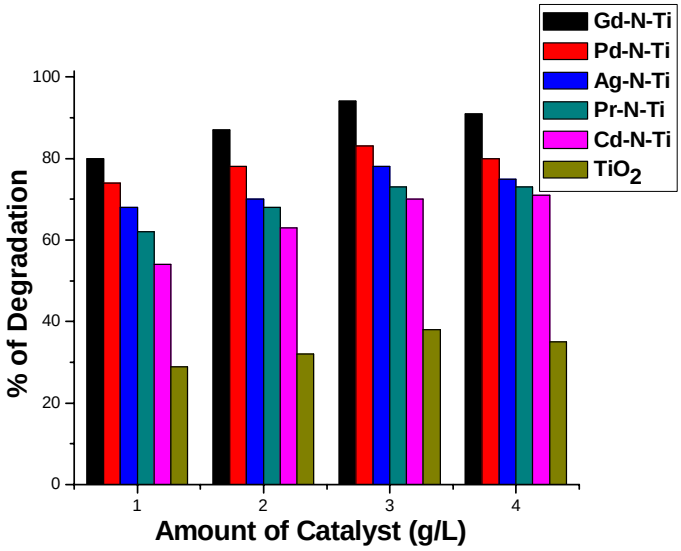

Fig. 4.5. % degradation of Metolachlor against catalysts amount

4.2.2. (c) Effect of Time

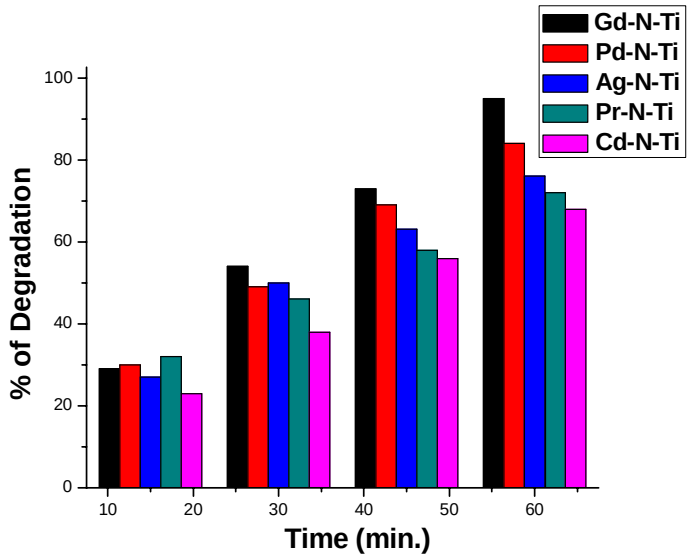

Fig. 4.6. % Degradation of Metolachlor against time

In this case, a total of 50 ml aqueous solution of Metolachlor was taken in a beaker and catalyst amount of 3 g/L was added. The experimental set up and the conditions used are same as before. It is clear from the figure that percent of degradation increases with increase of irradiation and reaches around 95% with an irradiation time of 60 minutes. Further increase of time does not have much effect on photocatalytic activity. Here maximum degradation was observed with Gd(1wt%)-N-Ti system and least degradation was observed with Cd(1wt%)-N-Ti system. The degradation follows the same pattern as before. Increase of irradiation time on catalyst surface enhances the generation of photoexcited species. These intermediate species facilitates the generation of reactive oxygen species responsible for the degradation of adsorbed substrates. These generated reactive oxygen species are very unstable and non-specific in nature that affects the photo reaction positively.

4.2.2. (d) Recyclability Studies

Here also we conducted the recyclability studies with two of the most effective catalysts in order to understand the stability of the catalytic systems. The same experimental conditions were used. The concentration was analyzed by HPLC technique. The catalysts were found to be active up to two cycles without appreciable loss in its activity.

Table.4.4. Recyclability Studies

No. of Cycles	Catalysts	% Degradation	
1	Gd(1wt%)-N-Ti	94	82
2	Pd(1wt%)-N-Ti	89	80

4.3 Conclusion

The catalytic activity of the cost effective, sustainable and environmentally benign, metal, non-metal co-doped TiO_2 systems were checked in the photodegradation of recalcitrant and persistent herbicides such as Atrazine and Metolachlor. The catalysts were found to be very active for the effective degradation of the herbicides. The percentage degradation was analyzed using HPLC technique. Various parameters such as effect of different catalysts, effect of catalyst dosage, effect of time and recyclability were monitored for the same.

References

[1]. L. Gomathi Devi, G. Krishnamurthi, J. Phys. Chem. A. 115 (2011) 460.

[2]. S. Navarro, J. Fenoll, N. Vela, E. Ruiz, G. Navarro, J. Hazard. Mater. 172 (2009) 1303.

[3]. M. Vanclooster, J. J. T. I. Boesten, M. Trevisan, C. D. Brown, E. Capri, O. M. Eklo, B. Gottesbüren, V. Gouy, A.M.A. van der Linden, Agric. Water Manage. 44 (2000) 1.

[4]. S. Navarro, N. Vela, G. Navarro, Spanish J. Agric. Res. 5 (2007) 357.

[5]. R. D. Wauchope, S. Yeh, J. Linders, R. Kloskowski, K. Tanaka, B. Rubin, A. Katayama, W. Kördel, Z. Gerstl, M. Lane, J. B. Unsworth, Pest Manage. Sci. 58 (2002) 419.

[6]. D. Mackay, S. Paterson, Environ. Sci. Technol. 25 (1991) 427.

[7]. N. A. Quiroz, D. J. R. Gutierrez, S. S. Martínez, C. L. Bahena, Int. J. Geosciences. 2 (2011) 669.

[8]. L. Muszkat, D. Raucher, M. Mogaritz, D. Ronen, "Groundwater contamination by organic pollutants," Groundwater Contamination and Control, Marcel Dekker, New York, NY, USA, (1994).

[9]. J. A. Graham, Analytical Chemistry. 63 (1991) 613.

[10]. D. M. Blake, Bibliography of Work on the Photocatalytic Removalof Hazardous Compounds from Water and Air, National Renewal Energy Laboratory, Cole Boulevard Golden, Colo, USA, (2001).

[11]. Md. M. Rahman, Jang-Eok Kim, J. Korean Soc. Appl. Biol. Chem. 53 (2010) 458.

[12]. A. Gora, B. Toepfer, V. Puddu, G. L. Puma, Appl. Catal. B. Environ. 65 (2006) 1.

[13]. S. Parra, J. Olivero, C. Pulgarin, Appl. Catal. B. Environ. 36 (2002) 75.

[14]. K. Djebbar, A. Zertal, T. Sehili, Environ. Technol. 27 (2006) 1191.

[15]. M. H. Dehghani, A. Fadaei, Ind. J. Sci. and Technol. 6 (2013) 3876.

[16]. C. J. Hapeman-Somich, ACS Symposium Series. 459 (1991) 133.

[17]. P. Slade, Nature. 207 (1965) 515.

[18]. R. R. Giri, H. Ozaki, S. Taniguchi, R. Takanami, Int. J. Environ. Sci. Tech. 5 (2008) 17.

[19]. W. Bahnemann, M. Muneer, M. M. Haque, Catal. Today. 124 (2007) 133.

[20]. G. Palmisano, V. Augugliaro, M. Pagliaro, L. Palmisano, Chem. Commun. 33 (2007) 3425.

[21]. O. Legrini, E. Oliveros, and A. M. Braun, Chem. Rev. 93 (1993) 671.

[22]. K. Ikehata, M. G. El-Din, J. Environ. Eng. and Sci. 5 (2006) 81.

[23]. S. Parra, S. Malato, C. Pulgarin, Appl. Catal. B. Environ. 36 (2002) 131.

[24]. M. Hincapie, M. I. Maldonado, I. Oller, W. Gernjak, J. A. Sanchez-Perez, M. M. Ballesteros, S. Malato, Catal. Today. 101 (2005) 203.

[25]. O. Zaharaa, H. Y. Chen, M. Bouchy, Journal of Advanced Oxidation Technologies. 4 (1999) 1169.

[26]. D. Dvoranov, V. Brezov, M. Mazur, M. A. Malati, Appl. Catal. B. 37 (2002) 91.

[27]. A. Gora, B. Toepfer, V. Puddu, G. Li Puma, Appl. Catal. B. 65 (2006) 1.

[28]. A. Fujishima, T. N. Rao, D. A. Tryk, J. Photochem. Photobiol. C. 1 (2000) 1.

[29]. U. I. Gaya, A. H. Abdullah, J. Photochem. Photobiol. C. 9 (2008) 1.

[30]. W. E. Pereira, C. E. Rostad, Environ. Sci. Technol. 24 (1990) 1400.

[31]. I. K. Konstantinou, T. M. Sakellarides, V. A. Sakkas, T. A. Albanis, Environ. Sci. Technol. 35 (2001) 398.

[32]. S. J. Kalkhoff, K. E. Lee, S. D. Porter, P. J. Terrio, E. M. Thurman, J. Environ. Quality. 32 (2003) 1025.

[33]. M. Mamian, W. Torres, F. E. Larmat, Portugaliae Electrochimica Acta. 27 (2009) 371.

[34]. C. A. Guzman-Perez, J. Soltan, J. Robertson, Separation and Purification Technol-ogy. 79 (2011) 8.

[35]. V. K. Gupta, B. Gupta, A. Rastogi, S. Agarwal, A. Nayak, Water Research. 45 (2011) 4047.

[36]. G. -C. Chen, X. -Q. Shen, Y.-Q. Zhou, X.-E. Shen, H. -L. Huang, S. U. Khan, J. Hazard. Mater. 169 (2009) 912.

[37]. I. K. Konstantinou, T. A. Albanis, Appl. Catal. B. Environ. 42 (2003) 319.

[38]. E. Pelizzeti, V. Maurino, C. Minero, V. Carlin, E. Pramauro, O. Zerbinati, M. L. Tosato, Environ. Sci. Technol. 24 (1990) 1559.

[39]. G. Chesters, V. Simsiman, J. Leby, B. J. Alhajor, R. N. Fathulla, J. M. Harkin, Rev. Eviron. Contam. Toxicol. 110 (1989) 1.

[40]. Y. B. Kumar, N. Singh, S. B. Singh, J. Environ Anal Toxicol. 3 (2013) 196.

[41]. Extoxnet (2000) Extension Toxicology Network. Pesticide information profile: Metolachlor.

[42]. R. Frank, L. Logan, Arch. Environ. Contam. Toxicol. 17 (1988) 741.

[43]. R. J. Maguire, R.J. Tkatcz, Arch. Environ. Contam. Toxicol. 25 (1993) 220.

[44]. R. P. Richards, D. B. Baker, Environ. Toxicol. Chem. 12 (1993) 13.

[45]. A. A. Debora, S. Lacorte, T. Vinhas, P. Viana, D. Barcelo´, J. Chromatogr. A. 879 (2000) 13.

[46]. F. Han, V. S. R. Kambala, M. Srinivasan, D. Rajarathnam, R. Naidu, Appl. Catal. A: Gen. 359 (2009) 25.

[47]. Y. Liu, X. Chen, J. Li, C. Burda, Chemosphere. 61 (2005) 11.

[48]. M. Maicu, M. C. Hidalgo, G. Colon, J. A. Navio, J. Photochem. Photobiol. A. 217 (2011) 275.

[49]. R. Asahi, T. Morikawa, T. Ohwaki, K. Aoki, Y. Taga, Science. 293 (2001) 269.

[50]. J. Yu, T. Ma, S. Liu, Phys. Chem. Chem. Phys. 13 (2011) 3491.

[51]. I. Cacciotti, A. Bianco, G. Pezzotti, G. Gusmano, Chem. Eng. J. 166 (2011) 751.

[52]. D. W. Hwang, J. S. Lee, W. Li, S. H. Oh, J. Phys. Chemistry. B. 107 (2003) 4963.

[53]. Z. M. El-Bahy, A. A. Ismail, R. M. Mohamed, J. Hazard. Mater. 166 (2009) 138.

[54]. W. Choi, A. Termin, M. R. Hoffmann, J. Phys. Chem. 98 (1994) 13669.

[55]. Y. Cong, J. L. Zhang, F. Chen, M. Anpo, D. N. He, J. Phys. Chem. C. 111 (2007) 10618.

[56]. H. Tang, K. Prasad, R. Sanjines, P. E. Schmidd, F. Levy, J. Appl. Phys. 75 (1994) 2042.

[57]. M. Qamar, M. Saquib, M. Muneer, Desalination. 171 (2004) 185.

[58]. H. K. Singh, M. Muneer, D. Bahnemann, Photochem. Photobiol. Sci. 2 (2003) 151.

.....ൠ.....

Chapter 5

Photo – oxidation of Some Polycyclic Aromatic Hydrocarbons (PAHs)

Contents

The use of light in chemistry has aroused much attention during the last two three decades. The reason for this is that semiconductor catalysis in the presence of light can have the ability to clean the environment in a sustainable manner which has a minimal environmental impact. Photocatalysis in organic synthesis concerns the use of light to induce chemical transformations onto organic substrates which are transparent in the wavelength range employed. There are actually two methods for the removal of pollutants from the ecosystem. Complete mineralization is the one way to remove the pollutants. Conversion of toxic compounds to other compounds having toxicity less than the initial starting compound is the second way. In this chapter, we are concentrating on the second aspect and discuss the photo-oxidation of some polycyclic aromatic hydrocarbons by using metal, non-metal modified TiO_2 systems.

5.1. Introduction

Heterogeneous photocatalysis in selective organic synthesis is not frequently employed although nowadays the demands for replacement of

traditional oxidation methods with cleaner ones are increasing [1]. Photo-oxidation can be considered as one of the important classes of photocatalytic reactions responsible for the conversion of organic substrates in a greener and cost effective way. Irradiation of a suspension containing semiconductor powder, mostly of the inexpensive and environmentally benign TiO_2 is an effective method for the oxidation of organic substrates [1-6]. These kinds of heterogeneous photocatalytic reactions are possible in both aqueous and non-aqueous medium [7-11]. Mineralization of organic pollutants using TiO_2 is a well-known area but studies on photo induced organic transformation based on TiO_2 are comparatively rare. Every organic functional group containing either a non-bonded lone pair of any π conjugation can be activated towards TiO_2 photocatalyzed oxidative reactivity [12]. TiO_2-sensitized organic photosynthetic reactions include oxidation and oxidative cleavage, reduction, isomerization, substitution and polymerization. Oxidatively inert solvents provide suitable medium for these kinds of reactions [14]. The C-H bond activation is one of the most challenging chemical problems and also has a lot of practical applications. Generally, the formation of oxidation products depends mainly on the reaction medium [15]. Conversion of 1-decene and 2-hexene to their corresponding carbonyls and epoxides by irradiated photocatalyst has been reported [16,17]. The selectivity of the epoxidation reaction in a mixture of acetonitrile and butyronitrile was improved using rutile (instead of anatase) and visible light [18]. Hydrogenation of propyne to propene by noble metals -loaded TiO_2 was reported, of which Pd/TiO_2 presents the highest photocatalytic activity [19]. Photo-oxidation of cyclohexane to cyclohexanol and cyclohexanone has also been reported in the liquid

phase at room temperature and atmospheric pressure [20-22]. Due to the stability of aromatic nucleus, photocatalytic reactions occur in aqueous solutions and especially facilitate various side chain reactions. The reaction rate is sensitive to ring substitution. The electron-donating groups enhance and electron-withdrawing groups decrease the rate of the reaction [23]. This type of reactions may present a convenient method for the oxidation of benzene ring substituents.

The photo-oxidation of toluene leads to benzaldehyde and subsequently to benzoic acid in MeCN which is accelerated by the presence of small amounts of H_2SO_4 [24]. It is assumed that the HSO_4^- anions promote the reaction by mediating the oxidation of the organic substrate by reacting with the photogenerated hole to form highly oxidizing $HSO_4^{\cdot}$ radicals. They also suggested that the formation of benzoic acid is favoured by stronger electron-withdrawing substituents. The reaction scheme is shown in Fig. 5.1.

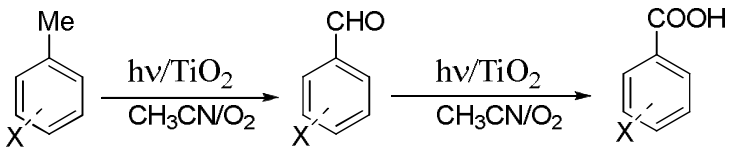

Fig.5.1. Reaction Scheme for the Photo-oxidation of Substituted Toluene

Another study revealed that the oxidation rate of the alkyl chain of alkylbenzenes in UV-irradiated acetonitrile solutions decreases with the number of carbon atoms and carbon atom in the 'α' position with respect to the aromatic ring is more reactive [25]. 2-formylcinnamaldehyde was formed from Naphthalene in a mixed solution of water and MeCN.

The best selectivity of 85% and the highest reaction rate were obtained using a photocatalyst containing 90% rutile and 10% anatase [26]. Photocatalytic oxidation of methylpyridines (picoline) in acetonitrile leads to inorganic products due to the poor stability of pyridine nucleus compared to benzene nucleus [5]. Selective oxidation of alcohols to carbonyls is one of the most important chemical transformations in industrial chemistry and these carbonyl compounds such as ketones and aldehydes are precursors for many drugs, vitamins and fragrances and are important intermediates in many complex syntheses [27,28]. Most of reactions use toxic, corrosive or require expensive oxidants and drastic conditions such as high pressure, temperature or strong mineral acids [29,30]. But photocatalysis is an effective and easy way for the preparation of these industrially important compounds. Photo-oxidation of Benzhydrol to Benzophenone over TiO_2 modified with Lanthana was also reported [31]. Aldehydes, ketones, acids and amines are also converted to specific products by using semiconductor mediated photocatalysis [32-34]. It is also applicable in the synthesis of heterocyclic compounds [35]. In this chapter we are concentrating on the photo-oxidation of some substituted anthracene derivatives.

Polycyclic aromatic hydrocarbons (PAHs), also known as poly-aromatic hydrocarbons or polynuclear aromatic hydrocarbons, are fused aromatic rings and do not contain hetero-atoms or substituents [36]. These are found naturally and also formed by the incomplete combustion of oil, garbage etc. These are one of the structural constituents of dyes, plastics and pesticides. Effluents from coir and textile industries contain anthracene based PAHs which results in the contamination of drinking

water. Due to the presence of stable benzene rings, most of the PAHs show strong inhibition towards biological degradation and the common methods employed for their removal [37]. Naphthalene is the simplest polycyclic aromatic hydrocarbon. PAHs are ubiquitous pollutants that occur in natural phase such as soil, sediment, water, air and are harmful to environment and health of human being due to their high degree of mutagenicity and carcinogenicity [38-40]. These compounds may be classified as low molecular weights or high molecular weights (HMW) depending on the number of rings present. Low molecular weight (LMW) PAHs are relatively soluble in water but those containing 4-5 rings are hydrophobic in nature. Biodegradation of these heavier PAHs are not easy due to their poor water solubility [41,42]. The tendency to strongly adsorb on particulate matter renders the HMW PAHs less available and thus less susceptible to remediation (Cerniglia & Heitkamp, 1989). HMW PAHs have high resonance energies due to the dense clouds of π-electrons surrounding the aromatic rings making them persistent in the environment and recalcitrant to degradation (Johnson, Wick, & Harms, 2005). Low molecular weight PAHs are sometimes removed by microbial degradation and evaporation. But these conventional methods are not sufficient for the removal of stable HMW PAHs [43]. Heterogeneous photocatalysis, especially using titanium dioxide (TiO_2) have been extensively investigated to remove PAHs in aqueous solution [4,44,45]. Due to the extremely low solubility of PAHs in water, the studies mentioned above had to use organic solvent to dissolve PAHs or use surfactants to increase their solubility [15] which makes the sample analysis arduous [46,47]. Iron oxide acts as natural photocatalysts to catalyze the degradation of organic pollutants and Li et al. reported the photodegradation of pyrene

using iron oxide in solid phase [48]. Irradiation of aromatic compounds by light produces partially oxidized intermediates which are more susceptible to biodegradation than parent compounds. Thus photodegradation has been suggested as pre-treatment strategy for biodegradation [49]. This chapter discusses the photo-oxidation of some anthracene derivatives in CH_3CN using metal, non-metal modified TiO_2 under visible light.

5.2. Photo-oxidation of substituted anthracene derivatives

PAHs' chronic health effect, carcinogenicity, microbial recalcitrance, high bioaccumulation potential and low removal efficiency in treatment process is a serious concern nowadays. So removal or degradation of these things from the environment is very necessary. Here comes the importance of advanced oxidation process (AOP). The substrates and catalysts used in the photo-oxidation reactions are shown below.

Substrates

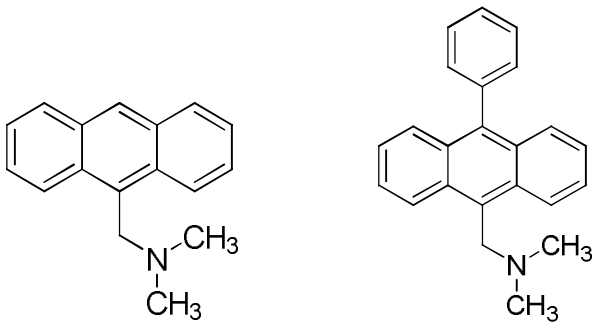

Fig. 5.2. 9-(*N*,*N*-Dimethylaminomethyl)anthracene and its phenyl substituted derivative

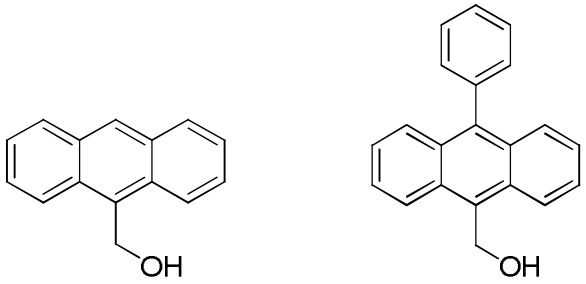

Fig.5.3. 9-Anthracenemethanol and its phenyl substituted derivative

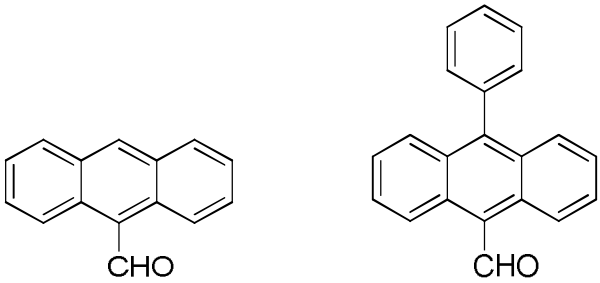

Fig. 5.4. 9-Anthraldehyde and its phenyl substituted derivative

Catalysts used for photo-oxidation

a) Gd(1wt%)-N-Ti

b) Pd(1wt%)-N-Ti

c) Ag(1wt%)-N-Ti

5.2.1. Photo-oxidation of 9-(*N,N*-Dimethylaminomethyl)anthracene systems

Irradiated semiconductor materials are suitable candidates for some organic transformations. Here the three catalysts mentioned above have been employed for the photo-oxidation of some 9-(*N,N*-Dimethylaminomethyl) anthracene systems. Very simple conditions were used for the reaction. Anthracenemethanamines and phenyl substituted anthracenemethanamines can very effectively shut the communication between donor and the

acceptor species so that we can easily study the photoinduced electron transfer reactions in these systems with the presence of a catalyst. Catalysts do not have any directing nature here; it can only alter the rate of the reaction. So we obtained same products with all the three catalysts. Light response of all the three catalysts are purely in the visible region. But light absorption ability and the rate of formation of the reactive oxygen species are different for various catalysts. That may affect the yield of the products and the time taken for the reaction to be completed. The light source was either 100 W or 150 W Xe ozone free lamps with average life of 1500h. A 420-630 nm dichoric mirror (cold mirror) filter was used in order to get visible radiation which gave an irradiance of 64.7 mW/cm^2 (100 W) and 96.8 mW/cm^2 (150 W) respectively. Photo-oxidation reactions were carried out as follows. 9-(*N*,*N*-Dimethylaminomethyl)anthracene system in CH_3CN (0.03M) was taken in a 100 ml beaker and 0.1g of the Gd(1wt%)-N-Ti catalyst was added to it. The mixture was stirred for about 30 minutes to achieve an adsorption/desorption equilibrium before placing under the lamp setup. Then the suspension was irradiated using a Xenon ozone free lamp. Anthraquinone (AQ) was the only product obtained with 90% yield within 2.5h using 150 W lamps. As a control, we also carried out the same reaction without the catalyst. But no products were formed within the above said time period. In the second case, 10th position of the 9-(*N*,*N*-Dimethylaminomethyl)anthracene (0.3M) was protected by a phenyl ring and conducted the photo-oxidation and expected the same product as in the former case. Surprisingly within the time limit of 2.5h, an intermediate species 9-hydroxy 9-phenylanthrone (9H9PA) could be obtained in good yield (150 W). When the reaction time was increased to 4h, anthraquinone was obtained as the major product (89%, 150 W). The

results are tabulated in Table 5.1. The resultant mixture was centrifuged and filtered using Whatman No. 42 filter paper. This was further purified by silica column chromatography using 70:30 hexane/DCM mixtures as the mobile phase. Isolated products were thoroughly characterized using various techniques such as melting point measurement (MP), FT-IR, ^{1}H NMR and GCMS analysis.

Table 5.1. Photo-oxidation of Tertiary Amine Derivatives by using Gd(1wt%)-N-Ti System

Substrate	**Time (h)**	**Products**	**Yield (%)**
9-(*N*,*N*-Dimethylaminomethyl)anthracene	2.5	AQ	90
10-phenyl-9-(*N*,*N*-Dimethylaminomethyl)anthracene	2.5	9H9PA	74
		AQ	14
10-phenyl-9-(*N*,*N*-Dimethylaminomethyl)anthracene	4	AQ	89

Table 5.2. Photo-oxidation using Pd(1wt%)-N-Ti System

Substrate	**Time (h)**	**Products**	**Yield (%)**
9-(*N*,*N*-Dimethylaminomethyl)anthracene	2.5	AQ	81
10-phenyl-9-(*N*,*N*-Dimethylaminomethyl)anthracene	2.5	9H9PA	68
		AQ	12
10-phenyl-9-(*N*,*N*-Dimethylaminomethyl)anthracene	4	AQ	80

Table 5.3. Photo-oxidation using Ag (1wt%)-N-Ti System

Substrate	**Time (h)**	**Products**	**Yield (%)**
9-(*N*,*N*-Dimethylaminomethyl)anthracene	3	AQ	82
10-phenyl-9-(*N*,*N*-Dimethylaminomethyl)anthracene	3	9H9PA	70
		AQ	8
10-phenyl-9-(*N*,*N*-Dimethylaminomethyl)anthracene	4	AQ	80

Similar products were obtained with Pd(1wt%)-N-Ti and Ag(1wt%)-N-Ti system. But the yield and time taken for completion of the reaction were different. The light absorption ability of these catalysts are somewhat low compared to Gd(1wt%)-N-Ti, which adversely affects the formation of reactive oxygen species thereby the photo-oxidation efficiency. The results are presented in the Table 5.2 and 5.3.

The amount of the catalyst was chosen to be 0.1g since a lower amount (0.05g) gave a marginal yield and a higher amount (0.15g) made the suspension very thick for the light to transmit and resulted in a poor yield. The effect of lamp power was also studied for all the reactions using two photoreactors having powers 100 W and 150 W respectively. As expected the yield was higher with a lamp power of 150 W.

5.2.2. Photo-oxidation of 9-Anthracenemethanol

The concentration of the substrate, light source, catalyst, catalyst amount and experimental conditions are same as before. Anthraquinone (AQ) was the only product obtained after photo-oxidation of 9-Anthracenemethanol with 85% yield within 2.5h using 150 W lamp. Protection of 10^{th} position of the compound by phenyl group leads to the formation of 9-hydroxy 9-phenylanthrone (9H9PA) in good yield. When the reaction time was increased to 4h, we obtained anthraquinone as the major product with 80% yield. But with Pd(1wt%)-N-Ti system, it takes around 3h for the completion of the reaction and the yield obtained was somewhat low. With Ag(1wt%)-N-Ti, the complete conversion of phenyl protected derivative of the substrate takes place within 3.5h. C-N bond cleavage is easy compared to C-C bond cleavage. That is, functional groups present on the anthracene systems affect the reaction time and

yield of the products. Functional groups also affect the interaction of reactive oxygen species with the substrate and the easier cleavage of the functional group reduces the time taken for the complete conversion of the substrate. The photo-oxidation results are tabulated in Table 5.4, 5.5 and 5.6.

Table. 5.4. Photo-oxidation of Anthracenemethanol using Gd(1wt%)-N-Ti

Substrate	Time (h)	Products	Yield (%)
9-Anthracenemethanol	2.5	AQ	85
10-phenyl-9-anthracenemethanol	2.5	9H9PA	70
		AQ	11
10-phenyl-9-anthracenemethanol	4	AQ	80

Table. 5.5. Photo-oxidation of Anthracenemethanol using Pd(1wt%)-N-Ti

Substrate	Time (h)	Products	Yield (%)
9-Anthracenemethanol	3	AQ	81
10-phenyl-9-anthracenemethanol	3	9H9PA	69
		AQ	9
10-phenyl-9-anthracenemethanol	4	AQ	77

Table. 5.6. Photo-oxidation of Anthracenemethanol using Ag(1wt%)-N-Ti

Substrate	Time (h)	Products	Yield (%)
9-Anthracenemethanol	3	AQ	80
10-phenyl-9-anthracenemethanol	3.5	9H9PA	70
		AQ	8
10-phenyl-9-anthracenemethanol	4	AQ	76

5.2.3. Photo-oxidation of 9-Anthraldehyde

Nanoparticles such as metal, metal oxide and metal sulfides can catalyze many chemical transformations in organic synthesis including reduction, oxidation, cross coupling or hydrogenation [50-52]. The experimental set up and reaction conditions are same as before. Anthraquinone (82%) was obtained from anthraldehyde with a time period of 3.5h using Gd(1wt%)-N-Ti. Photo-oxidation of phenyl protected anthraldehyde favored 9-hydroxy 9-phenylanthrone (9H9PA) with 70% yield. The formed intermediate species eventually transformed to anthraquinone as the time increased to 4h. Same products were obtained with the other two catalysts. Here the aldehyde group is directly attached to the anthracene moiety. Cleavage of C-O bond is rather difficult than C-C and C-N cleavages. The rate of formation of reactive oxygen species and its feasibility to interact with the substrate affects the yield and time of the reaction. The results are tabulated in Table 5.7, 5.8 and 5.9.

Table. 5.7. Photo-oxidation of Anthraldehyde by Gd(1wt%)-N-Ti

Substrate	Time (h)	Products	Yield (%)
9-Anthraldehyde	3.5	AQ	82
10-phenyl-9-anthraldehyde	3.5	9H9PA	70
		AQ	9
10-phenyl-9-anthraldehyde	4.5	AQ	78

Table. 5.8. Photo-oxidation of Anthraldehyde using Pd(1wt%)-N-Ti

Substrate	Time (h)	Products	Yield (%)
9-Anthraldehyde	3.5	AQ	79
10-phenyl-9-anthraldehyde	4	9H9PA	65
		AQ	12
10-phenyl-9-anthraldehyde	4.5	AQ	78

Table.5.9. Photo-oxidation of Anthraldehyde by Ag(1wt%)-N-Ti

Substrate	Time (h)	Products	Yield (%)
9-Anthraldehyde	4	AQ	70
10-phenyl-9-anthraldehyde	4	9H9PA	58
		AQ	11
10-phenyl-9-anthraldehyde	5	AQ	69

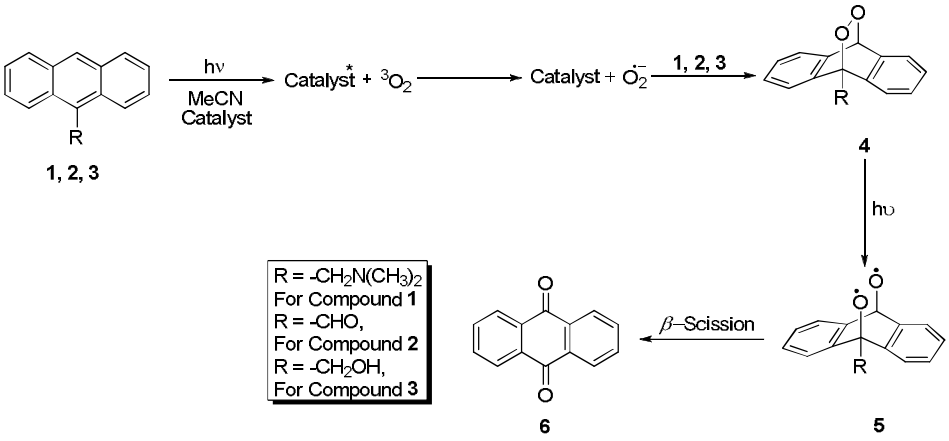

Fig. 5.5. General Reaction Mechanism for Anthracene Derivatives

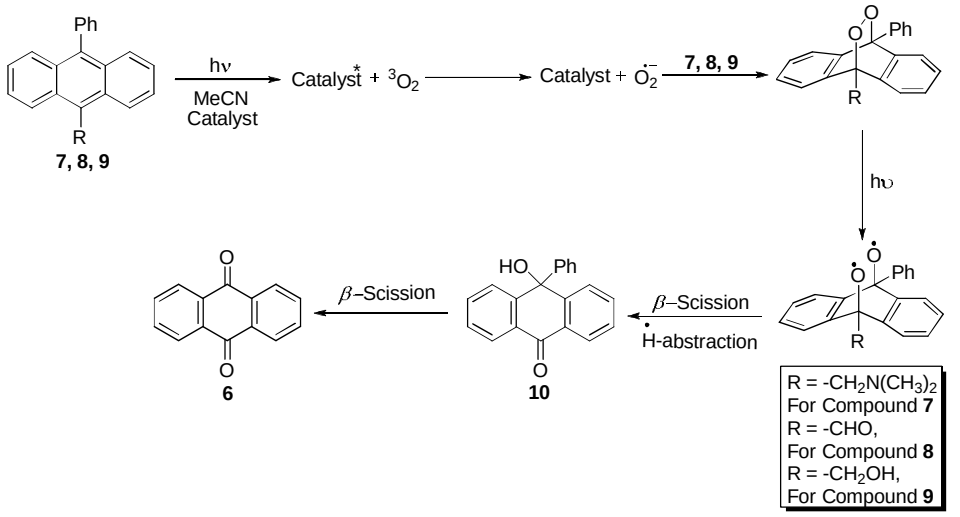

Fig. 5.6. Reaction Mechanism for Phenyl Protected Anthracene Derivatives

Light and molecular oxygen are the two major driving forces in photo-oxidation reactions. The reaction does not occur without catalyst, oxygen or in the dark. In this reaction, molecular oxygen was not added to the reaction mixture externally. However, the reaction efficiencies in oxygen atmosphere and air atmosphere are comparable. Upon irradiation with visible light, electrons in the valance band of the catalyst could get excited and get accumulated in the conduction band. These electrons could easily be captured by molecular oxygen adsorbed on the catalyst surface to form some reactive oxygen species which in turn react with the substrate molecules. Molecular oxygen not only acts as a scavenger for electrons but is also responsible for producing some reactive species. The superoxide anion (reactive oxygen species) formed reacts with the substrate to form endoperoxide. This was eventually decomposed to anthraquinone through β-Scission. The phenyl ring at the 10^{th} position reduces the feasibility of photo-oxidation reaction and the stability of the

intermediate compound allows its easy identification and separation. Increasing the reaction time leads to extensive degradation resulting in the loss of phenyl group to form anthraquinone (AQ). The intermediate species 9-hydroxy 9-phenylanthrone (9H9PA) was formed from endoperoxide through β-Scission and hydrogen abstraction. It then rearranges to form the final product via β-Scission.

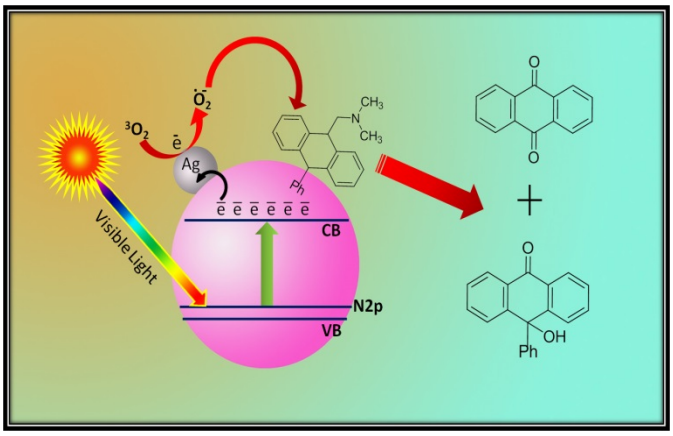

Fig.5.7. Plausible way of interaction of reactive oxygen species with the substrate in Ag,N co-doped TiO_2 system

Usually, metals can exist as a metal island on the surface of the catalyst. It can act as the scavenger for electrons excited from the valance band upon irradiation only when the work function of these metals are high compared to the semiconductor materials. So these electrons can easily be captured by molecular oxygen adsorbed on the surface through metal to form reactive oxygen species. It then interacts with the substrate molecule adsorbed on the surface favoring the products.

5.3. Characterization of Anthraquinone (AQ)

Melting point of the compound was found to be 284°C which is well in accordance with the reported results. FT-IR spectrum of the compound shows a strong band around 1670 cm^{-1} corresponding to C=O stretching vibration. The band at 896 cm^{-1} represents the stretching of substituted benzene ring. ^{1}H NMR spectrum of the compound shows two doublet of doublets at 'δ' value in the range of 7.8-8.34 ppm indicating two sets of four equivalent protons. GCMS spectrum shows m/z value at 208 corresponds to the M^{+} peak of anthraquinone and it shows an M-28 peak at 180. All these characterizations confirm the formation of compound Anthraquinone (AQ).

5.4. Characterization of 9-hydroxy 9-phenylanthrone (9H9PA)

The melting point (MP) of the compound is 216°C which agrees with the already reported results. FT-IR spectrum shows two strong bands at 3416 cm^{-1} and 1600 cm^{-1} corresponding to the O-H stretching and bending vibrations respectively. Another prominent peak at 2922 cm^{-1} corresponds to C-H stretching vibration. Proton NMR spectrum of the compound shows multiplets having 'δ' value around 7.07-7.75 ppm representing the 13 aromatic protons. Compound 4 (9-hydroxy 9-phenyl anthrone) shows M^{+} peak at m/z 286 and M-77 peak at 209.

5.5. Conclusion

Semiconductor catalysis is an effective and greener way for the removal of environmentally harmful substances. Cost effective, recyclable and environmentally benign co-doped TiO_2 catalysts were successfully employed for the photo-oxidation of some anthracene derivatives in the

visible region. Here all the three catalysts showed comparable activity. Yield of the product and the time taken for the completion of the reaction are different for all the catalysts. The catalysts were found to be very active for the photo conversion of anthracene derivatives to Anthraquinone, a compound having diverse applications in industrial as well as medical fields. Substitution of the 10^{th} position by a phenyl ring favored 9-hydroxy 9-phenylanthrone (9H9PA) as an intermediate species. The toxicity of this compound was also found to be lower compared to the starting compounds.

References

[1]. O. Carp, C. L. Huisman, A. Reller, Progress in Solid State Chemistry. 32 (2004) 33.

[2]. A. Mills, S. Le Hunte, J. Photochem. Photobiol. A. Chem. 108 (1997) 1.

[3]. P. Pichat, Handbook of Heterogeneous Photocatalysis, eds, G. Ertl, H. Knoezinger, J. Wietkamp, Wiley, New York (1997) 2111.

[4]. M. R. Hoffmann, S. T. Martin, W. Choi, D. W. Bahnemannt, Chem. Rev. 95 (1995) 69.

[5]. P. Pichat, Catal. Today. 19 (1994) 313.

[6]. P. V. Kamal, Chem. Rev. 93 (1993) 267.

[7]. N. N. Rao, P. Natarajan, Curr. Sci. 66 (1994) 742.

[8]. M. A. Fox, Top. Curr. Chem. 142 (1987) 71.

[9]. H. Kisch, J. Prakt. Chem. 336 (1994) 635.

[10]. E. Baciocchi, C. Rol, G. V. Sebastiani, L. Taglieri, J. Org. Chem. 59 (1994) 5272.

[11]. R. Kuenneth, C. Feldmer, F. Knoch, H. Kisch, Chem. Eur. J. 1 (1995) 441.

[12]. L. Cermenati, M. Mella, A. Albini, Tetrahedron. 54 (1998) 2575.

[13]. M. A. Fox, M. T. Dulay, Chem. Rev. 93 (1993) 341.

[14]. R. Terzian, N. Serpone, C. Minero, E. Pelizzetti, H. Hidaka, J Photochem. Photobiol. A. Chem. 63 (1990) 829.

[15]. P. PichatIn: M. Schiavello, editor. Photoelectrochemistry, photocatalysis and photoreactors. Dordrecht: D. Reidel; (1985) 425.

[16]. T. Ohno, K. Nakabeya, M. Matsumura, J. Catal. 176 (1998) 76.

[17]. T. Ohno, T. Kigoshi, K. Nakabeta, M. Matsumura, Chem. Lett. 877 (1998).

[18]. T. Ohno, Y. Masaki, S. Hirayama, M. Matsumura, J. Catal. 204 (2001) 163.

[19]. J. L. Zhang, M. Anpo, Chem. J. Chin. Univ.—Chin. 25 (2004) 733.

[20]. A. Sclafani, J. M. Hermann, J. Phys. Chem. 100 (1996).

[21]. P. Boarini, V. Carassiti, A. Maldotti, R. A. Madelli, Langmuir. 14 (1998) 2080.

[22]. C. B. Almquist, P. Biswas, Appl. Catal. A: Gen. 214 (2001) 259.

[23]. M. T. Dulay, D. Washington-Dedeaux, J. Photochem. Photobiol. A: Chem. 61 (1991)153.

[24]. D. Worsley, A. Mills, K. Smith, M. G. Hutchings, J. Chem. Soc. Chem. Commun. (1995) 1119.

[25]. O. Beaume, A. Finiels, P. Geneste, P. Graffin, A. Guida, J. L. Olive et al., M. Guisneteditor, Heterogenouscatalysis and fine chemicals III. Studies in surface science and catalysis, Amsterdam: Elsevier. 78 (1993) 401.

[26]. T. Ohno, K. Tokieda, S. Higashida, M. Matsumura, Appl. Catal. A: Gen. 244 (2003) 383.

[27]. R. A. Sheldon, J. K. Kochi, Metal-catalyzed oxidation of organic compounds. New York: Academic Press; (1981).

[28]. M. Hudlicky, Oxidation in organic chemistry. Washington (DC): American Chemical Society; (1990).

[29]. R. C. Larock, Comprehensive organic transformation. New York: VCH; (1989).

[30]. G. Canelli, G. Cardillo, Chromium oxidations in organic chemistry. Berlin: Springer, (1984).

[31]. N. B. Shali, S. Sugunan, J. Sol-Gel Sci. Tech. 42 (2007) 101.

[32]. H. L. Chum, M. Ratcliff, F. L. Posey, A. J. Nozik, J. A. Turner, J. Phys. Chem. 87 (1983) 3089.

[33]. Y. J. Lin, A. Lee, L. S. Teng, H. T. Lin, Chemosphere. 48 (2002) 1.

[34]. M. A. Fox, J. N. Younathan, Tetrahedron. 42 (1986) 6235.

[35]. K. V. Subba Rao, M. Subrahmanyam, J. Photochem. Photobiol. Sci. 1 (2002) 597.

[36]. J. C. Fetzer, "The Chemistry and Analysis of the Large Polycyclic Aromatic Hydrocarbons". Polycyclic Aromatic Compounds (New York: Wiley) 27 (2) (2000) 143.

[37]. X. Sun, H. Liu, J. Dong, J. Wei, Y. Zhang, Catal. Lett. 135 (2010) 219.

[38]. J. Jacob, The significance of polycyclic aromatic hydrocarbons as environmental carcinogens, Pure Appl. Chem. 68 (1996) 301.

[39]. C. Menzie, B. B. Potocki, J. Santodonato, Environ. Sci. Technol. 26 (1992) 1278.

[40]. P. Henner, M. Schiavon, J. L. Morel, E. Lichtfouse, Anal. Mag. 25 (1997) 56.

[41]. A. Masih, A. Taneja, Chemosphere. 65 (2006) 449.

[42]. S. K. Samanta, O.V. Singh, P. K. Jain, Trends Biotechnol. 20 (2002) 243.

[43]. D. Dąbrowska1, A. Kot-Wasik, J. Namieśnik, Polish J. of Environ. Stud. 17 (2008) 17.

[44]. A. Fujishima, K. Hashimoto, T. Watanabe, TiO_2 Photocatalysis Fundamental and Application, BKC, Tokyo, (1999).

[45]. D. S. Bhatkhande, V. G. Pangarkar, A. A. C. M. Beenackers, J. Chem. Technol. Biotechnol. 77 (2001) 102.

[46]. M. E. Sigman, P. F. Schuler, M. M. Ghosh, R. T. Dabestani, Environ. Sci. Technol. 32 (1998) 3980.

[47]. S. Wen, J. Zhao, G. Shen, J. Fu, P. Peng, Chemosphere. 50 (2003) 111.

[48]. Y. Wang, C. S. Liu, F. B. Li, C. P. Liu, J. B. Liang, J. Hazard. Mater. 162 (2009) 716.

[49]. K. M. Lehto, E. Vuorimaa, H. Lemmetyinen, J. Photochem. Photobiol. A. 136 (2000) 53.

[50]. P. Christopher, H. Xin, S. Linic, Nat. Chem. 3 (2011) 467.

[51]. B. Oregan, M. Gratzel, Nature. 353 (1991) 737.

[52]. A. Corma, H. Garcia, Chem. Soc. Rev. 37 (2008) 2096.

.....ൠ.....

Chapter 6

Cu/Pd Bimetallic Supported on TiO_2 for Suzuki Coupling Reaction

Contents

Bimetallic catalysts, composed of two metal elements in either alloy or intermetallic form, often emerge as materials of a new category with catalytic properties different from monometallic catalysts, depending on the composition and size/morphology. The term "bimetallic catalysts" was introduced by Sinfelt in the early 1960s [1]. Generally, bimetallic catalysts are more superior to mono metallic catalyst and provide a better platform for the development of novel catalysts with enhanced activity, selectivity and stability. This chapter discusses the preparation of Cu/Pd bimetallic supported on TiO_2 by Sol-Gel followed by impregnation method, its characterization and applications in Suzuki coupling reaction.

6.1. Introduction

The deposition of noble metal nanoparticles on the support used as catalysts is attracting immense attention because of the widespread use of these particles in heterogeneous catalysis [2]. Due to the presence of an altered electronic or surface structure of the metal particles, metal

nanoparticle catalysts composed of two (or more) different metal elements may result in improved catalyst quality or properties and hence are of great interest from both technological and scientific views [3]. Bimetallic catalysts are well known materials for exhibiting properties that are different from those of the corresponding monometallic catalysts [1,4]. Correlation of electronic properties of bimetallic surfaces with reaction pathways is a difficult task and it has been demonstrated that bimetallic surfaces also play a significant role in controlling their electronic and catalytic properties [5-7]. There have been a lot of reports on the synthesis and assembly of bimetal materials such as Pd-Pt [8], Au-Ag [9], Pt-Co [10] and Ni-Mo [11]. Agrawal et al. conducted a lot of studies on bimetallic or multimetallic nanoparticle catalysts such as Au-Ag, Au-Cu and Au-Ag-Cu [12]. Due to mechanical and chemical resistance under reaction conditions, Alumina-based supports are commonly employed in these catalysts. Generally, bimetallic systems are highly active than monometallic systems. Grondelle et al. reported higher activity for ammonia oxidation on alumina supported silver/copper catalyst than catalysts with pure silver or copper particles on alumina [13]. Zhao et al. reported the epoxidation of styrene over Ag/Cu bimetallic supported on Alumina [14]. Noble metals (Pd and Pt) in combination with various promoters such as Cu [15–19], Sn [20], In [21], Ag and Au [22] dispersed on solid supports are highly active for nitrate conversion. The role of promoters in this catalyst system is to curtail undesirable side reactions with simultaneous increase in the catalytic activity. Higher catalytic activity of Pd-Cu bimetallic particles supported on ceria [23], alumina [24] and titania [25] compared to monometallic Pd catalyst have been reported elsewhere. Hirai et al. [26] reported the aerobic oxidation of

2-propanol to acetone under visible light using supported Au-Cu nanoalloy. Selective oxidation of benzylic alcohols to the corresponding aldehydes has been reported with SBA-16 immobilized Au-Pd catalyst [27]. Hutchings et al. have demonstrated the oxidation of primary C–H bonds in toluene to benzyl benzoate compounds with high selectivity under mild solvent-free conditions by Au-Pd/C and Au-Pd/TiO_2 [28]. Chen et al. evaluated γ-Al_2O_3 supported Pt-Ni catalysts for the hydrogenation of benzene and 1,3-butadiene and the results revealed that catalysts with a smaller Pt/Ni ratio exhibited higher levels of activity [29]. Norskov et al. reported the selective hydrogenation of acetylene by Ni-Zn nanocatalyst. This particular catalyst is less expensive and more readily available than the Ag-modified Pd hydrogenation catalyst which is currently used industrially for the removal of trace acetylene from ethylene. Liu et al. successfully conducted the selective hydrogenation of 2-chloronitrobenzene using Pt-Ru nanoparticles supported on SnO_2 [30]. Qiu et al. selectively hydrogenated 2-chloronitrobenzene to 2-chloroaniline using a three-dimensional flower-like Co-Ni/C catalyst [31]. Keane et al. compared the activity of Ni/Al_2O_3 and Au/Al_2O_3 nanoparticles prepared by the impregnation method with that of Au-Ni/Al_2O_3 nanoparticles prepared by the reductive deposition of Au onto Ni in the catalytic gas-phase conversion of 2,4-dichlorophenol [32]. He et al. evaluated the catalytic activities of different Ru and Ru-Re bimetallic nanoparticles supported on SiO_2, ZrO_2, TiO_2, H-β and H-ZSM5 in the hydrogenolysis of glycerol to propanediols and found that Ru-Re catalyst showed higher activity than Ru catalyst [33]. Asakura et al. developed Ru-Fe/CNT system for the selective hydrogenolysis of an aqueous 20% (w/w) glycerol solution to glycols [34]. These bimetallic catalysts are also applicable in coupling reactions.

Pd-catalyzed cross-coupling reactions have become some of the most important organic transformations in synthetic chemistry for forming C–C bonds [35] and the use of Pd nanoparticles in these coupling reactions has been extensively investigated [36–39]. Recent studies are focused to enhance the activity, selectivity and stability of the catalysts used as well as elucidating the catalytic reaction mechanisms by designing a variety of novel Pd-based bimetallic materials. Chen et al. prepared and evaluated the alloy and the core-shell Au-Pd particles confined in silica nanorattles in order to enhance the activity, selectivity and stability of catalysts for the Suzuki coupling reaction [40]. A highly active catalyst based on Pd-Co alloy nanoparticles supported on polypropylenimine grafted on graphene could effectively carry out Sonogashira coupling reaction, reported by Shaabani et al. [41]. Choi et al. synthesized a variety of carbon-supported bimetallic Pd-M (M = Ag, Ni, and Cu) nanoparticles by γ-irradiation at room temperature and the resulting Pd-Cu/C nanoparticles exhibited high catalytic efficiency in the Suzuki and Heck-type coupling reactions [42]. Gao et al. reported the effectiveness of montmorillonite supported Pd-Cu for Sonogashira coupling reaction [43]. Ultimately bimetallic catalysts are found to be more effective than mono metallic catalysts for coupling reactions. Here we report the Suzuki coupling reaction by using Cu/Pd bimetallic supported on TiO_2. Various parameters such as effect of catalysts, effect of solvents and effect of bases were evaluated for the same.

6.2. Preparation of catalysts

Cu/Pd bimetallic TiO_2 was prepared by Sol-Gel followed by impregnation method. 10 ml of $Ti[OCH(CH_3)_2]_4$ was dissolved in 30 ml

of ethanol by vigorous stirring at room temperature. To this 0.23g of $Pd(NO_3)_2$ in 25 ml of water was added and the whole solution was sonicated for about 5h to form a clear sol. After proper aging, the obtained gel was dried at 80°C and crushed to finally divided particles. Around 0.09g of $Cu(NO_3)_2.3H_2O$ in 50 ml water was added to the finely divided particles in a beaker and stirred for 8h. The final mixture was washed perfectly with various solvents in order to remove the impurities completely. Then it was dried and calcined at 500°C for 3h to get the desired Cu(1wt%)-Pd(4wt%)-Ti system. We have prepared various bimetallic catalysts by varying the concentration of dopants.

Monometallic Cu-TiO_2 and Pd-TiO_2 were prepared by sonication assisted Sol-Gel method. 10 ml of $Ti[OCH(CH_3)_2]_4$ was dissolved in ethanol/acetic acid (1:1 v/v) mixture by stirring. To this solution around 0.20g of $Cu(NO_3)_2.3H_2O$ in water was added and sonicated for about 5h to form a clear sol. After proper ageing, the obtained Gel was dried at 80°C and calcined at 500°C for 3h. The obtained catalyst was designated as Cu(2wt%)-Ti. Another fraction of the catalysts was prepared by varying the concentration of dopant.

Monometallic Pd-TiO_2 was also prepared by the same method discussed above. Here also 10 ml of $Ti[OCH(CH_3)_2]_4$ was dissolved in ethanol/acetic acid (1:1 v/v) mixture by vigorous stirring. This solution was mixed with 0.23g of Palladium nitrate in 25 ml of water and stirred continuously to get a clear sol. After aging, the sol was transformed to gel. This was dried at 80°C and calcined at 500°C for 3 hours to get the required Pd(4wt%)-Ti.

6.3. Characterization of bimetallic Cu/Pd-TiO_2

6.3.1. X-ray Diffraction Analysis (XRD)

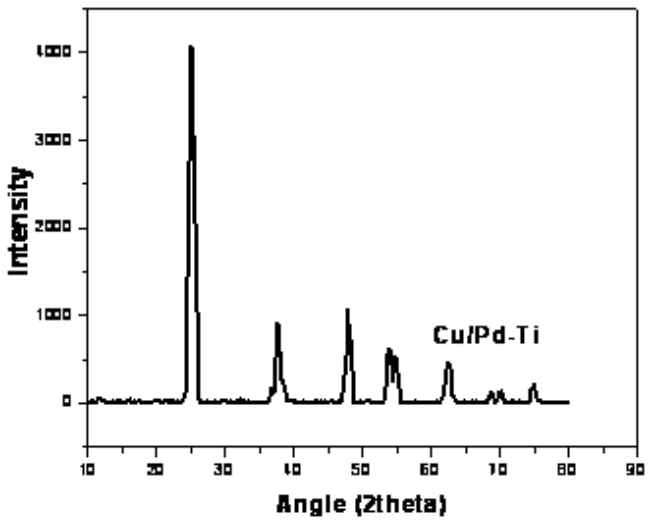

Fig. 6.1. XRD pattern of Cu-Pd-Ti

Fig. 6.1 represents the XRD pattern of Cu(2wt%)-Pd(4wt%)-Ti system. Sharp and intense peaks after calcination at 500°C represent the highly crystalline nature of the material. Here the dominant phase is anatase with an angle of 2θ = 25.3°. No peak corresponding to rutile or brookite phases was observed. The peaks corresponding to Pd and Cu were also absent due to their low concentration. Crystallite size of the sample was calculated from Scherrer equation by using full width at half maximum (FWHM) of the (101) peak of the anatase phase. The average crystallite size was calculated to be 18.1 nm. Here the crystallite size was found to be higher due to the agglomeration of particles.

6.3.2. Thermal Analysis

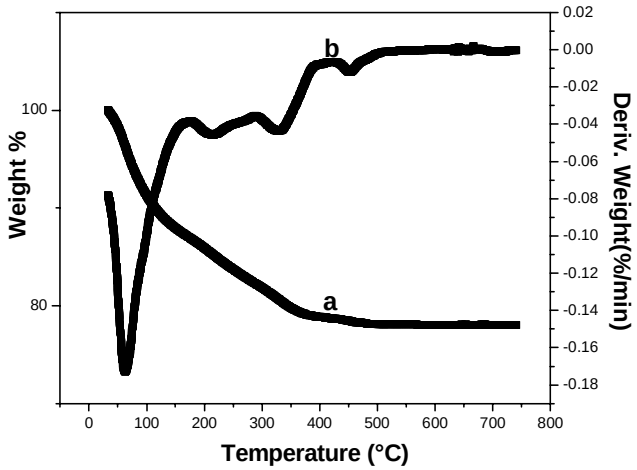

Fig. 6.2. a) TG Curve b) DTG Curve of Cu-Pd-Ti

Thermal analysis is used to understand the stability of the prepared catalyst. Fig. 6.2 represents the TG and DTG curves of Cu/Pd-Ti system. A weight loss around 100°C may be due to the loss of adsorbed water. Three weight losses located below 460°C is due to the complete decomposition of precursors. After 460°C, there is no noticeable weight loss on DTG which indicates the stability of the catalyst and hence the calcination temperature was fixed at 500°C.

6.3.3. Scanning Electron Microscopy

From the SEM images, we could understand that all the particles are irregular in shape. The shapeless structures in the image are mainly due to agglomeration and that would have happened during synthesis. Irregularity of Cu(2wt%)-Pd-Ti system was high compared to Cu(1wt%)-Pd-Ti. This may be due to the greater degree of agglomeration resulting from the higher concentration of dopants. Particle aggregation results in an increase of particle size thereby decreasing the surface area. The

surface area data is tabulated in Table 6.1. Compared to pure TiO_2, surface area of bimetallic modified TiO_2 was found to be somewhat high.

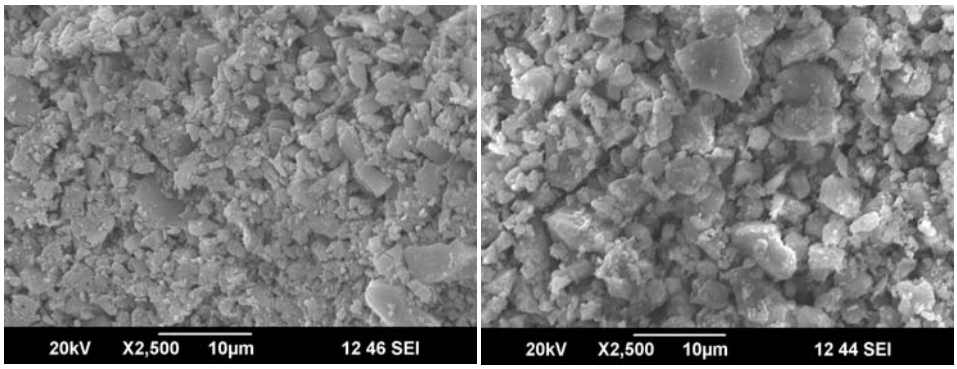

Cu(1wt%)-Pd-Ti Cu(2wt%)-Pd-Ti

Fig. 6.3. SEM Images of Cu(1wt%)-Pd-Ti and Cu(2wt%)-Pd-Ti Systems

Table. 6.1. Surface Area of $TiO_2$and Cu-Pd-Ti Systems

Catalyst	Surface area (m^2/g)
TiO_2	59
Cu(1wt%)-Pd-Ti	67
Cu(2wt%)-Pd-Ti	76

6.3.4. Energy Dispersive X-ray Analysis

EDX is a qualitative technique used to estimate approximate percentage of elements present in the prepared system. The intensity of the peak is directly related to the concentration of elements. EDX spectrum of Cu/Pd bimetallic TiO_2 with different concentration of copper is shown in Fig. 6.4. Spectra showed the presence of Cu and Pd along with Ti and O. So EDX give a qualitative idea about the composition of the system. The atom percentages of impurities are tabulated in Table. 6.2.

Table. 6.2. Atom percentage of impurities present in Cu-Pd-Ti System

Name of the Catalyst	Atom % of Dopants	
Cu(1wt%)-Pd-Ti	Cu-1.9	Pd-3.9
Cu(2wt%)-Pd-Ti	Cu-2.6	Pd-4.1

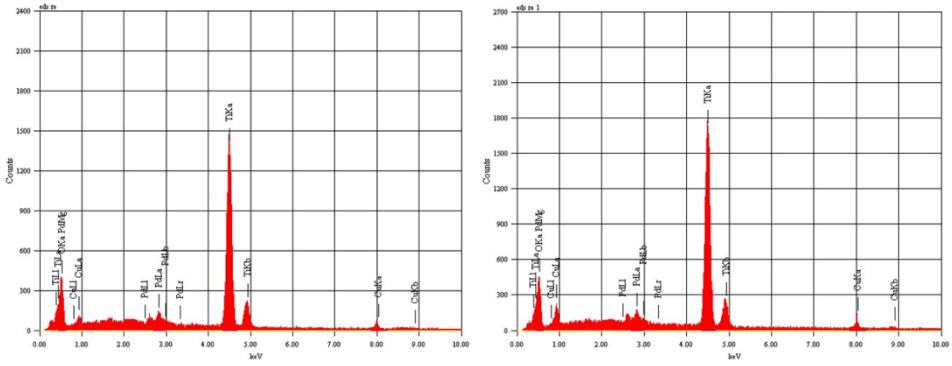

(a) **(b)**

Fig.6.4. EDX Spectum of a) Cu(1wt%)-Pd-Ti b) Cu(2wt%)-Pd-Ti

6.3.5. X-ray Photoelectron Spectroscopy (XPS)

Fig.6.5. shows the survey scan of Cu(2wt%)-Pd(4wt%)-Ti and its high resolution scan over various core levels such as Ti2p, O1s, Pd3d and Cu2p. Peaks observed at 458 eV and 464 eV due to spin orbit splitting corresponding to the $Ti2p_{3/2}$ and $Ti2p_{1/2}$ levels confirmed Ti^{+4} species. O1s signal at 528.1 eV indicates O^{2-} ions in the lattice of TiO_2. The binding energy values of $Pd3d_{5/2}$ (334 eV) and $3d_{3/2}$ (341 eV) revealed that palladium was in the form of PdO in the prepared system. Peak at binding energy of 932 eV corresponds to $Cu2p_{3/2}$ and another peak at 952 eV with a binding energy difference of 20 eV represents $Cu2p_{1/2}$ confirmed the presence of Cu(II) species. These two peaks indicate the good dispersion of metal into TiO_2 matrix.

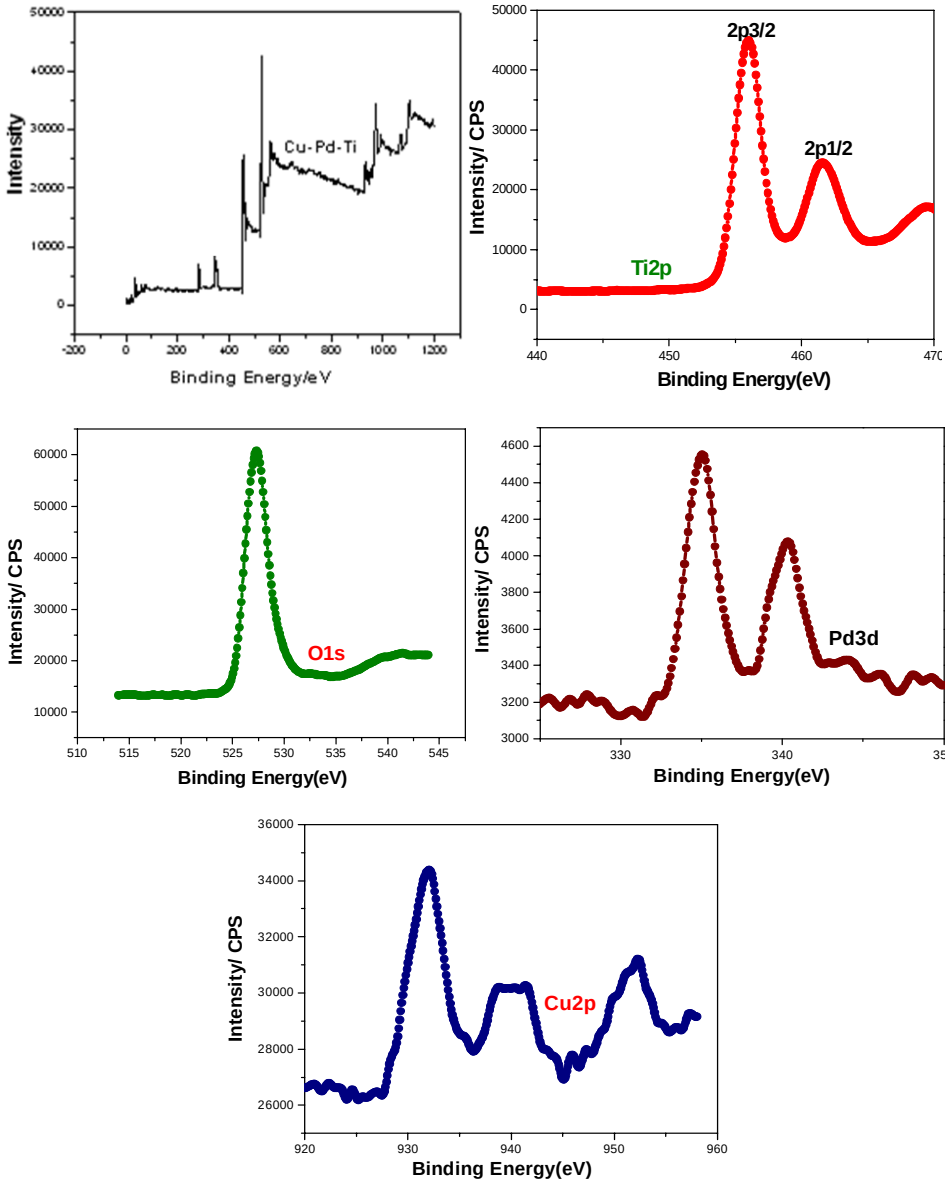

Fig. 6.5. XPS Spectrum of Cu(2wt%)-Pd(4wt%)-TiO_2

6.4. Suzuki Coupling Reaction

Transition-metal catalysed cross-coupling reactions are powerful tools for the formation of new carbon–carbon bonds which has got

immense significance in industrial as well as synthetic points of view. Palladium catalyzed coupling of aryl halide and phenyl boronic acid in the presence of a base is known as Suzuki Coupling reaction. Extensive work has been carried out on Suzuki coupling reaction in a homogeneous way, however it suffers from a number of drawbacks such as catalyst decomposition, poor reagent solubility etc. In this chapter, we made an attempt to evaluate the activity of Cu/Pd-Ti catalyst in Suzuki coupling reactions. Reaction scheme is shown below.

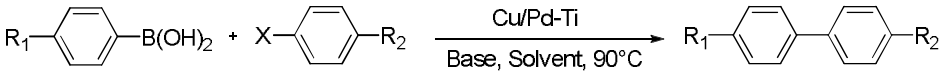

Fig. 6.6. Suzuki Coupling Reaction Catalyzed by Cu/Pd-Ti

Five different catalysts were employed to carry out Suzuki coupling reaction. The results are shown in Table. 6.3. A marginal yield was obtained with catalyst having 1wt% of Copper. But the product yield was increased to 21% as the concentration of the copper was increased. Monometallic Pd(4wt%)-Ti system showed better activity compared to copper modified TiO_2 because 'Pd' is the active component in the catalytic system. Around 52% yield was obtained with monometallic Pd modified TiO_2 system. Combination of Cu and Pd on TiO_2 improved the product yield which unambiguously proved the effectiveness of bimetallic catalytic system. In the bimetallic system, copper acts as a promoter which alters the rate of the reaction and also improves the selectivity towards a particular product. Synergistic effect due to Pd and Cu is also responsible for the improved activity of bimetallic systems. From the table, it is clear that Cu(2wt%)-Pd(4wt%)-Ti system was superior to other

catalysts and produced around 71% of the product biphenyl using DMF as the solvent. We have again checked the activity of the three effective catalysts by varying water as the solvent. Here also the results followed the same pattern and around 60% of biphenyl was obtained with Cu(2wt%)-Pd(4wt%)-Ti catalytic system. The results are presented in Table. 6.4.

Table.6.3. Suzuki Coupling Reaction Using Different Catalysts

Catalysts	% Yield
Cu(1wt%)-Ti	11
Cu(2wt%)-Ti	21
Pd(4wt%)-Ti	52
Cu(1wt%)-Pd(4wt%)-Ti	63
Cu(2wt%)-Pd(4wt%)-Ti	71

Reaction Conditions: Bromobenzene (3 mmol), Phenyl boronic acid (3.6 mmol), K_2CO_3 (9 mmol), Temperature (90°C), DMF (10 ml), Reaction Time (20h), Catalyst amount (0.1g).

Table.6.4. Effect of three active catalysts in Suzuki reaction using water as the solvent

Catalyst	% Yield
Pd(4wt%)-Ti	41
Cu(1wt%)-Pd(4wt%)-Ti	53
Cu(2wt%)-Pd(4wt%)-Ti	60

Reaction conditions: Bromobenzene (3 mmol), Phenyl boronic acid (3.6 mmol), K_2CO_3 (9 mmol), Temperature (90°C), Water (10 ml), Time (20h), Catalyst amount (0.1g).

Suzuki coupling reaction was carried out in polar protic, polar aprotic and non-polar aprotic solvents in order to understand its influence on this reaction. The results are tabulated in Table.5.

Compared to non-polar solvents, good results were obtained with polar solvents. Smooth interaction between the substrates and the active sites of the catalyst takes place very effectively in polar solvents due to its easier diffusion effect compared to non-polar solvents. That is why yield of the product biphenyl was found to be higher with polar solvents. Among different solvents, dimethyl formamide (DMF) showed higher yield of around 72% using Cu(2wt%)-Pd(4wt%)-Ti as the catalytic system. Poor yield of around 28% was obtained with non-polar aprotic solvent xylene. Poor reagent solubility and lesser interaction between the substrate and catalytic active site results in poor yield. The results are tabulated in Table 6.5. We have again checked the activity only in polar solvents using Cu(2wt%)-Pd(4wt%)-Ti by changing the base as NaOH. Here the activity followed the same pattern as before and higher yield (59%) was obtained with DMF as the solvent. The results are summarized in Table.6.6.

Table.6.5. Effect of Solvent on Suzuki Coupling Reaction

Solvents	% Yield
DMF	72
Dioxane	59
DMSO	39
Water	65
Ethanol	70
Acetic acid	56
Toluene	32
Xylene	28

Reaction conditions: Bromobenzene (3 mmol), Phenyl boronic acid (3.6 mmol), K_2CO_3 (9 mmol), Catalyst used (Cu(2wt%)-Pd(4wt%)-Ti, Temperature (90°C), Solvent (10 ml), Time (20h), Catalyst amount (0.1g).

Table. 6.6. Effect of Polar Solvents on Suzuki Reaction using NaOH as the Base

Solvents	% Yield
DMF	59
Ethanol	49
Water	51

Reaction Conditions: Bromobenzene (3 mmol), Phenyl boronic acid (3.6 mmol), NaOH (9 mmol), Catalyst used (Cu(2wt%)-Pd(4wt%)-Ti, Temperature (90°C), Solvent (10 ml), Time (20h), Catalyst amount (0.1g).

Base is an inevitable part of Suzuki coupling reaction. Without the presence of a base, these reactions are not feasible. Boron containing compounds can be activated in the presence of a base and also facilitate the formation of R1Pd-OR from R1Pd-X. But exact understanding of this parameter is still unclear. We have tried four different bases to understand its effect on Suzuki reaction. The yield was different with different bases. Higher yield of around 72% was obtained with Cu(2wt%)-Pd(4wt%)-Ti system using K_2CO_3 as the base and poor yield was obtained in triethyl amine. The results are presented in the Table. 6.7.

Table. 6.7. Effect of different bases on Suzuki coupling reaction

Base	% yield
K_2CO_3	71
Na_2CO_3	67
KOH	57
Et_3N	61

Reaction conditions: Bromobenzene (3 mmol), Phenyl boronic acid (3.6 mmol), Base (9 mmol), Catalyst used (Cu(2wt%)-Pd(4wt%)-Ti, Temperature (90°C), DMF (10 mL), Time (20 hours), Catalyst amount (0.1g).

We have conducted the recycling studies by washing the Cu(2wt%)-Pd(4wt%)-Ti using different solvents and then calcined at 500°C for 1h. No significant loss of catalytic activity was observed after three cycles. The results are shown in Table. 6.8.

Table.6.8. Recycling studies

No. of cycles	% yield
1	72
2	68
3	65

Reaction Conditions: Bromobenzene (3 mmol), Phenyl boronic acid (3.6 mmol), Base (9 mmol), Catalyst used (Cu(2wt%)-Pd(4wt%)-Ti, Temperature (90°C), DMF (10 ml), Time (20h), Catalyst amount (0.1g).

6.4.1. Mechanistic Details of Suzuki Coupling Reaction

Oxidative addition, Transmetalation and Reductive elimination are the three major steps involved in Suzuki coupling reaction [44]. Oxidative

addition can be considered as the rate determining step in this catalytic cycle [45]. The aryl halide reacts with copper present in the Cu-Pd-Ti system giving aryl copper halide in the first step which upon transmetalation gave aryl palladium halide. This Ar-Pd-X reacts with Ar-$B(OH)_2$ to give Ar-Pd(II)-Ar and $XB(OH)_2$. This trans Ar-Pd(II)-Ar undergoes reductive elimination, gives the product and regenerates Pd(0) catalyst which can actively participate in other catalytic cycles. The reaction proceeds with complete retention of stereochemistry for alkenyl halide and with inversion for allylic and benzylic halides. Mechanism of Suzuki coupling reaction is shown in scheme 1.

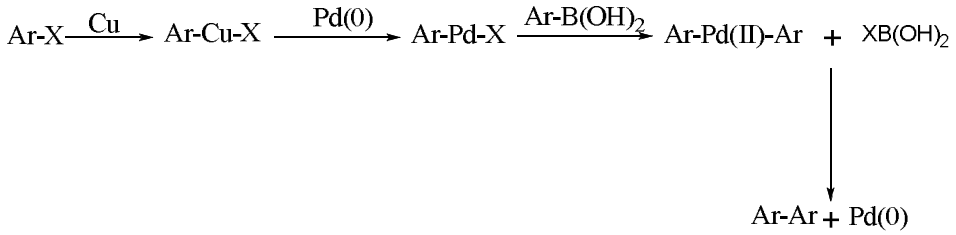

Fig. 6.7. Mechanism of Cu/Pd-Ti Catalyzed Suzuki Coupling Reaction

6.4.2. Characterization of the product

The product biphenyl was separated and purified by column chromatography using hexane as the mobile phase. The product was characterized by ^{1}HNMR, FTIR and GCMS analysis.

^{1}HNMR (400 MHz; CDCl3): δ7.35-7.59 (m, 10H). FT-IR (υ_{max}(cm^{-1}): 2925-2956 (=CH- stretching, 1400-1500 (-C=C- stretching).

6.5. Conclusion

Cu/Pd-bimetallic supported on TiO_2 was prepared by Sol-Gel followed impregnation method and well characterized by techniques such as XRD, TG-DTG, SEM-EDX and XPS. The prepared catalytic systems were successfully employed for Suzuki coupling reactions. Effective solvent, base and catalyst were DMF, K_2CO_3 and Cu(2wt%)-Pd(4wt%)-Ti respectively. The bimetallic catalyst was found to be active up to three cycles without appreciable loss in its activity.

References

[1]. J. H. Sinfelt, Bimetallic Catalysts: Discoveries, Concepts, and Applications. New York: John Wiley & Sons, (1983).

[2]. W. Guobin, D. Wei, L. Qian, C. Weiliang, Z. Jingchang, China Petroleum Processing and Petrochemical Technology. 14 (2012) 59.

[3]. J. H. Sinfelt, J. Catal. 29 (1973) 308.

[4]. J. A. Rodriguez, Surf. Sci. Rep. 24 (1996) 225.

[5]. B. Hammer, J. K. Norskov, Surf. Sci. 343 (1995) 211.

[6]. B. Hammer, J. K. Norskov, Adv. Catal. 45 (2000) 71.

[7]. J. Greeley, M. Mavrikakis, Nat. Mater. 3 (2004) 810.

[8]. N. Toshima, M. Harada, T. Yonezawa, K. Kushihashi, K. Asakura, J. Phys. Chem. 95 (1991) 7448.

[9]. J.-H. Liu, A.-Q. Wang, Y.-S. Chi, H.-P. Lin, C.-Y. Mou, J. Phys. Chem. B. 109 (2005) 40.

[10]. S. C. Tsang, N. Cailuo, W. Oduro, A. T. S. Kong, L. Clifton, K. M. K. Yu, B. Thiehaut, J. Cookson, P. Bishop, ACS Nano. 2 (2008) 2547.

[11]. L. Zhao, K. Fang, D. Jiang, D. Li, Y. Sun, Catal. Today. 158 (2010) 490.

[12]. V. V. Agrawal, P. Mahalakshmi, G. U. Kulkarni, C. N. R. Rao, Langmuir. 22 (2006) 1846.

[13]. L. Gang, B. G. Anderson, J. V. Grondelle, J. Catal. 206 (2002) 60.

[14]. H. -K. Wang, C. -Y Yi, L. Tian, W. –J. Wang, J. Fang, J. –H. Zhao, W. –G. Shen, J. Nanomaterials. 2012 (2011) 1.

[15]. A. Pintar, Catal. Today. 77 (2003) 451.

[16]. F. Deganello, L. F. Liotta, A. Macaluso, A. M. Venezia, G. Deganello, Appl. Catal. B: Environ. 24 (2000) 265.

[17]. J. Batista, A. Pintar, J. P. Gomilsek, A. Kodre, F. Bornette, Appl. Catal. A: Gen. 217 (2001) 55.

[18]. S. Kerkeni, E. Lamy-Pitara, J. Barbier, Catal. Today. 75 (2002) 35.

[19]. E. F. Gauthard, J. Barbier, Appl. Catal. A: Gen. 237 (2002) 253.

[20]. H. Berndt, I. Monnich, B. Lucke, M. Menzel, Appl. Catal. B: Environ. 30 (2001) 111.

[21]. L. Lemaignen, C. Tong, V. Begon, R. Burch, D. Chadwick, Catal. Today. 75 (2002) 43.

[22]. F. Gauthard, F. Epron, J. Barbier, J. Catal. 220 (2003) 182.

[23]. F. Epron, J. Gauthard, J. Barbier, J. Catal. 206 (2002) 363.

[24]. Y. –X. Chen, Y. Zhang, G. –H. Chen, Water Res. 37 (2003) 2489.

[25]. W. Gao, N. Guan, J. Chen, X. Guan, R. Jin, H. Zeng, Z. Liu, F. Zhang, Appl. Catal. B: Environ. 46 (2003) 341.

[26]. Y. Sugano, Y. Shiraishi, D. Tsukamoto, S. Ichikawa, S. Tanaka, T. Hirai, Angew. Chem. Int. Ed. 52 (2013) 5295.

[27]. Y. T. Chen, H. M. Lim, Q. H. Tang, Y. T. Gao, T. Sun, Q. Y. Yan, Y. H. Yang, Appl. Catal. A. 380 (2010) 55.

[28]. L. Kesavan, R. Tiruvalam, M. H. Ab Rahim, M. I. bin Saiman, D. I. Enache, R. L. Jenkins, N. Dimitratos, J. A. Lopez-Sanchez , S. H. Taylor, D. W. Knight, C. J. Kiely, G. J. Hutchings, Science. 331 (2011) 195.

[29]. W. W. Lonergan, D. G. Vlachos, J. G. Chen, J. Catal. 271 (2010) 239.

[30]. M. H. Liu, Q. Bai, H. L. Xiao, Y. Y. Liu, J. Zhao, W. W. Yu, Chem. Eng. J. 232 (2013) 89.

[31]. Y. L. Xie, N. Xiao, Z. Ling, Y. Liu, C. Yu, J. S. Qiu, Chin. J. Catal. 33 (2012) 1883.

[32]. M. A. Keane, S. Gomez-Quero, F. Cardenas-Lizana, W. Q. Shen, Chem- Cat. Chem. 1 (2009) 270.

[33]. L. Ma, D. H. He, Top Catal. 52 (2009) 834.

[34]. B. D. Li, J. Wang, Y. Z. Yuan, H. Ariga, S. Takakusagi, K. Asakura, ACS Catal. 1 (2011) 1521.

[35]. C. C. C. Johansson Seechurn, M. O. Kitching, T. J. Colacot, V. Snieckus, Angew. Chem. Int. Ed. 51 (2012) 5062.

[36]. M. Hyotanishi, Y. Isomura, H. Yamamoto, H. Kawasaki, Y. Obora, Chem. Commun. 47 (2011) 5750.

[37]. C. C. Li , R. Sato, M. Kanehara, H. B. Zeng, Y. Bando, T. Teranishi, Angew. Chem. Int. Ed. 48 (2009) 1.

[38]. R. Z. Zhang, J. M. Liu, F. W. Li, S. F. Wang, C. G. Xia, W. Sun, Chin. J. Chem. 29 (2011) 525.

[39]. Y-M. Shen, Y-J. Du, M-F. Zeng, D. Zhi, S-X. Zhao, L-M. Rong, S-Q. Lv, L. Du, C-Z. Qi, Appl. Organomet. Chem. 24 (2010) 631.

[40]. L. F. Tan, X. L. Wu, D. Chen, H. Y. Liu, X. W. Meng, F. Q. Tang, J. Mater. Chem. A. 1 (2013) 10382.

[41]. A. Shaabani, M. Mahyari, J. Mater. Chem. A. 1 (2013) 9303.

[42]. S-J. Kim, S-D. Oh, S. Lee, S-H. Choi, J. Ind. Eng. Chem. 14 (2008) 449.

[43]. W. Xu, Y. L. Sun, M. H. Guo, W. Q. Zhang, Z. W. Gao, Chin. J. Org. Chem. 33 (2013) 820.

[44]. K. Matos, J. A. Soderquist, J. Org. Chem. 63 (1998) 461.

[45]. N. Miyaura, A. Suzuki, Chem. Rev. 95 (1995) 2457.

.....ꕥ.....

Chapter 7

Photovoltaic Applications of TiO_2 Thin Films

Contents

Due to energy crisis, the whole world is looking for a new sustainable energy source. Harnessing solar energy is one of the most promising ways to tackle this issue. The present dominant photovoltaic (PV) technologies are based on inorganic materials. But the high material cost, low power conversion efficiency and manufacturing cost limits its popularization [1]. A lot of research has been conducted towards the development of low-cost PV technologies, of which organic photovoltaic (OPV) devices are quite promising. During the last two decades, organic electronic devices such as organic light-emitting diodes (OLEDs), organic thin film transistors, OPVs and organic memory devices have attracted much attention because of their low cost, stability and high performance

characteristics. This chapter discusses the fabrication of inverted hetero junction solar cells using conducting polymer as photo active layer. Here TiO_2 was used as the electron transport layer. Two fullerene derivatives were introduced into the device in order to improve the power conversion efficiency.

7.1. Introduction

Organic photovoltaic devices are based on organic semiconductors whose backbones are comprised mainly of alternating C–C and C=C bonds. Semiconducting properties of OPV devices are mainly attributed to the electron delocalization along the conjugated backbone [2]. OPVs are divided mainly into two different categories according to whether their constituent molecules small or large. Synthesis, purification and device fabrication processes of these two classes of materials are different. Polymer solar cells (PSCs) are processed from solution in organic solvents whereas solar cells based on small-molecules are processed mainly using thermal evaporation deposition techniques in a high-vacuum environment. Easy thin-film fabrication, low material consumption resulting from a high absorption coefficient, use of organic materials which are abundant, low manufacturing energy requirements, low specific weight, mechanical flexibility, tunable material properties and high transparency are the major advantages of PSCs over other OPVs based on small-molecules [3]. A donor–acceptor bilayer planar heterojunction was introduced to the OPV cell in 1979 by Tang and achieved power-conversion efficiencies (PCEs) of around 1% [4,5]. Introduction of C_{60} fullerene and its derivatives (such as [6,6]-phenyl-C_{61}-butyric acid methyl ester, PCBM) to replace n-type molecules is one of the

major breakthroughs in OPV technology [6]. C_{60} derivatives have become standard n-type molecules in OPV devices due to their strong electro negativity and high electron mobility. Effective electron transfer between conjugated polymer and fullerene derivatives were independently demonstrated by Heeger et al. and Yoshino et al. in early 1990s [7,8]. They observed an extremely fast femto second (fs) photoinduced electron transfer process which dominates over all other photophysical processes present and this provided a solid foundation for OPV technology. Reduced interfacial area between donor and acceptor species is the major drawback of planar junction; while less durability is the main limitation of bulk heterojunction devices. In order to overcome these difficulties, inverted heterojunction device was introduced. Materials design, morphology and manipulation and interface engineering are the three major concerns while fabricating a polymer based solar cell device. In inverted heterojunction, inorganic materials such as zinc oxide, titanium oxide and cadmium selenide can also function as acceptors for polymer donors, for which efficiencies of over 3% have been demonstrated [9-11]. Short circuit current (J_{sc}), open circuit voltage (V_{oc}) and fill factor (FF) are the three important parameters to be tuned to get good power conversion efficiency. A donor polymer with a lower HOMO level will give a higher V_{OC} and the HOMO level of the polymer in a PSC can be effectively lowered by utilizing groups that are less electron-rich [12-15]. Narrowing the band gap is an effective way to improve Jsc but it is also affected by factors such as carrier mobility, intermolecular interaction and molecular chain packing. Simultaneous improvement of V_{OC} and J_{SC} can be achieved by structural fine-tuning [16-19]. Side-chain tuning also has considerable effects on improving the FF and Frechet et al. optimized the

side-chain patterns for N-alkylthieno[3,4-c] pyrrole-4,6-dione (TPD)-based polymers [20]. Side-chain tuning helped to optimize π-stacking, polymer crystallinity and material miscibility and caused the FF to increase and recently reported an efficiency of 7% for a TPD–silole copolymer [21]. The bottom layer of a PSC is traditionally a layer of the transparent conductive material, indium tin oxide (ITO) and in inverted heterojunction devices, solution processed transition metal oxides have been applied in place of PEDOT:PSS to get long term stability [22,23]. Developing novel acceptors such as fullerene derivatives can also improve the PCE of PSCs [24-28]. n-type inorganic metal oxides such as TiOx [29] and zinc oxide (ZnOx) [30] have been shown to be good candidates for organic electronics. The inverted architecture has received increasing attention since 2006. Yang et al. demonstrated an inverted PSC structure using V_2O_5 as the top p-type interface layer. Nanostructure forms such as TiO_2 nanotube [31] and ZnO nanoridge [32] have also been applied as n-type materials in the fabrication of inverted PSCs. The most popular n-type buffer materials are TiOx, ZnOx and Cs-doped TiOx, while the most popular p-type buffers are V_2O_5, MoO_3, WO_3, NiO and PEDOT:PSS. Wantz et al. studied the light activation phenomenon in TiO_2 based inverted organic solar cells and achieved a power conversion efficiency of 4% [33]. Aplarslan et al. fabricated a device using buffer layers of Mn-doped TiO_2 with P3HT:PCBM as active layer and observed that the efficiency of the device with doped titania was increased by 38% in comparison to layer without Mn-dopant [34]. The inverted solar cells with Nb-doped titania were proposed by Lira-Cantu et al. using MEH-PPV (Poly[2-methoxy-5-(2-ethylhexyloxy)-1,4-phenylenevinylene]) as the photo active layer [35,36]. Non-metal doped TiO_2 was also introduced in

inverted heterojunction devices and a power conversion efficiency of around 1.6% was obtained with N-TiO_2 [37]. ITO/CdS/P3HT:PCBM/Ag type inverted solar cells were fabricated by Yavuz et al. by employing CdS films between ITO and the blend film of P3HT:PCBM and achieved a power conversion efficiency of 0.3% [38]. Liang et al. employed vertically aligned ZnO nanowalls as electrode in inverted polymer solar cells and obtained an efficiency of 2.14% [39]. A thermal annealing free inverted polymer solar cell using ZnO nanoparticles (NPs)/Cs_2CO_3 bilayer as an electron-selective layer (ESL) and the blend of poly(3-hexylthiophene)(P3HT):phenyl C_{61}-butryric acid methyl ester (PCBM) as an active light-absorbing layer has been reported by Cheng et al. [40]. The effect of Al doping in sol-gel derived AZO layer on the performance of P3HT:PCBM bulk heterojunction with an inverted structure have been demonstrated by Aprilia et al. [41]. Rajesh et al. successfully fabricated an inverted polymer heterojunction device by using In_2S_3 as the electron transport layer with MEH-PPV as the photo active layer and achieved a power conversion efficiency of 0.075% [42]. This chapter discusses the fabrication of the device using TiO_2 as the electron transport layer with MEH-PPV as the hole transport layer.

7.2. Preparation of TiO_2 Thin Films

10 ml of $Ti[OCH(CH_3)_2]_4$ was mixed with 30 ml of water and stirred for about 5h. The resulted mixture was dried at 100°C to get titanyl hydroxide ($TiO(OH)_2$). Around 0.3g of titanyl hydroxide was dissolved in 1:1 volume mixture of H_2O/HNO_3 led to the formation of titanyl nitrate which is a water soluble salt. Then 6g of poly vinyl alcohol (PVA) in 50 ml of water was refluxed at 80°C for about 12h resulted viscous clear

solution of PVA. 1:1 volume mixture of PVA/titanyl nitrate was used as the precursor for TiO_2. Cost effective spin coating technique was adopted for the fabrication of thin film. We have prepared two TiO_2 films having different thickness by varying the volume of precursor. Specified amount of precursor was spin coated on indium doped tin oxide (ITO) at 3000 rpm. The acceleration and time used was 3000 and 1min respectively. Finally TiO_2 thin film was obtained by calcination of this spin coated ITO plate at 500°C for 2h. 1 ml of precursor solution resulted TiO_2 thin films having a thickness of 200 nm and 300 nm films was obtained by spin coating 1.5 ml of precursor solution. The thickness of the fabricated films was measured using Stylus profiler. Both the above prepared films were used for fabrication of the device.

7.3. Preparation of Thin Films of poly[2-methoxy-5-(2'-ethylhexyloxy)-*p*-phenylenevinylene] (MEH-PPV)

MEH-PPV was purchased from Sigma Aldrich. Around 10mg of MEH-PPV was dissolved in 1 ml of chlorobenzene. 0.3 ml of MEH-PPV in chlorobenzene was spin coated on ITO plate at 1000 rpm. The acceleration and time used for fabrication was 1000 and 40s respectively. The thickness of the film was measured to be 100 nm by Stylus profiler. This 100 nm MEH-PPV film was used throughout the device fabrication. During device fabrication, two fullerene derivatives such as [6,6]-phenyl-C_{61}-butyric acid methyl ester (PCBM) and indene C_{60} bisadduct (ICBA) were added along with MEH-PPV solution in order to improve the power conversion efficiency. Both these fullerene derivatives are p-type materials and can accept the electrons transferred from the photoactive layer (MEH-PPV). Around 20mg of fullerene derivatives were mixed

with 10mg of MEH-PPV in chlorobenzene. Then 0.3 ml of this mixture was spin coated on the top of TiO_2 thin film in the device.

7.4. Characterization of TiO_2 Thin Films

7.4.1. X-ray Diffraction Analysis (XRD)

From the XRD pattern it is clear that anatase is the dominant phase with an angle of 2θ = 25.1°. Calcination temperature used was 500°C which is the phase forming temperature of metastable anatase phase. No peak corresponding to brookite and rutile was observed. Sharp and intense peaks represent the crystalline nature of the TiO_2 thin film. Compared to powder form, the intensities of peaks are very less in film form due to the low concentration of TiO_2. Here the film thickness was 300 nm which is very less compared to substrate concentration. The crystallite size was calculated by using Scherrer formula and was found to be 31nm.

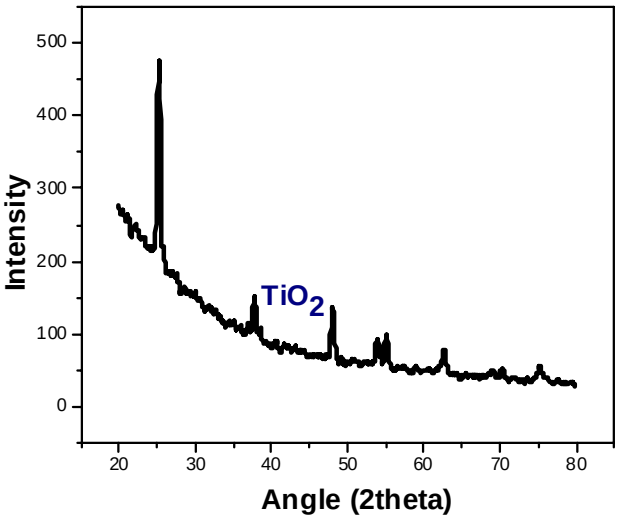

Fig. 7.1. XRD pattern of TiO_2 Thin Film

7.4.2. Atomic Force Microscopy (AFM)

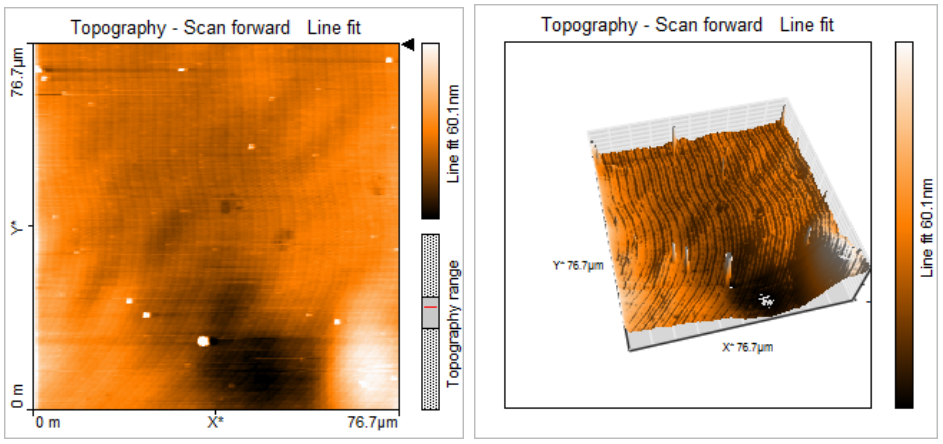

(a) TiO_2 Film Calcined at 500°C **(b)** 3D map of TiO_2 Film Calcined at 500°C

(c) TiO_2 Film Calcined at 550°C **(d)** 3D map of TiO_2 Film Calcined at 550°C

Fig.7.2. AFM Images of TiO_2 Thin Films

The Fig.7.2 (a) and (b) represent the AFM images of TiO_2 calcined at 500°C for 2h with its 3D map and showed a uniform nature. Area roughness of the film was found to be around 252 nm. All the films were fabricated by Spin coating the precursor solution so that there is a chance for crystal growth during calcination. Fig. 7.2 (c) and (d) correspond to

TiO_2 thin films calcined at 550°C for 2h with its 3D map. A calcination temperature of 550°C facilitated the crystal growth towards nanofiber morphology. We have repeated the experiment 4-5 times and obtained the same morphology in this particular temperature. Area roughness of this film was found to be 592 nm. Area roughness was less for uniform morphology but high temperature destructed the uniform behavior so that area roughness was found to be higher. Due to uniform nature, the films obtained at 500°C showed less resistance compared to sample calcined at higher temperature. So we have used the uniform film having less resistance for the fabrication our photovoltaic device.

7.4.3. Conductivity Measurement

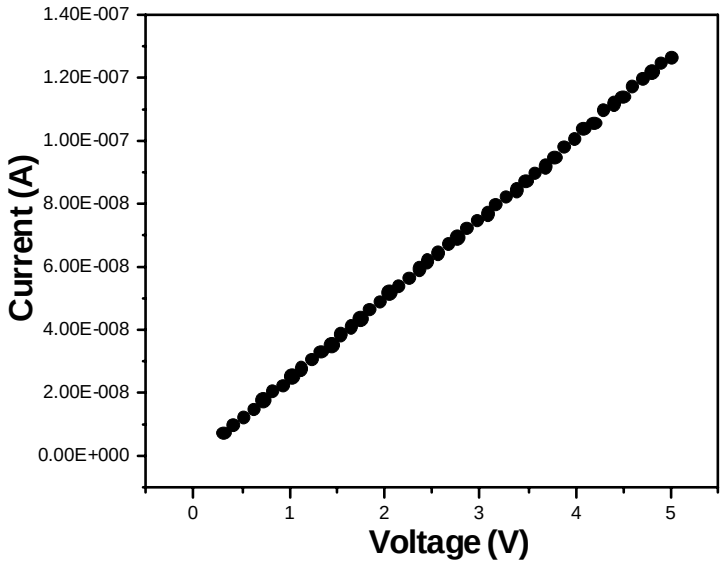

Fig.7.3. I-V Plot of TiO_2 Thin Film

Conductivity measurements are purely based on ohms law. Conductivity of TiO_2 thin film was measured by two probe Keithley 2420-C system and that was calculated to be around 1.25×10^{-1} $\Omega^{-1}cm^{-1}$. This value

is purely in the semiconducting range. This conductivity measurement confirmed the presence of TiO_2 thin film on ITO surface.

7.5. Fabrication of Inverted Heterojunction Device

The base structure of most of the solar cell devices is indium doped tin oxide (ITO). ITO can collect both electrons and holes because the work function of ITO is in between the HOMO and LUMO of conjugated polymers. Top layer influences the polarity of ITO electrode. TiO_2 films having various thicknesses were fabricated on ITO plate by spin coating technique. The method of fabrication has been reported earlier. TiO_2 is an n-type material and electron deficient in nature so that it can act as an electron transport layer. Photo active layer of this device was a p-type conjugated conducting polymer MEH-PPV. A Mixture of MEH-PPV and fullerene derivatives (PCBM and ICBA) in chloroform was coated on the top of TiO_2 by spin coating technique. Both PCBM and ICBA are fullerene derivatives but LUMO level of these materials are different. Very cost effective spin coating technique was adopted for the fabrication of the entire device. Low work function metal, silver (Ag) was vacuum deposited on the top of photo active layer at a pressure of $\sim 6 \times 10^{-6}$ Torr. In this device ITO can act as the negative electrode and vacuum deposited silver can be considered as the positive electrode. The device structure is shown in Fig. 7.4.

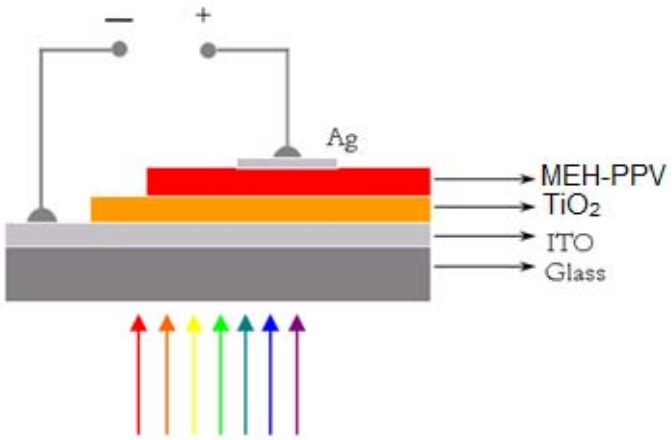

Fig.7.4. Schematic Representation of Inverted Heterojunction Device

7.6. Energy Level Diagram of ITO/TiO_2/Polymer/Ag device

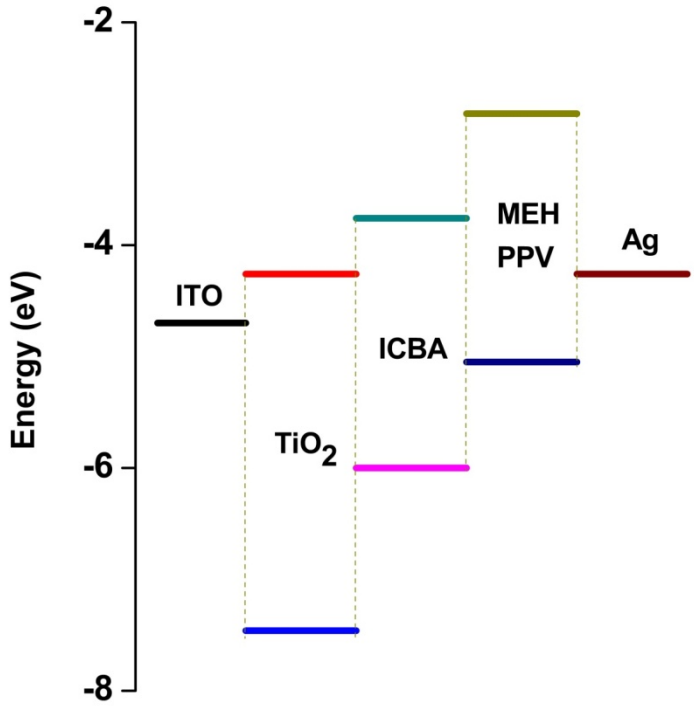

Fig.7.5. Energy Level Diagram of Inverted Heterojunction Device

Fig.7.5. represents the energy level diagram of the fabricated inverted heterojunction device. Here ITO is the base electrode and Ag is the top electrode. The photo active layer used here was a mixture of MEH-PPV and fullerene derivative ICBA. We have fabricated the device using two different acceptor molecules. The conduction band edge of TiO_2 is -4.1 eV. The LUMO level of the polymer ranges from -2.3 to -3.1 eV. So the level of acceptor must be between -3.5 to -3.8 eV. The LUMO level of PCBM is somewhat similar to that of TiO_2 which adversely affect the charge transfer. But the LUMO level of ICBA is -3.74. This compatible energy level facilitates an effective charge transfer in the device. The effective charge transfer between conjugated polymer and the acceptor molecule is evidenced from fluorescence quenching studies.

7.7. Fluorescence Quenching Studies

10mg of MEH-PPV and 20mg of ICBA were mixed via sonication in 1ml of chlorobenzene. Desired amount of this solution was spin coated on glass substrate at 1000 rpm. The acceleration and time used was 1000 and 40s respectively. We have also prepared bare MEH-PPV film on glass substrate using the same method. Both these prepared films were employed for fluorescence studies. Excitation source used in this study was blue LED having a wavelength of 458 nm. Emission maximum of bare MEH-PPV was measured to be around 585 nm. But this emission peak was completely disappeared in the mixture of MEH-PPV and ICBA. That is, the fluorescence was quenched due to the effective charge transfer between the two materials. Compatible energy level between the

two materials is mainly responsible for the complete quenching of fluorescence. The fluorescence spectrum is shown in Fig. 7.6.

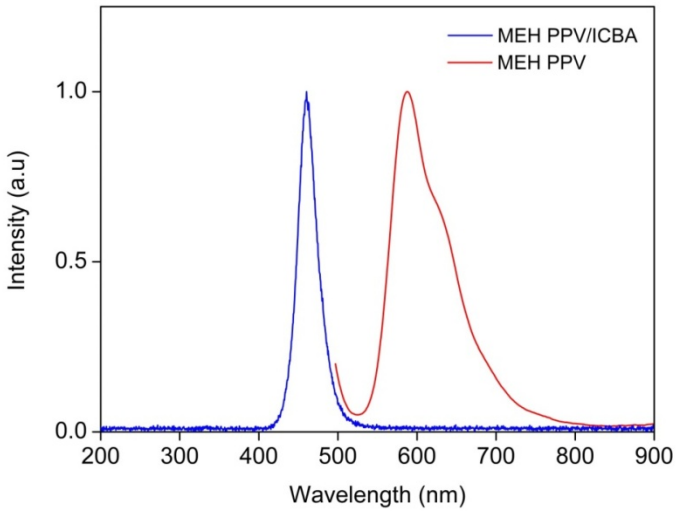

Fig.7.6. Fluorescence Spectrum of 1:2 Mixtures of MEH-PPV and ICBA

7.8. J-V Characteristics of ITO/TiO_2/Polymer+PCBM/Ag Heterojunction

The device fabrication has been described earlier. Here the acceptor used was PCBM. Thicknesses of TiO_2 and MEH-PPV used in this study were 300 nm and 100 nm respectively. We have optimized the thicknesses by trial and error method. The J-V characteristics are shown in Fig. 7.7. Fig.7.7a represents the J-V characteristic of the heterojunction in dark which unambiguously proved the formation of diode. In the dark, the diode is purely ohmic in nature. But the device showed rectification after irradiation with a Xenon lamp of 150 W. Based on this we have calculated short circuit current (Jsc), open circuit voltage (Voc), fill factor (FF) and finally efficiency of the fabricated device. Jsc, Voc and FF were found to be 0.33 mA/cm^2, 563 mV and 30% respectively. The efficiency of the device was calculated to be 0.05%.

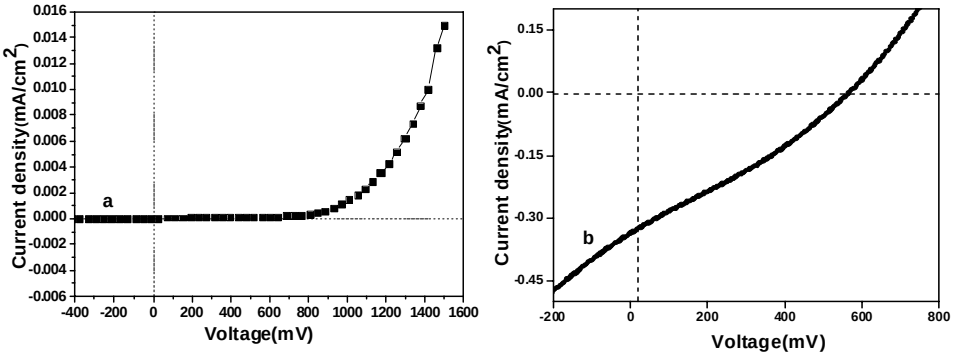

Fig.7.7. J-V Characteristics of Inverted Heterojunction Using 300 nm TiO_2 Thin Film

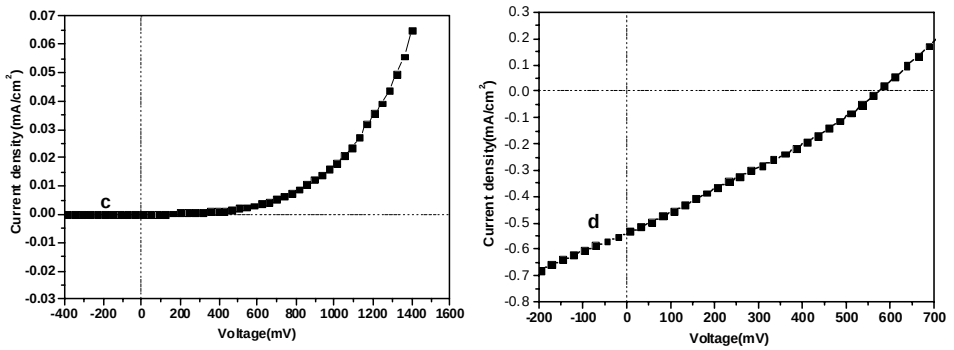

Fig.7.8. J-V Characteristics of Inverted Heterojunction Using 200 nm TiO_2 Thin Film

Fig.7.8 shows the J-V characteristics of inverted heterojunction using 200 nm TiO_2 thin film where the thickness of photo active layer was kept constant. TiO_2 thin film having a thickness of 100 nm was not sufficient to form the diode due to its low concentration and polymer films having thickness above 100 nm could not absorb light effectively resulting low power conversion efficiency. Fig. 7.8c indicates the J-V properties of the device in dark which confirmed the formation of diode. It is clear from the graph that no rectification was there in the dark. But the device showed rectifying character upon irradiation with a light source (150 W, Xenon lamp). The device exhibited a short circuit current density

of (Jsc) of 0.53 mA/cm^2 and an open circuit voltage (Voc) of 572 mV. The fill factor (FF) and power conversion efficiency were calculated to be 28.63% and 0.082% respectively. The resistance of TiO_2 film is a main constraint while fabricating the device. Techniques such as inversion cooling and doping is somewhat sufficient for reducing the resistance of the semiconductor film which helps to improve the power conversion efficiency to a much higher extend.

7.9. J-V characteristics of ITO/TiO_2/Polymer+ICBA/Ag Heterojunction

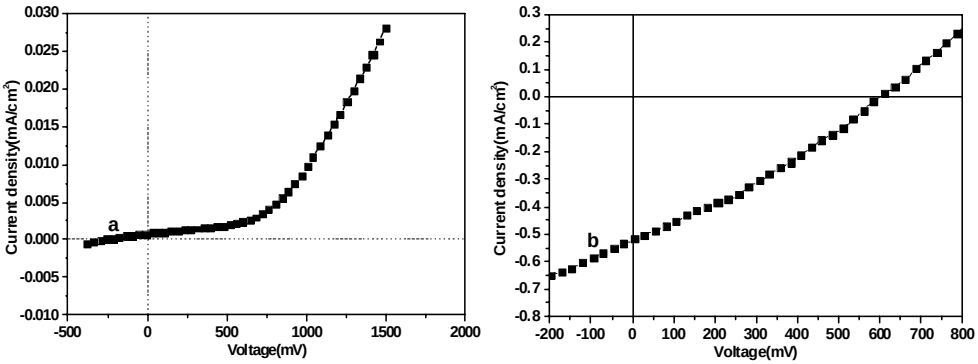

Fig.7.9. J-V characteristics of Heterojunction Device Using 300 nm TiO_2 Thin Film as Electron Transport Layer

The Fig.7.9a indicates the J-V characteristics of the device in the dark. From the graph it is clear that the device exhibited some rectifying behavior in the dark which may be due to the barrier formed at the TiO_2/polymer interface. The formation of diode is obvious from the graph. The device showed higher rectification after illumination with a 150 W Xenon lamp with an irradiance of 96.9 mW/cm^2. Under illumination the heterojunction showed a short circuit current density (Jsc) of

0.52 mA/cm^2 and an open circuit voltage (Voc) of 601 mV. The fill factor and efficiency of the device was calculated to be 30.15% and 0.095% respectively. The energy level of the ICBA is more compatible with the conducting polymer. The effective charge transfer improved the power conversion efficiency of the device.

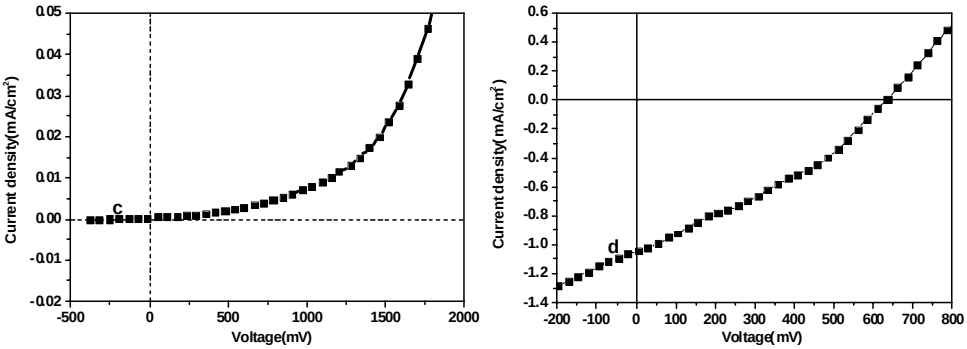

Fig.7.10. J-V Characteristics of Heterojunction Device Using Electron Transport ayer as 200 nm TiO_2 Thin Film

J-V characteristics of Fig.7.10c exhibited the formation of diode. In the dark, the device was not rectifying in nature. But upon illumination, the device showed a much higher rectification compared to other fabricated devices. The device showed a short circuit current density of 0.70 mA/cm^2 and an open circuit voltage of 672 mV after illumination. The fill factor and power conversion efficiency were calculated to be 48.2% and 0.22% respectively. 0.22% was the maximum efficiency obtained from our work. From this we could understand that TiO_2 thickness and nature of fullerene derivative played a vital role in the efficiency of the device.

7.10. Conclusion

Fabricated inverted heterojunction devices using TiO_2 as the electron transport layer and conjugated polymer MEH-PPV as the hole transport layer. Two fullerene derivatives such as PCBM and ICBA were introduced in the device in order to improve the power conversion efficiency. The maximum power conversion efficiency of around 0.22% was obtained by using ICBA as the acceptor molecule. The optimum thicknesses of electron transport layer and hole transport layer in order to get better efficiency were found to be 200 nm and 100 nm respectively.

References

[1]. www.eia.gov/aer

[2]. M. Pope, C. E. Swenberg, Electronic Processes in Organic Crystals and Polymers 2nd edn. Oxford Univ., (1999).

[3]. G. Dennler, M. C. Scharber, C. J. Brabec, Adv. Mater. 21 (2009) 1323.

[4]. C. W. Tang, US patent 4, 164 (1979) 431.

[5]. C. W. Tang, Appl. Phys. Lett. 48 (1986) 183.

[6]. J. C. Hummelen, J. Org. Chem. 60 (1995) 532.

[7]. N. S. Sariciftci, L. Smilowitz, A. J. Heeger, F. Wudl, Science. 258 (1992) 1474.

[8]. S. Morita, A. A. Zakhidov, K. Yoshino, Solid State Commun. 82 (1992) 249.

[9]. M. D. McGehee, MRS Bull. 34 (2009) 95.

[10]. S. Dayal, N. Kopidakis, D. C. Olson, D. S. Ginley, G. Rumbles, Nano Lett. 10 (2010) 239.

[11]. J. Weickert, R. B. Dunbar, H. C. Hesse, W. Wiedemann, L. Schmidt-Mende, Adv. Mater. 23 (2011) 1810.

[12]. N. Blouin, A. Michaud, M. Leclerc, Adv. Mater. 19 (2007) 2295.

[13]. Q. M. Zhou, Appl. Phys. Lett. 84 (2004) 1653.

[14]. A. Gadisa, Adv. Funct. Mater. 17 (2007) 3836.

[15]. L. J. Huo, J. H. Hou, S. Q. Zhang, H. Y. Chen, Y. Yang, Angew. Chem. Int. Ed. 49 (2010) 1500.

[16]. Y. Y. Liang, J. Am. Chem. Soc. 131 (2009) 7792.

[17]. H. Y. Chen, Nature Photon. 3 (2009) 649.

[18]. S. C. Price, A. C. Stuart, L. Q. Yang, H. X. Zhou, W. You, J. Am. Chem. Soc. 133 (2011) 4625.

[19]. H. X. Zhou, Angew. Chem. Int. Ed. 50 (2011) 2995.

[20]. C. Piliego, J. Am. Chem. Soc. 132 (2010) 7595.

[21]. T. Y. Chu, J. Am. Chem. Soc. 133 (2011) 4250.

[22]. K. X. Steirer, Adv. Energy Mater. 1 (2011) 813.

[23]. C. P. Chen, Y. D. Chen, S. C. Chuang, Adv. Mater. 23 (2011) 3859.

[24]. M. Lenes, Adv. Mater. 20 (2008) 2116.

[25]. D. W. Laird, US patent 20080319207A1 (2008).

[26]. R. B. Ross, Nature Mater. 8 (2009) 208.

[27]. Y. J. He, H. Y. Chen, J. H. Hou, Y. F. Li, J. Am. Chem. Soc. 132 (2010) 1377.

[28]. G. J. Zhao, Y. J. He, Y. F. Li, Adv. Mater. 22 (2010) 4355.

[29]. J. Y. Kim, Adv. Mater. 18 (2006) 572.

[30]. J. Gilot, I. Barbu, M. M. Wienk, R. A. Janssen, J. Appl. Phys. Lett. 91 (2007) 113520.

[31]. G. K. Mor, K. Shankar, M. Paulose, O. K. Varghese, C. A. Grimes, Appl. Phys. Lett. 91 (2007) 152111.

[32]. N. Sekine, C. H. Chou, W. L. Kwan, Y. Yang, Org. Electron. 10 (2009) 1473.

[33]. S. Chambon, E. Destouesse, B. Pavageau, L. Hirsch, G. Wantz, J. Appl. Phys. 112 (2012) 094503(1-6).

[34]. Z. Alparslan, A. Ksemen, O. Ornek, Y. Yerli, S. E. San, Int. J. Photoenergy. (2011) 734618.

[35]. M. Lira-Cantu, A. Chafiq, J. Faissat, I. Gonzalez-Valls, Y. Yu, Sol. Energy Mater. Sol. Cells. 95 (2011) 1362.

[36]. M. Lira-Cantu, M. KhodaSiddiki, D. Mu~noz-Rojas, R. Amade, N. I.Gonzalez-Pech, Sol. Energy Mater. Sol. Cells. 94 (2010) 1227.

[37]. K. Siuzdak, M. Abbas, L. Vignau, M. Devynck, G. V. Dubacheva, A. Lisowska-Oleksiak, J. Appl. Phys. 112 (2012) 123110(1-5).

[38]. N. Yavuz, S. A. Yuksel, A. Karsli, S. Gunes, Sol. Energy Mater. Sol. Cells. 116 (2013) 224.

[39]. Z. Liang, R. Gao, J. L. Lan, O. Wiranwetchayan, Q. Zhang, C. Li, G. Cao, Sol. Energy Mater. Sol. Cells. 117 (2013) 34.

[40]. G. Cheng, W. –Y. Tong, K. –H. Low, C. –M. Che, Sol. Energy Mater. Sol. Cells. 103 (2012) 164.

[41]. A. Aprilia, P. Wulandari, V. Suendo, Herman, R. Hidayat, A. Fujii, M. Ozaki, Sol. Energy Mater. Sol. Cells. 111 (2013) 181.

[42]. M. R. Rajesh Menon, M. V. Maheshkumar, K. Sreekumar, C. Sudha Kartha, K. P. Vijayakumar, Sol. Energy Mater. Sol. Cells. 94 (2010) 2212.

.....ooo.....

Chapter 8

Nonlinear Optical Properties of TiO_2 and Modified TiO_2 Thin Films

Contents

Search for new effective materials for optoelectronics, microelectronics and molecular electronics is constantly carried out by scientists all over the world. This improves the performance of electronic devices and contribution from NLO materials for this purpose is inevitable. The potential applications of non-linear optics in photonics and optoelectronics have got immense interest nowadays. During the last two decades, a lot of materials were developed as NLO materials for diverse technological applications. But most of the materials developed have some limitations in practical applications. Difficulty in preparation, high cost, toxicity, durability and incorporation into devices are the main constraints of the developed materials. So researchers are now concentrating to develop low cost, sustainable and stable materials for NLO applications. Here comes the importance of semiconductor materials. This chapter discusses the fabrication of noble metal modified TiO_2 thin films by spray pyrolysis

technique and its characterization. The nonlinear optical properties of the prepared materials were investigated by Z-Scan technique.

8.1. Introduction

'Non-linear optics is a phenomenon where the optical properties of matter depend in a reversible manner on the intensity 'I' of the incident light field [1]. Progress in the field was closely connected with the evolution of lasers. Nonlinearity in optics is manifested by changes in the optical properties of a medium as the intensity of the applied field is increased or when one or more other fields are introduced. Here fields refer to any external variables such as electric field, magnetic field, acoustic wave or piezo-electric field (mechanical stress) [2]. The optical nonlinearity can be classified as intrinsic or extrinsic. Intrinsic nonlinearity violates the principle of superposition arising from a nonlinear response of the individual molecule or unit cell to the fields of two or more light waves while extrinsic nonlinearity is related to changes of the composition of the medium due to the absorption or emission of light. In either type of nonlinearity, the optical property of the medium is directly related to the intensity of light. The order of nonlinearity can be assigned according to the power of the intensity involved. This chapter focusses on the third order non-linear optical properties of pristine and noble metal modified TiO_2 thin films. Wide band gap semiconductor nanocrystals (NCs) have attracted increasing attention because of their tunable optical properties arising from the quantum size effect and have a lot of importance in science and technology [3-8]. Non-linear optical phenomena in semiconductors can be classified into two according to the mode of activation. If the non-linearity is due to real or virtual optical excitation in the electronic system

of the semiconductor, it is known as 'photoelectronic' optical nonlinearity and if it is due to sample heating by the absorbed light due to non-radiative recombination, it can be referred as 'photothermal' optical non-linearity. Non-linear optical properties of nanomaterials have emerged as a significant research area due to their potential applications in high-speed information processing [9-13], nanolasers [14], optical limiters [15] and all-optical switching [16,17]. There is a significant demand for thin film nonlinear optical materials which can be integrated into an optoelectronic device. Fabrication of thin films of semiconductor materials is easy, cheap and possesses good NLO behavior due to wide band gap and minimal scattering. The basic criteria for a material to show third order non-linear optical behavior is mainly based on two photon absorption (TPA). Among various optical properties of nano materials, two photon absorption (TPA) has got immense significance due to its effectiveness in imaging [18,19] and nanolaser pumping [20-22]. The TPA effect mainly depends on the polarization effect of the incident laser and the anisotropy of the semiconductor crystals [23-28]. Semiconductors and its different modified forms are known to be better candidates to show third order nonlinear optical properties. Among various semiconductors, TiO_2 and ZnO can be considered as highly efficient NLO materials. ZnO nanowire is considered as an important building block for fabricating various nano devices. There are a few reports on the study of polarization effect of the SHG of ZnO films [25], SHG and THG of the ZnO nanowire [29] and Raman effect of the ZnO nanorod [30]. Large third-order nonlinear optical susceptibility and fast response time of nanoparticles of noble metals (e.g., Ag, Au, Cu) embedded in dielectric matrices have been widely investigated for many years which are essential for future optical device applications [31-33].

Theoretical studies indicated that the anisotropy of both the shape and distribution of the metal nanoparticles could greatly enhance the third-order nonlinear optical susceptibility $\chi^{(3)}$ [34,35]. Non-spherical 'Au' particles embedded in Au/SiO_2 multilayer composite films and oriented 'Ag' clusters in $Ag/BaTiO_3$ composite films showed an enhancement of $\chi^{(3)}$ via geometric anisotropy [36,37]. Enhanced third order nonlinearity in these noble metal modified systems is due to the surface plasmon resonance (SPR) effect. Usually gold and silver nanoparticles dispersed in a transparent matrix, an absorption peak due to SPR is observed in the visible spectral region [38-41]. In Au and Cu nanocrystals, the inter band transition of the 'd' band to 'sp' bands lies in the same spectral region as the SPR. Consequently, both the SPR and the inter band transition contribute to the nonlinear optical processes and it is very difficult to discriminate the SPR contribution to the nonlinear properties. Schwerzel et al. [42] and Du et al. [43] have measured the nonlinear optical properties of CdS-NCs embedded in polymers with nanosecond laser pulses and Lin et al. [44] have reported a large optical Kerr coefficient of -8.4×10^{-14} cm^2/W for CdS-NCs in poly(methyl methacrylate) (PMMA) with femtosecond laser. Morphology, aspect ratio, size, orientation and density of crystal have great effects on the properties and applications of semiconductor materials. So far, variety of morphologies such as belt like [45], flower like [46], tubular [47], tower like [48] and plate-like [49] ZnO have been reported using different techniques for various applications [50]. Nonlinear absorption is a phenomenon defined as nonlinear change (increase or decrease) in absorption with increasing intensity. This can be mainly divided into two types: saturable absorption (SA) and reverse saturable absorption (RSA). Nonlinear

absorption properties of the materials depend on the pump intensity and absorption cross-section at the excitation wavelength. With increasing intensity, if the excited states show saturation owing to their long lifetimes, the transmission will show 'SA' characteristics. Here absorption decreases with increase of intensity. If, however, the excited state has strong absorption compared with that of the ground state, the transmission will show 'RSA' characteristics. A. Thankappan et al. reported optical limiting applications of ZnO nanoplates embedded in polymer matrices. The fabricated material showed a lower optical liming threshold of 46.86 MW/cm^2 at a pump power of 436 MW/cm^2 and with negative refractive index [51]. Zhang Chun-feng et al. reported large off-resonant third order nonlinearity of Ag:TiO_2 composite films. The local field enhancement in the nanostructure positively influences the non-linear optical behavior [52]. Q Wang et al. observed a large third order non-linear susceptibilities of (Au, Ag)–TiO_2 three component composite films annealed at 600°C in air [53]. K. Iliopoulos et al. investigated the non-linear optical response of TiO_2 nanostructured thin films by low temperature hydrothermal growth technique [54]. H. Long et al. also studied the third order non-linearity of single-phase anatase and rutile TiO_2 films fabricated by pulsed laser deposition (PLD) technique on fused quartz and Si(100) substrates [55]. Divya et al. reported the effect of nature of excitons on the third order non-linear optical properties of amorphous TiO_2 and its crystalline forms such as anatase and rutile [56]. This chapter discusses the NLO properties of anatase TiO_2 thin films and its modified forms.

8.2. Fabrication of Bare and Noble Metal Modified Thin Films

Spray pyrolysis technique was adopted for the fabrication of thin films. $Ti[OCH(CH3)_2]_4$ (TTIP) was dissolved in 1:1 v/v of CH_3CH_2OH/CH_3COOH. This homogeneous solution was used as the precursor for TiO_2. The glass substrate was maintained at a temperature of 400±5ºC. Spray rate was 2 ml/min and the time was limited to 10 minutes. After spraying, the substrate was cooled to room temperature. The thickness of the prepared film was calculated to be around 250 nm using Stylus profiler.

Noble metal modified films were also prepared through the same manner. Here also homogeneous solution of TTIP in CH_3CH_2OH/CH_3COOH was the precursor for TiO_2. Aqueous solutions of $HAuCl_4$, $Pd(NO_3)_2$ and $AgNO_3$ were used as the precursors for Au, Pd and Ag respectively. In this case, TiO_2 precursor to aqueous metal salt solutions was taken in a 1:1 molar ratio. Titania precursor and metal salt solutions were mixed together and subjected to spray pyrolysis as before. The glass substrate was maintained at a temperature of 400±5ºC. Here also the spray rate was 2 ml/min and the time was limited to 10 minutes. Different volumes of metal salt solutions were added to titania precursor in order to prepare thin films with varied amount of metal content. The film thickness was found to be around 250 nm by Stylus profiler.

8.3. Characterization of Metal Modified TiO_2 Thin Films

8.3.1. X-ray Diffraction Analysis (XRD)

From the XRD patterns, it is clear that anatase is the major phase with an angle of $2\theta = 25.3°$. Sharp and intense peaks support the crystalline nature of the thin films. Compared to powder form intensities

of the peaks are reduced drastically. Rutile and brookite phases were not observed because the calcination temperature used was 400°C. No visible peaks corresponding to Au, Ag and Pd were observed due to their low concentration. Sharp peaks also represent the periodicity of the prepared samples. Crystallite size of the prepared samples was found to be greater than 30 nm.

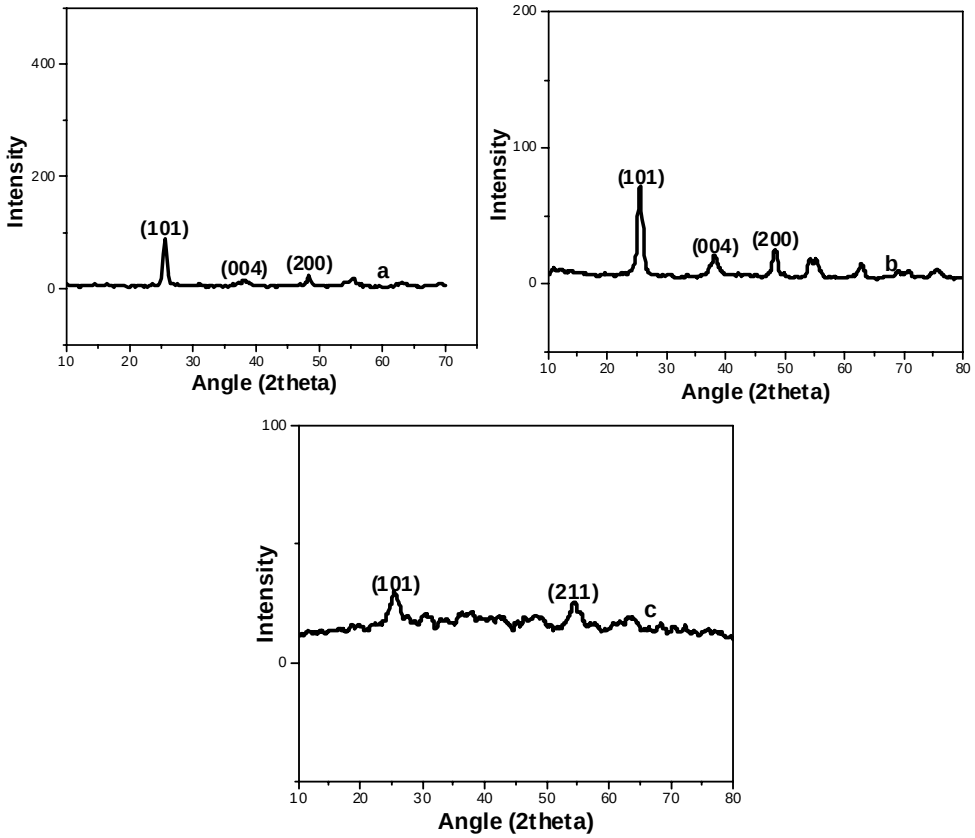

Fig.8.1. XRD Patterns of a) Au-TiO_2 b) Ag-TiO_2 c) Pd-TiO_2

8.3.2. Scanning Electron Microscopy

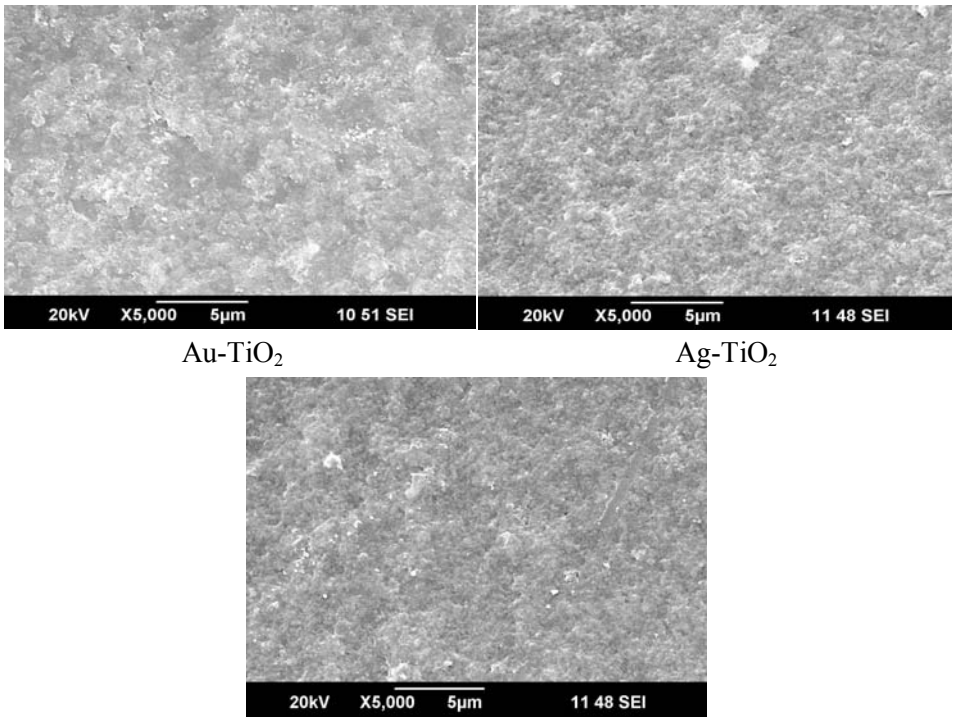

Au-TiO_2 Ag-TiO_2

Pd-TiO_2

Fig.8.2. SEM Images of Noble Metal Modified TiO_2 Thin Films

SEM micrographs were used to understand the morphology of the prepared systems. It reveals the uniform nature of noble metal modified thin films. Shapeless structures due to agglomeration or special geometries could not be seen from SEM images. This uniform surface geometry is a positive factor that enhances the nonlinear optical properties. Random distribution of particles on film surface reduces the nonlinear optical properties due to scattering effect. Scattering is inversely related to nonlinear optical behavior. Compared to any other forms, scattering was found to be less for film form due to uniform nature. Third

order nonlinear optical properties of these films were found to be higher due to minimum scattering.

8.3.3. Energy Dispersive X-ray Analysis (EDX)

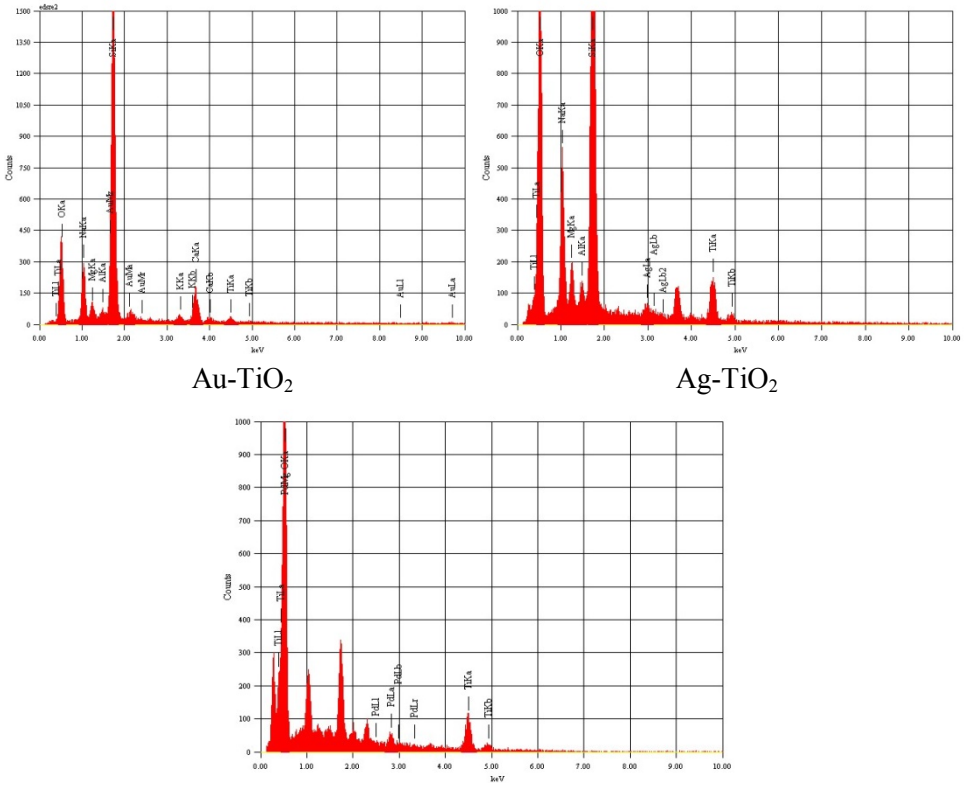

Au-TiO_2 Ag-TiO_2

Pd-TiO_2

Fig. 8.3. EDX Spectra of Noble Metal Modified Thin Films

EDX is a qualitative technique used to understand the elemental composition and also estimate other materials such as impurities or adducts in the sample approximately. These impurities are sometimes occur accidently or added for modification of the base structure. Intensity of EDX peaks are directly related to the percentage of elements present in the system. Fig. 8.3 represents the EDX patterns of Au(0.75)-Ti, Ag(2.5)-

Ti and Pd(2)-Ti. The digits in the bracket represents the volume of the metal salt solution in milliliter. EDX patterns showed the presence of variety of elements other than Ti, O and metals. The peaks corresponding to other elements were coming from the glass substrate. Here compared to thin films, the concentration of glass substrate was higher. Compared to other elements, the concentration of oxygen was found to be higher in all the samples. This may be due to the combined contribution of oxygen from TiO_2 and from silica substrate. The atom percentage of metals and Ti are tabulated in table 1.

Table 8.1. Atom Percentage of Dopants and Ti in the Thin Films

Catalyst	% of Dopant and Ti	
Ag-TiO_2	Ag-1.30	Ti-8.30
Pd-TiO_2	Pd-1.64	Ti-7.36
Au-TiO_2	Au-0.89	Ti-6.0

8.4. Nonlinear Absorption Phenomena

Nonlinear absorption describes the change in absorption of a material as a function of intensity or fluence [57]. The probability of a material absorbing more than one photon before relaxing to the ground state can be greatly enhanced at high intensities. There are many types of nonlinear absorption phenomena. Among them saturable absorption (SA) and reverse saturable absorption (RSA) have got great significance due to its heavy applications in electronic devices.

Two-photon absorption (TPA) is the process by which the energy gap between two real states is bridged by the simultaneous absorption of two photons which do not have the same frequency. But both photons do

not have sufficient energy to complete the transition alone and TPA phenomenon is thus observed in the spectral range where the material is normally transparent. An optical transition can take place only when the two photons are present together for a fleeting instant of time. The first photon making a virtual transition to a non-existent state between the two real energy states and if the second photon appears within the virtual lifetime of that state, the absorption sequence to the upper state can be completed. To have an appreciable rate of TPA, both photons will be present during the virtual lifetime. Because the virtual lifetime is so short, photon fluxes must be high and therefore power levels from laser beams are required. The proximity of the input photons to a real state of the system controls the efficiency of TPA. When the intermediate state of TPA is also a system resonance, the situation is commonly referred to as excited state absorption (ESA), which is a sequence of two linear absorption processes that leads to an effective third-order nonlinearity. Schematic of TPA is shown in Fig. 8.4.

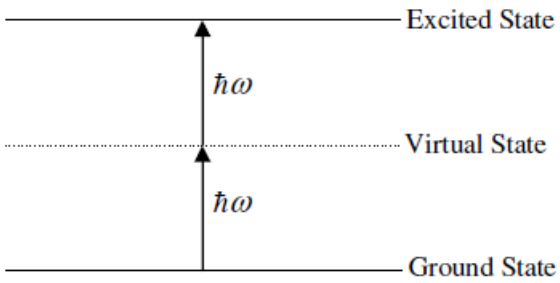

Fig.8.4. Schematic Representation of Two Photon Absorption (2PA)

Saturable absorption (SA) means the decrease of absorption with increase of intensity. When the absorption cross-section from excited state

is smaller than that from the ground state, the absorption of the system will be decreased when the system is pumped with high intensity laser beam. This process is called saturable absorption. But on the other hand, when the absorption cross-section from excited state is larger than that from the ground state, the absorption of the system will be increased under intense laser fields. This process is called reverse saturable absorption (RSA). In semiconductors, the irradiation of a photon with energy greater than the band gap will excite an electron to the conduction band where it is a free carrier. The excited electron will rapidly relax to the bottom of the conduction band. From there it will undergo recombination with an excited hole in the valence band. However, at sufficiently high intensities, it can absorb another photon while it is still in the conduction band. This process is called free carrier absorption (FCA).

8.5. Techniques for NLO Measurements

Some of the methods used for studying NLO properties are Z-Scan, three wave mixing, optical Kerr effect, ellipse rotation, interferometric methods, excitation-induced increase or bleaching of absorption, pump and probe beam spectroscopy, laser-induced grating spectroscopy and photoacoustic techniques. Among these, Z-scan technique has been employed in investigating NLO properties of TiO_2 and noble metal modified TiO_2 thin films in this thesis.

8.5.1. Z-Scan Technique

Z-Scan is a single beam technique developed by Sheik Bahaeto measure the magnitude and sign of nonlinear refraction (NLR). It is also useful for characterizing nonlinear absorption (NLA) and differentiating

the effects of NLR from NLA [58,59]. The technique is based on the principle of spatial beam distortion but offers simplicity in use as well as high sensitivity comparable to interferometric methods. Using a single focused laser beam, the transmittance of the sample is measured through a partially obscuring circular aperture placed in the far field. The transmittance is determined as a function of the sample position (Z) measured with respect to the focal plane. Employing a Gaussian spatial profile beam simplifies the analysis. A laser beam propagating through a nonlinear medium will experience both amplitude and phase variations.

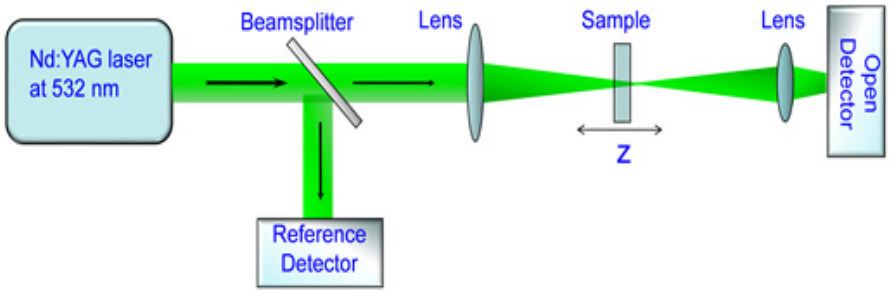

Fig.8.5. Schematic Representation of Z-Scan Technique

The experimental set up for Z-Scan technique is shown in Fig. 8.5. Z-Scan techniques can be divided in to open aperture and closed aperture according to the mode of operation. Closed and open aperture Z-Scan methods can be considered as real and imaginary parts of nonlinear susceptibility $\chi^{(3)}$ respectively. In closed aperture Z-Scan, transmitted light is measured through an aperture placed before the detector with respect to focal plane and is related to both nonlinear absorption and nonlinear refraction. But in open aperture Z-Scan, the transmitted light is measured without an aperture and is sensitive only to nonlinear absorption. In

Z-Scan technique, the thickness of the material should be less than Rayleigh's range Z_0 which is given by

$$Z_0 = \frac{k\omega_0^2}{2} \text{ ---------- (8.1)}$$

where k is the wave vector and ω_0 is the beam waist radius given by $\omega_0 = f\lambda/D$, where 'f' is the focal length of the lens used, 'λ' is the wavelength of the source and 'D' is the beam radius at the lens. Z-Scan technique depends mainly on beam profile and also the thickness of the sample. So in order to maintain a steady beam profile, the sample thickness should always be kept less than the Rayleigh's range. Generally, electronic Kerr effect will be dominant at low irradiance levels whereas TPA induced FCA will be dominant at high irradiance levels [60]. This chapter involves the measurement of third order nonlinear optical properties of titania based thin films through open aperture method. In the case of an open aperture Z-Scan, the transmitted light measured is sensitive only to intensity variations and thus phase variations of the beam are not taken into consideration. The intensity dependent nonlinear absorption coefficient α(I) can be written in terms of linear absorption coefficient α and TPA coefficient β as

$$\alpha(I) = \alpha + \beta I \text{ ---------- (8.2)}$$

Here 'α' and 'β' represent linear and nonlinear absorption coefficient respectively. In this study, we have calculated the third order nonlinear absorption coefficient 'β' by using Z-Scan technique comprising of Nd-YAG laser (532 nm, 7 ns and 10Hz). The sample is moved in the direction of light incidence near the focal point of the lens with a focal

length of 200 mm. The Rayleigh length Z_0 is estimated to be 7.4 mm which is much higher than the thickness of the sample cuvette (1mm), is an essential requirement for Z-Scan experiments. From this the nonlinear coefficients were obtained by fitting the experimental Z-Scan plot with the theoretical plots. The normalized transmittance for open aperture condition is given by

$$T_{(z)} = \frac{c}{q_{0\sqrt{\pi}}} \int_{-x}^{x} 1n(1+q_0 e^{-t^2})dt \quad \text{---------- (8.3)}$$

Where $q_0(z,r,t) = \beta I_0(t) L_{eff}$ and

$$L_{eff} = \frac{1-e^{-\alpha 1}}{\alpha} \quad \text{---------- (8.4)}$$

Here L_{eff} is the effective thickness of the film with linear absorption coefficient 'α' and 'I_0' is the irradiance at focus.

8.6. Open aperture Z-Scan Measurements

8.6.1. NLO Characterization of Pristine TiO_2 films

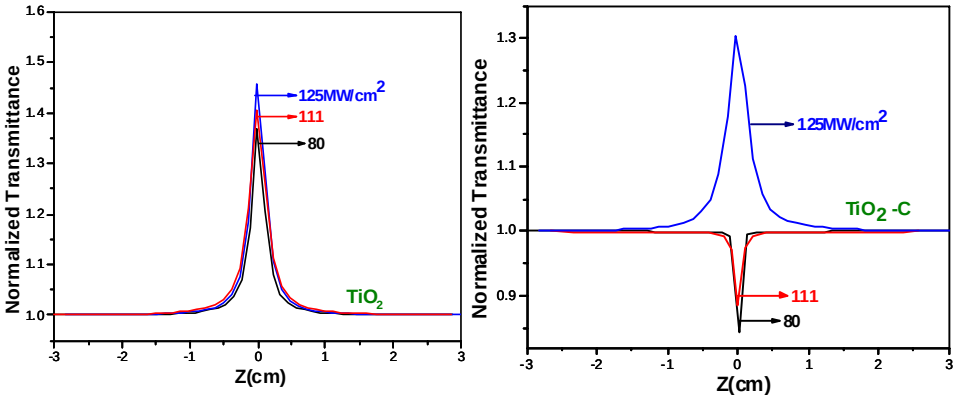

Fig. 8.6. Open aperture Z-Scan Traces of Bare and Calcined TiO_2 Thin Films at Various Intensities for an Irradiation Wavelength of 532 nm

Open aperture Z-Scan measurements of the bare and calcined TiO_2 corresponding to normalized transmittance as a function of distance from the focal point of the lens at various intensities are shown in Fig. 8.6. Bare TiO_2 film exhibited the saturation of ground state absorption upon moving the film towards the focus which results in an increase of transmittance (SA). Increase of laser intensity does not have any special influence on the switching of saturable absorption behavior in bare titania thin film. But increase of intensity increases the nonlinear optical properties (SA) of thin films. 'SA' process mainly depends on laser intensity because it induces bleaching in the ground state absorption. The nonlinear optical properties of titania film at an intensity of 125 MW/cm^2 was found to be higher. The films at various intensities exhibited saturable absorption and bleaching and are more susceptible to thermal effects. Heating of semiconductors reduces the Fermi energy level and thereby increases the concentration of carriers in the conduction band. This destabilizes the ground state and induces bleaching in the ground state absorption which ends up in 'SA' process. Generally, polarization responses of bound electrons are the main basis of optical nonlinearity but the contribution from conduction band electrons in semiconductors is unavoidable. The negative values of nonlinear absorption coefficient in these films are due to the absorption saturation of defect states. The results are tabulated in Table 8.2. Higher absorption cross-section of the ground state than the excited state produced strong 'SA' behavior in these films rather than induced absorption. The thickness of the film used here was calculated to be 250 nm. Thickness is one of the parameters affecting the absorption properties of thin films. Compared to thicker films, less localized defect states are present in thin films and thus low input intensities are very

sufficient to fill up these states. This supports saturable absorption behavior. But on the other hand, thicker films cannot be populated at low input intensities due to the higher concentration of localized defect states. Saturation occurs only if the life times of defect states are higher than the duration of megawatt pulses [61]. But calcination of these films at 400°C for about 3h changed the absorption characteristics. Saturable absorption property (transmittance peak) of the titania film was retained only at a laser intensity of 125 MW/cm^2 after calcination. But calcined samples at other laser intensities exhibited a normalized transmittance valley indicating the presence of reverse saturable absorption (RSA). Two photon absorption (TPA) followed by free carrier absorption (FCA) is the most dominant mechanism contributing to induced absorption in these calcined films at various intensities. Nonlinear optical properties with laser beam illumination at 532 nm usually corresponds to Two-Photon Absorption process because the photon energy of 532 nm laser is within the range $Eg < 2h\nu < 2Eg$, where $h\nu = 2.33$ eV. Absorption cross-section of excited states of RSA materials are high compared to ground state at the excitation radiation wavelength. These materials have a positive value for imaginary part of susceptibility $Im(\chi^{(3)})$ which is a measure of induced absorption. But on the other hand, a saturable absorber will show a negative value for susceptibility. Optical limiting is the most important application of these kinds of materials. Saturable absorption is the most significant third order nonlinear optical property that can have applications in volatile computer memory, the dynamic random access memory (DRAM), optical switching and laser pulse narrowing. The strong nonlinear optical properties of bare and calcined TiO_2 films can be attributed to intense two photon absorption. Calcination of TiO_2 films at 400°C favoured anatase as the major phase.

Among all the polymorphs of TiO_2, anatase was found to show higher third order nonlinear optical properties. Anatase is characterized by bound excitons and hence possesses large excitonic binding energy. Usually, large optical oscillator strength of associated optical transition positively influences the nonlinear optical properties of the material. It was reported that bound excitons have giant oscillator strengths that are higher than that of the oscillator strengths of the free excitons [62]. The confinement of excitonic wave function is another significant factor to improve the oscillator strength by a factor of R^3/a_B^3 where 'R' is the particle size and a_B is exciton effective Bohr radius. Defects and disorders present in anatase also contribute to the nonlinear optical properties.

Table 8.2. β values of TiO_2 thin films

Name of the System	$\beta = q/(I_0 \times L_{eff})$ (m/W)
TiO_2	-8.99666×10^{-7}
	-7.51713×10^{-7}
	-6.10771×10^{-7}
TiO_2-C	9.14716×10^{-6}
	3.92181×10^{-7}
	-5.09607×10^{-7}

8.6.2. NLO Characterization of Pd Modified TiO_2 Thin Films

Pd(1ml)-Ti was fabricated by spraying aqueous solution of palladium nitrate and precursor for titania in 1:10 volume ratio and that of Pd(2ml)-Ti was prepared by spraying the precursors in 2:10 volume ratio. From the Fig. 8.7, it is clear that palladium modified titania showed higher NLO properties than bare TiO_2. Saturable absorption induces peak shapes in open aperture curves. Here saturable absorption was dominated

in bare and calcined samples and the open aperture curve showed peak shapes. Calcination did not change the nonlinear absorption behavior of the palladium modified TiO_2 thin films. The nonlinear absorption coefficients of 1ml palladium modified titania films were found to be higher compared to Pd(2ml)-Ti films. The values obtained are tabulated in Table 8.3. The saturable absorption behavior of the films was retained at various laser intensities. Here the increase of laser intensity increases the nonlinear optical property. Bare and calcined sample showed higher 'β' values at an intensity of 125 MW/cm^2.

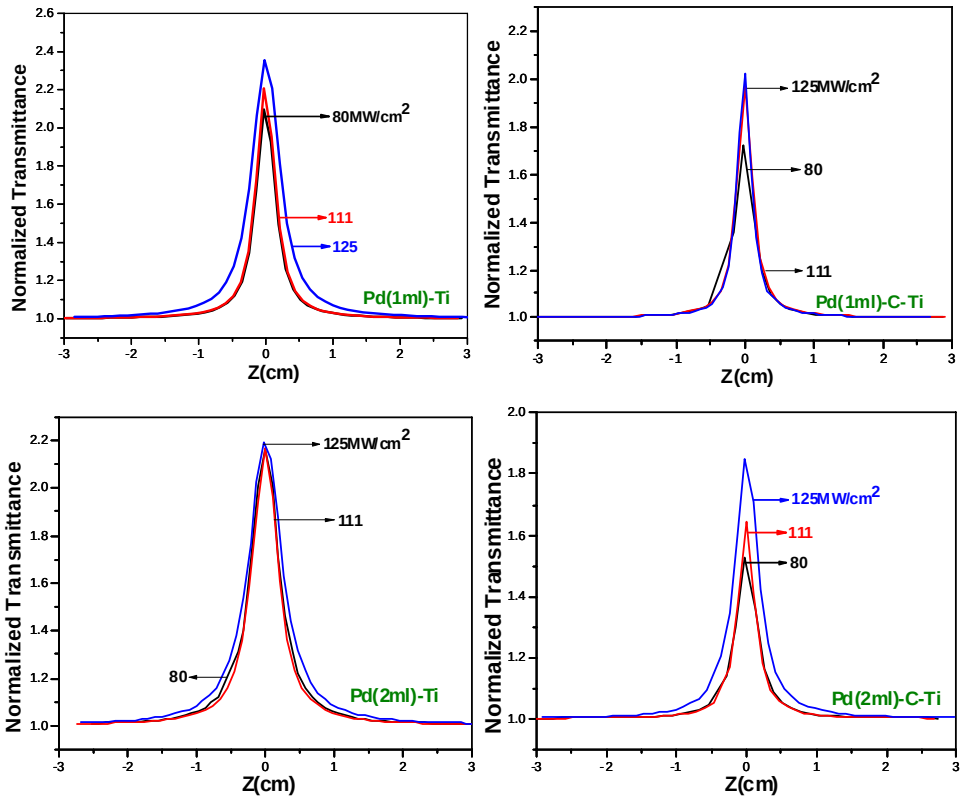

Fig. 8.7. Open Aperture Z-Scan Measurement of Bare and Calcined Palladium Modified Titania Thin Films atVarious Intensities for an Irradiation Wavelength of 532 nm

Strong surface polarization between Pd nanoparticles and the TiO_2 matrix leads to dielectric confinement effect of TiO_2 nanoparticles in the system which improved the nonlinear optical properties to a major extend. Electrical charge interaction between the metal part and TiO_2 produced an electric dipole layer at the nanoparticle surface which helps to separate the excited species effectively and enhances the electric field inside the nanoparticles which in turn affects the NLO behavior positively [63]. An excitation wavelength of 532 nm used in the experiment is farther away from the surface plasmon resonance (SPR) of palladium which is present in the UV region. So this SPR does not have any effect on the observed optical nonlinearity.

Table. 8.3. β values of 'Pd' modified TiO_2 thin films

Name of the system	$\beta = q/(I_0 \times L_{eff})$ (m/W)
Pd(1ml)-Ti	-1.57311×10^{-6}
	-1.17624×10^{-6}
	-1.0868×10^{-6}
Pd(1ml)-C-Ti	-9.711×10^{-7}
	-1.30351×10^{-6}
	-1.06718×10^{-6}
Pd(2ml)-Ti	-1.59473×10^{-6}
	-1.15213×10^{-6}
	-1.03182×10^{-6}
Pd(2ml)-C-Ti	-8.94699×10^{-7}
	-8.82605×10^{-7}
	-1.10551×10^{-6}

8.6.3. NLO Characterization of Au Modified TiO_2 Thin Films

Various 'Au' modified titania films were prepared by varying the concentration of the metal content. The digits in the bracket represent the

volume of metal precursor added to 10 ml of titania precursor. In the case of Au(0.25)-Ti, higher nonlinear absorption coefficient was obtained at an intensity of 125 MW/cm^2. Increase of concentration of the dopant increases the nonlinear properties. In all the samples, higher 'β' values were obtained at an intensity of 125 MW/cm^2 and the values are shown in Table 8.3. Presence of transmittance peak indicates the saturable absorption behavior of the prepared 'Au' modified TiO_2 thin films. Calcination and fluence does not switch the nonlinear properties of the modified thin films. Among all the samples, Au(0.75)-Ti showed highest nonlinear property. Higher amount of dopant increases the growth of TiO_2 grains, agglomerates them and shifts the absorption band to visible region. Agglomeration results in an increase of particle size and corresponding enhancement of nonlinear optical properties with increasing dimension in the weak confinement regime originates from the size dependent enhancement of oscillator strength of coherently generated excitons [64]. In 'Au' nanocrystals, the interband transition lies in the same spectral region as the SPR. As a result, both the SPR and interband transition contribute to NLO properties. So it is very difficult to find out the individual contribution of SPR to NLO properties. In the case of Au and Ag dispersed in a matrix, the surface plasmon resonance (SPR) absorption is usually observed in the visible spectral region [65,66]. The saturable absorption behavior observed in all the samples may be attributed to the resonant plasmon absorption of 'Au' particles in titania matrix. The value of nonlinear absorption coefficient was found to be negative for all the samples. This showed the strong SA behavior of the prepared films. Absence of induced absorption and the presence of strong SA imply that the absorption cross section of the ground state is higher than that of the absorption cross section of excited state. Saturable absorption and resonant plasmon

absorption phenomena were suggested to contribute to the total nonlinear absorption behavior of the prepared Au-TiO_2 thin films. SPR phenomenon associated with 'Au' particles mostly plays an important role to enhance the NLO properties and it allows inhibiting the Two-photon absorption of the titania thin film.

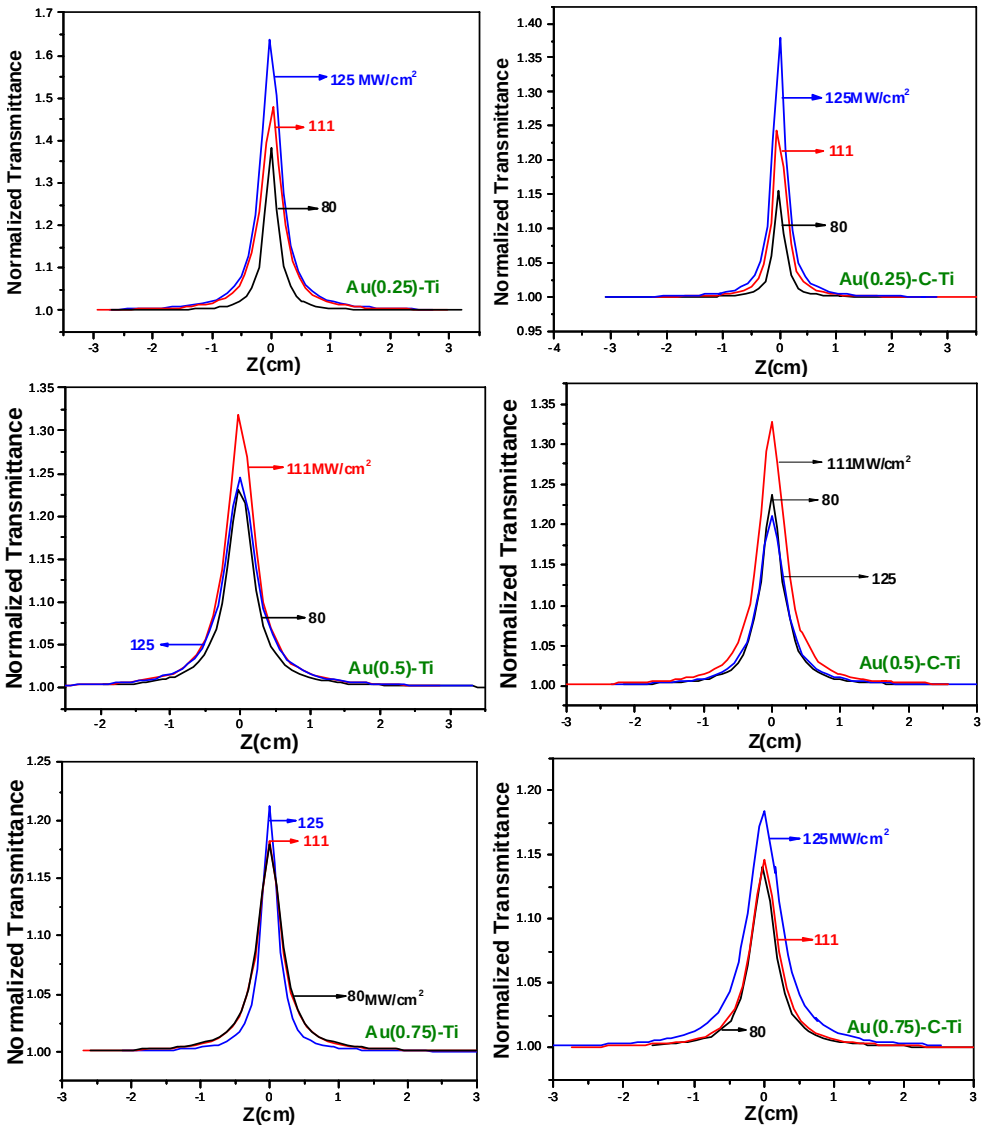

Fig. 8.8. Open Aperture Z-Scan Traces of Au Modified Titania Thin Films at Various Intensities for an Irradiation Wavelength of 532 nm

Table. 8.3. β values of 'Au' modified TiO_2 thin films

Name of the system	**$\beta = q/(I_0 \times L_{eff})$ (m/W)**
Au(.25)-Ti	-7.54591×10^{-7}
	-5.86626×10^{-7}
	-1.22117×10^{-6}
Au(.25)-C-Ti	-5.82484×10^{-7}
	-5.17615×10^{-7}
	-5.02155×10^{-7}
Au(.75)-Ti	-6.2112×10^{-7}
	-3.95853×10^{-7}
	-3.45965×10^{-7}
Au(.75)-C-Ti	-5.55028×10^{-7}
	-3.24403×10^{-7}
	-2.96441×10^{-7}
Au(.5)-Ti	-6.58847×10^{-7}
	-4.36114×10^{-7}
	-5.91844×10^{-7}
Au(.5)-C-Ti	-6.64079×10^{-7}
	-4.41303×10^{-7}
	-5.30492×10^{-7}

8.6.4. NLO Characterization of Ag Modified TiO_2 Thin Films

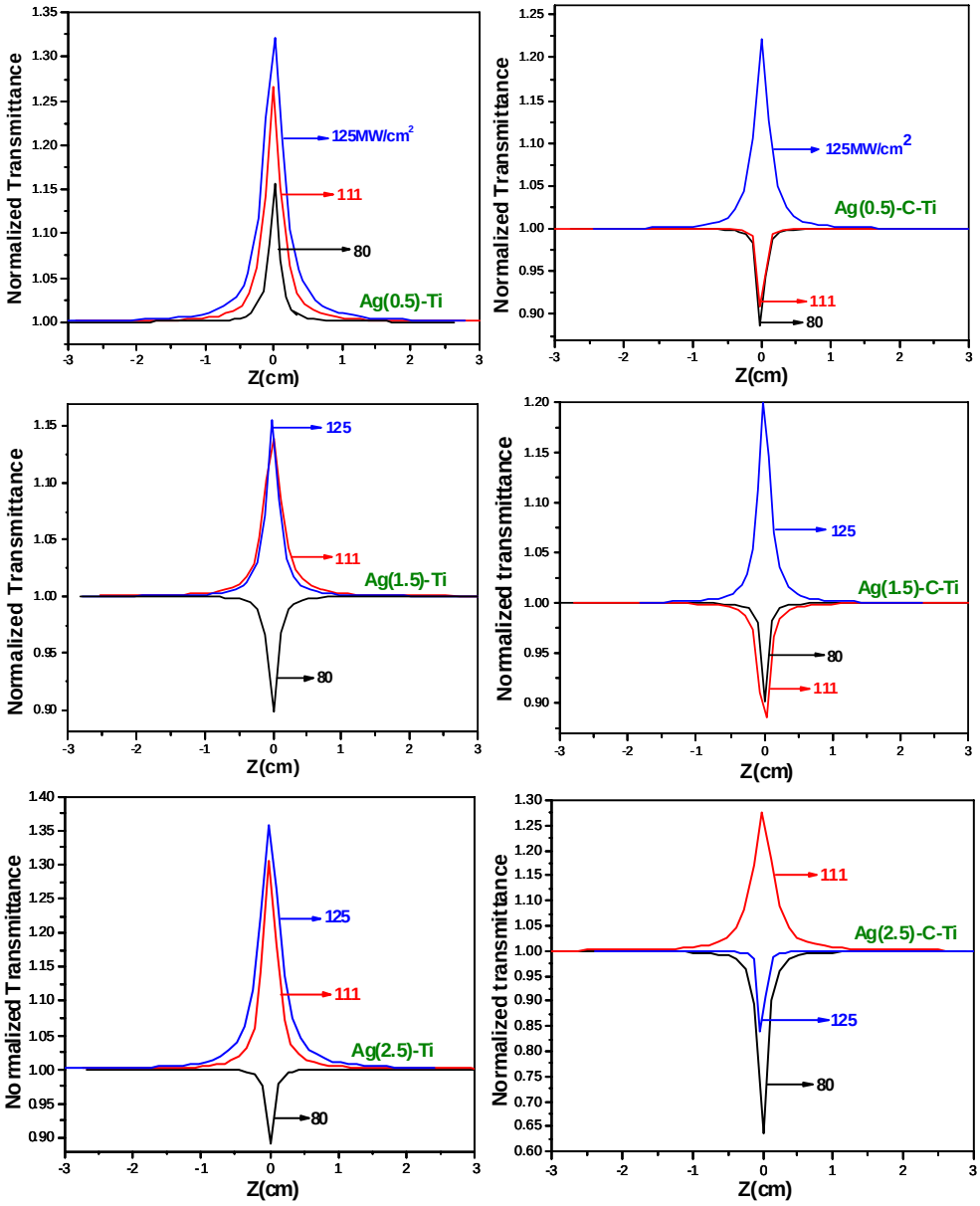

Fig.8.9. Open Aperture Z-Scan Results of Ag Modified TiO_2 Thin Films at Various Intensities for an Irradiation Wavelength of 532 nm

Here open aperture curves exhibited transmittance peaks (peak shapes) and normalized transmittance valleys at various intensities

indicating the presence of saturabe absorption and reverse saturable absorption behavior of the prepared thin films respectively. We have prepared different silver modified TiO_2 films by varying the concentration of metal part. In the case of Ag(0.5)-Ti, all the samples showed saturable absorption behavior at different intensities. Higher value of nonlinear absorption coefficient was observed at an intensity of 125 MW/cm^2. Upon calcination, switching of SA to RSA was observed in Ag(0.5)-Ti at intensities 80 MW/cm^2 and 111 MW/cm^2. Defect sites created during calcination contributes to nonlinearity and influences the switching of absorption properties. Here the SA behavior of the sample was retained at an intensity of 125 MW/cm^2. In Ag(1.5)-Ti, the SA behavior was observed at 111 MW/cm^2 and 125 MW/cm^2 intensities and switching to RSA was observed at 80 MW/cm^2. Here also the SA behavior was retained at 125 MW/cm^2 and RSA behavior was dominated at other intensities. Ag(2.5)-Ti showed negative nonlinear absorption coefficients at 125 MW/cm^2 and 111 MW/cm^2. The β values obtained are tabulated in Table 8.4. The sample showed a transmittance valley at an intensity of 80 MW/cm^2. Upon calcination, the sample retained SA property only at an intensity of 111 MW/cm^2. Here the RSA behavior was found to be higher at an intensity of 80 MW/cm^2. In the case of silver nanocrystals, the SPR contribution to the nonlinear optical properties is easily distinguishable because it is farther away from the interband transition energy [67]. The SPR band is sensitive to laser excitation. The excitation of interband and SPR transitions are not possible with a single photon of energy. So the nonlinearity observed in the Ag modified TiO_2 films may be due to the intraband transition of the free electrons. The intrinsic nonlinearity along with the local field effect enhances the third order nonlinearity.

The increase of nonlinear absorption coefficient in silver modified semiconductor can also be attributed to the enhancement of exciton oscillator strength. Two Photon Absorption followed by weak free carrier absorption is the main reason for the observed RSA behavior of silver modified TiO_2 thin films. Switching of SA to RSA imply that the absorption cross section of the ground state is higher than the excited state. Plasmon band bleach and optical limiting mechanism play an important role to change the signs of nonlinear absorption coefficient [68]. Fluence, concentration of dopants and calcination temperature are very important parameters deciding the NLO properties either as a saturable absorption or as a reverse saturable absorption.

Table. 8.4. β values of 'Ag' modified TiO_2 thin films

Name of the system	$\beta = q/(I_0 \times L_{eff})$ (m/W)
Ag(.5)-Ti	-7.23148×10^{-7}
	-5.26703×10^{-7}
	-3.56555×10^{-6}
Ag(.5)-C-Ti	1.0419×10^{-6}
	3.44349×10^{-7}
	-4.08708×10^{-7}
Ag(1.5)-Ti	4.709×10^{-7}
	3.22716×10^{-7}
	-3.11686×10^{-7}
Ag(1.5)-C-Ti	4.53689×10^{-7}
	5.14241×10^{-7}
	-3.82976×10^{-7}
Ag(2.5)-Ti	5.0367×10^{-7}
	-5.77058×10^{-7}
	-5.63626×10^{-7}
Ag(2.5)-C-Ti	1.70543×10^{-6}
	-5.34684×10^{-7}
	6.82502×10^{-7}

8.7. Conclusion

Noble metal modified TiO_2 thin films were prepared by spray pyrolysis technique and characterized by physico-chemical techniques such as XRD, SEM, EDX and absorption spectroscopy. Third order optical nonlinearities of the prepared films were evaluated by Z-Scan technique using 532 nm Nd-YAG lasers. The films exhibited both saturable absorption (SA) and reverse saturable absorption (RSA) behavior at different intensities. Compared to pure TiO_2 films, nonlinear optical properties of the modified films are found to be higher.

References

[1]. C. Klingshirn, Sernicond. Sci. Technol. 5 (1990) 457.

[2]. W. Nie, Adv. Mater. 5 (1993) 520.

[3]. D. Cotter, M. G. Burt, R. Manning, J. Phys. Rev. Lett. 68 (1992) 1200.

[4]. A. P. Alivisatos, Science. 271 (1996) 933.

[5]. G. P. Banfi, V. Degiorgio, D. Ricard, Adv. Phys. 47 (1998) 447.

[6]. Z. M. Pan, Z. R. Dai, Z. L. Wang, Science. 291 (2001) 1947.

[7]. Z. L. Wang, J. H. Song, Science. 312 (2006) 242.

[8]. M. Huang, S. Mao, H. Feick, H. Yan, Y. Wu, H. Kind, E. Weber, R. Russo, P. Yang, Science. 292 (2001) 1897.

[9]. D. Cotter, R. J. Manning, K. J. Blow, D. C. Rogers, Science. 286 (1999) 1523.

[10]. X. P. Liu, R. M. Osgood, Y. A. Vlasov, W. M. Green, Nat. Photonics. 4 (2010) 557.

[11]. B. Corcoran, C. Monat, L. O'Faolain, T. F. Krauss, Nat. Photonics. 3 (2010) 206.

[12]. J. Leuthold, C. Koos, W. Freude, Nat. Photonics. 4 (2010) 535.

[13]. M. A. Foster, A. C. Turner, M. Lipson, A. L. Gaeta, Nature. 441 (2006) 960.

[14]. M. H. Huang, S. Mao, H. Feick, P. D. Yang, Science. 292 (2001) 1897.

[15]. J. E. Riggs, D. B. Walker, Y. P. Sun, J. Phys. Chem. B. 104 (2000) 7071.

[16]. S. Tatsuura, M. Furuki, M. Tian, H. Mitsu, Adv. Mater. 15 (2003) 534.

[17]. Y. W. Zhu, H. I. Elim, Y. L. Foo, C. H. Sow, Adv. Mater. 18 (2006) 587.

[18]. D. R. Larson, W. R. Zipfel, R. M. Williams, W. W. Webb, Science. 300 (2003) 1434.

[19]. B. Dubertret, P. Skourides, D. J. Norris, A. Libchaber, Science. 298 (2002) 1759.

[20]. E. V. Chelnokov, N. Bityurin, W. Marine, Appl. Phys. Lett. 89 (2006) 171119.

[21]. H. Zhou, M. Wissinger, J. Fallert, H. Kalt, Appl. Phys. Lett. 91 (2007) 181112.

[22]. C. F. Zhang, Z. W. Dong, S. X. Qian, Opt. Lett. 31 (2006) 3345.

[23]. J. F. Wang, M. S. Gudiksen, X. F. Duan, C. M. Lieber, Science. 293 (2001) 1455.

[24]. R. De Salvo, M. Sheik-Bahae, E. W. Stryland, Opt. Lett. 18 (1993) 194.

[25]. U. Neumann, R. Grunwald, U. Griebner, W. Seeber, Appl. Phys. Lett. 87 (2005) 171108.

[26]. W. C. Hurlbut, Y. S. Lee, M. M. Fejer, Opt. Lett. 32 (2007) 668.

[27]. J. Zhang, Q. Lin, P. M. Fauchet, Appl. Phys. Lett. 91 (2007) 071113.

[28]. A. Ganany-Padowicz, I. Juwiler, O. Gayer, A. Arie, Appl. Phys. Lett. 94 (2009) 091108.

[29]. J. C. Johnson, H. Q. Yan, R. D. Schaller, R. Saykally, J. Nano Lett. 2 (2002) 279.

[30]. C. T. Chien, M. C. Wu, C. W. Chen, Y. F. Chen, Appl. Phys. Lett. 92 (2008) 223102.

[31]. D. Ricard, P. Roussignol, C. Flytzanis, Opt. Lett. 10 (1985) 511.

[32]. D. Cotter, R. J. Manning, K. J. Blow, A. D. Ellis, A. E. Kelly, D. Nesset, I. D. Phillips, A. J. Poustie, D. C. Rogers, Science. 286 (1999) 1523.

[33]. V. Keibig, M. Vollmer, Optical Properties of Metal Clusters, Springer, Berlin, (1995).

[34]. K. P. Yuen, M. F. Law, K. W. Yu, P. Sheng, Phys. Rev. E. 56 (1997) 1322.

[35]. K. P. Yuen, M. F. Law, K. W. Yu, P. Sheng, Opt. Commun. 148 (1998) 197.

[36]. H. B. Liao, W. Wen, G. K. L. Wong, Appl. Phys. A. 80 (2005) 861.

[37]. D. Guan, Z. Chen, W. Wang, H. Lu, Y. Zhou, K. -j. Jin, G. Yang, J. Opt. Soc. Am. B. 22 (2005) 1949.

[38]. Y. Hamanaka, A. Nakamura, N. Hayashi, S. Omi, J. Opt. Soc. Am. B. 20 (2003) 1227.

[39]. A. Lin, W. -T. Han, J. Nano photon. 1 (2007) 013554.

[40]. A. Lin, D. H. Son, I. H. Ahn, G. H. Song, W. -T. Han, Opt. Express. 15 (2007) 6374.

[41]. S. Ju, V. L. Nguyen, P. R. Watekar, B. H. Kim, C. Jeong, S. Boo, C. J. Kim, W. –T. Han, J. Nanosci. Nanotechnol. 6 (2006) 3555.

[42]. R. E. Schwerzel, K. B. Spahr, J. P. Kurmer, V. E. Wood, J. A. Jenkins, J. Phys. Chem. A. 102 (1998) 5622.

[43]. H. Du, G. Q. Xu, W. S. Chin, L. Huang, W. Ji, Chem. Mater. 14 (2002) 4473.

[44]. Y. Lin, J. Zhang, E. Kumacheva, E. H. Sargent, J. Mater. Sci. 39 (2004) 993.

[45]. M. Lucas, Z. L. Wang, E. Riedo, Phys. Rev. B. 81 (2010) 045415.

[46]. J. Li, L. Guicun, J. Qianmao, P. Hongrui, Mater. Lett. 61 (2007) 1964.

[47]. A. Wei, X. W. Sun, C. X. Xu, Z. L. Dong, Y. Yang, S. T. Tan, Nanotechnology. 17 (2006) 1740.

[48]. D. Da, T. S. Martin, R. Shriram, Nanoscale. 2 (2010) 2685.

[49]. S. Yin, T. Goto, F. Gobo, Y. F. Huang, P. L. Zhang, T. Sato, Mater. Sci. and Eng. 18 (2011) 042004.

[50]. X. Yue, U. Key, W. Jin, Jianwen, S. Dejain, Z. Ziqiang. Appl. Surf. Sci. 92 (2009) 6487.

[51]. A. Thankappan, S. Divya, S. Thomas, V. P. N. Nampoori, Optic & Laser Technology. 52 (2013) 37.

[52]. Z. Chun-feng, Y. Guan-Jun, D. Zhi-Wei, L. Ye, M. Guo-Hong, Q. Shi-Xiong, Chin. Phys. Lett. 22 (2005) 475.

[53]. Q. Wang, S. Wang, W. Hang, Q. Gong, J. Phys. D: Appl. Phys. 38 (2005) 389.

[54]. K. Iliopoulos, G. Kalogerakis, D. Vernardou, N. Katsarakis, E. Koudoumas, S. Couris, Thin Solid Films. 518 (2009) 1174.

[55]. H. Long, A. Chen, G. Yang, Y. Li, P. Lu, Thin Solid Films. 517 (2009) 5601.

[56]. S. Divya, I. Sebastian, V. P .N. Nampoori, P. Radhakrishnan, A. Mujeeb, Optics & Laser Technology. 56 (2014) 207.

[57]. R. L. Sutherland; "Handbook of nonlinear optics", CRC press (2003).

[58]. M. Sheik-Bahae, A. A. Said, T. H. Wei, D. J. Hagan, E. W. Van Stryland, IEEE J. Quantum Electron. 26 (1990) 760.

[59]. E. W. Van Stryland , M. Sheik-Bahae, "Z-Scan," in Characterization techniques and tabulations for organic nonlinear optical materials, M. G. Kuzyk, C. W. Dirk, Eds. New York: Marcel Dekker, (1998) 894.

[60]. P. K. Mandal, A. Samanta, J. Phys. Chem. B. 109 (2005) 15172.

[61]. M. Yüksek, U. Kürüm, H. G. Yaglioglu, A. Elmali, A. Ates, J. Appl. Phys. 107 (2010) 033115.

[62]. E. I. Rashba, G. E. Gurgenishvili, Soviet Physics – Solid State. 4 (1962) 759.

[63]. K. M. Rahulan, N. Padmanathan , G. Vinitha, C. C. Kanakam, Mat. Res. Bull. 48 (2013) 3037.

[64]. E. Hanamura, Phys. Rev. B. 37 (1988)1273.

[65]. A. Lin, W. -T. Han, J. Nanophoton. 1 (2007) 013554.

[66]. A. Lin, D. H. Son, I. H. Ahn, G. H. Song, W. -T. Han, Opt. Express. 15 (2007) 6374.

[67]. U. Kreibig, M. Vollmer, "Experimental results and discussion" in Optical Properties of Metal Clusters, J. P. Toennies ed. (Springer, Berlin, 1995).

[68]. J. He, W. Ji, G. H. Ma, S. H. Tang, H. I. Elim, W. X. Sun, Z. H. Zhang, W. S. Chin, J. Appl. Phys. 95 (2004) 11.

.....ooo.....

Chapter 9

Summary and Conclusions

The modern microelectronics applications are mainly based on semiconductor technologies. Moreover, building materials, health care products, materials for special applications and much more, often employ semiconductors due to their superior chemical and physical properties. A lot of semiconductor materials having different band gaps are available. But among them, titania paves more attention due to its stability, non-toxicity, environmental tolerance, low cost and better catalytic activity [1]. Strong oxidation and reduction power of photoexcited titanium dioxide (TiO_2) was realized after the photocatalytic splitting of water on TiO_2 electrode [2]. Since then, TiO_2 material has been extensively studied which has led to many promising applications in areas ranging from photovoltaics and photocatalysis to photo/electrochromics and sensors.

Photocatalysis is generally the acceleration of a photo reaction in the presence of a catalyst. Heterogeneous semiconductor photocatalysis has recently got immense significance due to its heavy application in environmental pollution control. TiO_2 is the most effective photocatalyst for water and air purification and for self-cleaning surfaces. Strong oxidative ability and super hydrophilicity makes TiO_2 a good antibacterial agent [3]. It is because of these reasons; TiO_2 can be considered as the

king of photocatalysts. TiO_2 crystallizes in three allotropic forms namely anatase, rutile and brookite out of which anatase is considered photocatalytically more active. Due to its large band gap (3.2 eV), the spectral response is limited in the UV region which constitutes only 4-5 % of the sunlight. Band gap narrowing is an effective way to shift the spectral response of TiO_2 and could be attained by anion doping [4-6]. Doping of TiO_2 by metals such as Pt, Ag, Au, Cu, Ni and Pd prevent the electron-hole (e^- - h^+) recombination resulting in an improved catalytic efficiency [7-9]. The above mentioned modifications however reduce the oxidative power and stability of the system concerned. The drawbacks of titania systems could be removed by another efficient method known as co-doping using Pd and N, V and N etc., where one element shifts the spectral response while the other lowers the electron-hole recombination [10-12]. Theoretical investigations revealed that the carrier lifetime in co-doped systems is longer than that in systems with single dopant. The use of light in chemistry has aroused much attention during the last two three decades. The reason for this is that, semiconductor catalysis in the presence of light can have the ability to clean the environment in a sustainable manner which has minimal environmental impact.

Photocatalysis in organic synthesis concerns the use of light to induce chemical transformations onto organic substrates which are transparent in the wavelength range employed. Heterogeneous photocatalysis with titanium dioxide has been extensively investigated as a method for oxidizing organic pollutants in water and air [13,14]. TiO_2 like other solid acid catalysts such as clays and alumina, cannot effectively favor thermal reactions. Acidic basic properties and oxidation

reduction properties associated with the surface sites present on TiO_2 is not so prominent. But on the other hand it can act as a better support which helps to carry out some thermal reactions in a heterogeneous way.

The whole world is nowadays suffered from global warming because of using fossil fuels such as coal and oil. Now the studies are more concentrating to produce clean, sustainable and low-cost energy due to the scarcity of fossil fuel resources. For this purpose, solar cells which convert solar energy to usable energy have become the centre of attraction. Generally, solar cells or photovoltaic cells are the devices which convert solar energy to electrical energy by using photovoltaic effect of semiconductors. Dye sensitized solar cell (DSSC) is a device that generates electric power from light without undergoing any permanent chemical transformation. DSSCs can be considered as the new technology in the category of solar cells, was found in 1991 by Gratzel. TiO_2 is the most commonly used semiconducting material in dye sensitized solar cells due to its low cost and high power conversion efficiency. A device which absorbs sun light with a layer of organic molecule and directly converts it to electric energy is known as organic solar cells. Recently most of the inorganic based solar cells are replaced by organic solar cells. TiO_2 can act as electron transport layer in hetero junction solar cells.

Nonlinear optics means the behavior of light in a nonlinear media. Here the dielectric polarization 'P' responds nonlinearly to the electric field of the light employed. It also deals with the variation of frequency, phase or other physical properties of the material due to the impact of an applied electric field. Nonlinear optics (NLO) is the basis of all photonic technologies where photons are used for signal transmission and

processing. Searching for new effective materials for optoelectronics, microelectronics and molecular electronics is constantly carried out by scientists all over the world. This improves the performance of electronic devices and contribution from NLO materials for this purpose is inevitable. The potential applications of non-linear optics in photonics and optoelectronics have got immense interest nowadays. During the last two decades, a lot of materials were developed as NLO materials for diverse technological applications. But most of the materials developed have some limitation in practical applications. Difficulty in preparation, high cost, toxicity, durability and incorporation into devices are the main constraints of the developed materials. So researchers are now concentrating to develop low cost, sustainable and stable materials for NLO applications. Here comes the importance of semiconductor materials.

Contents of the thesis:

This thesis is divided in to 9 chapters and deals with the modification of TiO_2 for various applications include photocatalysis, thermal reaction, photovoltaics and non-linear optics.

Chapter 1 involves a brief introduction of the topic of study. An introduction to the applications of modified titania systems in various fields are discussed concisely. Scope and objectives of the present work are also discussed in this chapter.

Chapter 2 explains the strategy adopted for the synthesis of metal, non-metal co-doped TiO_2 systems. Hydrothermal technique was employed for the preparation of the co-doped TiO_2 system, where $Ti[OCH(CH_3)_2]_4$,

urea and metal nitrates were used as the sources for TiO_2, N and metals respectively. In all the co-doped systems, urea to $Ti[OCH(CH_3)_2]_4$ was taken in a 1:1 molar ratio and varied the concentration of metals. Five different co-doped catalytic systems and for each catalysts, three versions were prepared by varying the concentration of metals. A brief explanation of physico-chemical techniques used for the characterization of the material was also presented in this chapter. This includes X-ray Diffraction (XRD), Raman Spectroscopy, FTIR analysis, Thermo Gravimetric Analysis, Energy Dispersive X-ray Analysis (EDX), Scanning Electron Microscopy(SEM), UV-Visible Diffuse Reflectance Spectroscopy (UV-Vis DRS), Transmission Electron Microscopy (TEM), BET Surface Area Measurements and X-ray Photoelectron Spectroscopy (XPS).

Chapter 3 contains the results and discussion of characterization techniques used for analyzing the prepared systems. Characterization is an inevitable part of materials research. Determination of physico-chemical properties of the prepared materials using suitable characterization techniques is very crucial to find its exact field of application. It is clear from the XRD pattern that photocatalytically active anatase phase dominates in the calcined samples with peaks at 2θ values around 25.4°, 38°, 48.1°, 55.2° and 62.7° corresponding to (101), (004), (200), (211) and (204) crystal planes (JCPDS 21-1272) respectively. But in the case of Pr-N-Ti sample, a new peak was observed at 2θ = 30.8° corresponding to the (121) plane of the polymorph brookite. There are no visible peaks corresponding to dopants, which may be due to their low concentration or it is an indication of the better dispersion of impurities in the TiO_2. Crystallite size of the sample was calculated from Scherrer equation by

using full width at half maximum (FWHM) of the (101) peak of the anatase phase. Crystallite size of all the co-doped TiO_2 was found to be lower than that of bare TiO_2 which indicates that the doping of metal ions having higher ionic radius into the lattice of TiO_2 causes some lattice distortion which suppress the growth of TiO_2 nanoparticles. The structural identity of the prepared system obtained from XRD pattern is further confirmed by Raman spectra measurements. Anatase has six Raman active modes. Band gap of the co-doped system was calculated using Kubelka-Munk equation and that was found to be lower than pure TiO_2. Stability of the prepared systems was understood from thermo gravimetric analysis. FT-IR was performed to understand the functional groups as well as to study the surface changes occurred during modification. EDX was used to determine the impurities present in the system. The EDX spectra of all the co-doped samples show signals directly related to the dopants. Spectra of all the co-doped systems contain O and Ti as the main components with low concentrations of doped elements. Morphologies of the prepared systems were obtained from SEM and TEM analysis. Average particle size of the systems was drawn from histogram data. Electronic structures of the samples were identified perfectly from XPS measurements.

Chapter 4 describes the photocatalytic degradation of herbicides Atrazine and Metolachlor using metal, non-metal co-doped titania systems. The percentage of degradation was analyzed by HPLC technique. Parameters such as effect of different catalysts, effect of time, effect of catalysts amount and reusability studies were discussed.

Chapter 5 deals with the photo-oxidation of some anthracene derivatives by co-doped catalytic systems. These anthracene derivatives come under

the category of polycyclic aromatic hydrocarbons (PAH). Due to the presence of stable benzene rings, most of the PAH show strong inhibition towards biological degradation and the common methods employed for their removal. According to environmental protection agency, most of the PAH are highly toxic in nature. TiO_2 photochemistry has been extensively investigated as a method for the catalytic conversion of such organic compounds, highlighting the potential of thereof in the green chemistry. There are actually two methods for the removal of pollutants from the ecosystem. Complete mineralization is the one way to remove pollutants. Conversion of toxic compounds to another compound having toxicity less than the initial starting compound is the second way. Here in this chapter, we are concentrating on the second aspect. The catalysts used were Gd(1wt%)-N-Ti, Pd(1wt%)-N-Ti and Ag(1wt%)-N-Ti. Here we were very successfully converted all the PAH to anthraquinone, a compound having diverse applications in industrial as well as medical fields. Substitution of 10^{th} position of desired PAH by phenyl ring reduces the feasibility of photo reaction and produced 9-hydroxy 9-phenyl anthrone (9H9PA) as an intermediate species. The products were separated and purified by column chromatography using 70:30 hexane/DCM mixtures as the mobile phase and the resultant products were characterized thoroughly by ^{1}H NMR, IR spectroscopy and GCMS analysis.

Chapter 6 elucidates the heterogeneous Suzuki coupling reaction by Cu/Pd bimetallic supported on TiO_2. Sol-Gel followed by impregnation method was adopted for the synthesis of Cu/Pd-TiO_2. The prepared system was characterized by XRD, TG-DTG, SEM, EDX, BET Surface area and XPS. The product was separated and purified by column chromatography using hexane as the mobile phase. Maximum isolated yield of biphenyl of around

72% was obtained in DMF using Cu(2wt%)-Pd(4wt%)-Ti as the catalyst. In this reaction, effective solvent, base and catalyst were found to be DMF, K_2CO_3 and Cu(2wt%)-Pd(4wt%)-Ti respectively.

Chapter 7 gives an idea about the photovoltaic (PV) applications of TiO_2 based thin films. Due to energy crisis, the whole world is looking for a new sustainable energy source. Harnessing solar energy is one of the most promising ways to tackle this issue. The present dominant photovoltaic (PV) technologies are based on inorganic materials. But the high material, low power conversion efficiency and manufacturing cost limits its popularization. A lot of research has been conducted towards the development of low-cost PV technologies, of which organic photovoltaic (OPV) devices are one of the promising. Here two TiO_2 thin films having different thickness were prepared by spin coating technique. The prepared films were characterized by XRD, AFM and conductivity measurements. The thickness of the films was measured by Stylus Profiler. This chapter mainly concentrated on the fabrication of an inverted hetero junction solar cell using conducting polymer MEH-PPV as photo active layer. Here TiO_2 was used as the electron transport layer. Thin films of MEH-PPV were also prepared using spin coating technique. Two fullerene derivatives such as PCBM and ICBA were introduced into the device in order to improve the power conversion efficiency. Effective charge transfer between the conducting polymer and ICBA were understood from fluorescence quenching studies. The fabricated Inverted hetero junction exhibited maximum power conversion efficiency of 0.22% with ICBA as the acceptor molecule.

Chapter 8 narrates the third order order nonlinear optical properties of bare and noble metal modified TiO_2 thin films. Thin films were fabricated

by spray pyrolysis technique. Sol-Gel derived $Ti[OCH(CH_3)_2]_4$ in CH_3CH_2OH/CH_3COOH was used as the precursor for TiO_2. The precursors used for Au, Ag and Pd were the aqueous solutions of $HAuCl_4$, $AgNO_3$ and $Pd(NO_3)_2$ respectively. The prepared films were characterized by XRD, SEM and EDX. The nonlinear optical properties of the prepared materials were investigated by Z-Scan technique comprising of Nd-YAG laser (532 nm,7 ns and10 Hz). The non-linear coefficients were obtained by fitting the experimental Z-Scan plot with the theoretical plots. Nonlinear absorption is a phenomenon defined as a nonlinear change (increase or decrease) in absorption with increasing of intensity. This can be mainly divided into two types: saturable absorption (SA) and reverse saturable absorption (RSA). Depending on the pump intensity and on the absorption cross- section at the excitation wavelength, most molecules show non- linear absorption. With increasing intensity, if the excited states show saturation owing to their long lifetimes, the transmission will show SA characteristics. Here absorption decreases with increase of intensity. If, however, the excited state has strong absorption compared with that of the ground state, the transmission will show RSA characteristics. Here in our work most of the materials show SA behavior and some materials exhibited RSA behavior. Both these properties purely depend on the nature of the materials and alignment of energy states within them. Both these SA and RSA have got immense applications in electronic devices.

The important results obtained from various studies are presented in **chapter 9.**

References

[1]. Y. M. Lin, Y. H. Tseng, J. H. Huang, C. C. Chao, C. C. Chen, I. Wang, Environ. Sci. Technol. 40 (2006) 1616.

[2]. A. Fujishima, K. Honda, Nature. 283 (1972) 37.

[3]. X. Fujishima, C. R. Zhang, Chimie. 9 (2006) 750.

[4]. J. Zhao, C. Chen, W. Ma, Top. Catal. 35 (2005) 267.

[5]. M. J. Anpo, Catal. 216 (2003) 233.

[6]. R. Asahi, T. Morikawa, T. Ohwaki, K. Aoki, Y. Taga, Science. 293 (2001) 269.

[7]. V. Brezova, A. Blazkova, L. Karpinsky, J. Groskova, B. Havlinova, V. Jorik, M. Ceppan, J. Photochem. Photobiol. A: Chem. 109 (1997) 177.

[8]. S. Ikeda, N. Sugiyama, B. Pal, G. Marci, L. Palmisano, H. Noguchi, K. Uosaki, B. Ohtani, Phys. Chem. Chem. Phys. 3 (2001) 267.

[9]. A. Fuerte, M. D. Hernandez-Alonso, A. J. Maira, A. Martinez-Arias, M. Fernandez-Garcia, J. C. Conesa, J. Soria, Chem. Commun. (2001) 2718.

[10]. A. T. Kuvarega, R. W. M. Krause, B. B. Mamba. J. Phys. Chem. C. 115 (2011) 22110.

[11]. J. Liu, R. Han, Y. Zhao, H. Wang, W. Lu, T. Yu, Y. Zhang, J. Phys. Chem. C. 115 (2011) 4507.

[12]. X. Sun, H. Liu, J. Dong, J. Wei, Y. Zhang. Catal. Lett. 135 (2010) 219.

[13]. M. A. Fox, M. T. Dulay, Chem. Rev. 93 (1993) 341.

[14]. M. R. Hoffman, S. T. Martin, W. Choi, D. W. Bahnemann, Chem. Rev. 95 (1995) 69.

.....ooo.....

List of Publications

1. K M Mothi, K P Sandhya, A H Salim, S Sugunan, International Journal of Environmental Science and Engineering Research. 4(3) (2013) 77-84.

2. K. M. Mothi, G. Soumya, A. H. Salim, S. Sugunan, J Sol-Gel Sci Technol. (Accepted)

3. K M Mothi, G Soumya, M J Honey, S Sugunan, Journal of Porous Materials (Communicated).

4. K M Mothi, S Sugunan, Bulletin of Chemical reaction Engineering and Catalysis (Communicated)

.....ꕥ.....